

Wind Resource Assessment for the Donadeo Innovation Centre for Engineering (DICE) building at the
University of Alberta North Campus

by

Hermes Gordon

A thesis submitted in partial fulfillment of the requirements for the degree of

Master of Science

Department of Mechanical Engineering
University of Alberta

© Hermes Gordon, 2017

Abstract

The implementation of small wind turbines in the urban environment with the intention of producing energy in high demand areas (cities), and reduce carbon footprint has been met generally with less than successful results. . The primary challenge in these projects is to understand the wind field, specially the turbulence structure around the buildings, which is characterized by large recirculation zones and flow separation. However, one possible advantage of the wind field around buildings is the concentration effect that could increase the wind power density compared to rural settlements.

This thesis studies the potential of harvesting wind energy at the Donadeo Innovation Centre for Engineering (DICE) building at University of Alberta North Campus. In order to conduct the wind resource assessment wind data were collected at the edge of the building with three wind monitors and one ultrasonic anemometer. Data were recorded with a constructed datalogger, which allowed us to reduce equipment cost.

Data of the month of February was processed and different statistical tools were used, including daily and hourly mean averages, wind roses, and Rayleigh wind probability distribution to determine the main wind direction and most probable wind speeds. Turbulence intensity was also computed for 10 min. and 1 min. averaging time, and the difference between the two approaches was studied.

One minute autocorrelations were computed for the windiest and most turbulent hours; and the integral time and length scale were determined based on Taylor's hypothesis. These calculations approximated the size of the turbulent elements present in the urban environment.

The DICE building presented higher wind speeds than the Tory building, and has a wind power density comparable to coastal areas. However the turbulence intensity is extremely high compared to the open ground and coastal zones. There was a small reduction in the turbulence intensity when using 1 min. averaging time, showing that 10 min. gives an upper estimation for turbulence intensity which can be used as a conservative approach when assessing a location for potential wind energy harvesting.

Acknowledgements

I would like to thank my supervisor, Dr. Brian Fleck for giving me the opportunity of completing a Masters in Science in Mechanical Engineering at the University of Alberta. I am grateful for all his support, guidance throughout the course of my degree and his enthusiasm that encouraged me to explore my new field of study. He consistently allowed this thesis to be my own work, and steered me in the right the direction whenever he thought I needed it.

I would also like to thank Dr. Carlos Lange and Dr. Mireille Tadie Fogaing for being involved in this research project. Their input and advice was valuable for the development of this thesis; and their knowledge in computational fluid dynamics helped me to visualize and understand key aspects that are studied in this work.

I want to thank Jorge Marin, for supporting me in the development of hardware equipment that was vital for the project. His input and expertise in electronics was important and allowed me to increase my knowledge in instrumentation and programming.

I am extremely grateful for all the support from my parents. They have always been a guide and a source of inspiration that encourages me to chase for the best and become better every day. I appreciate their unconditional understanding and support that has led me to this day. This accomplishment would not have been possible without them.

Finally, I want to express my gratitude to my sister, friends and all the special people that has made this journey a unique experience.

Table of Contents

1.	Introduction	1
1.1	Thesis objective	3
1.1.1	Specific objectives	3
1.2	Thesis format	3
2	Literature and Basic Concepts.....	4
2.1	Energy in Canada.....	4
2.2	Wind speed in the built environment.....	6
2.2.1	Vertical wind profile.....	6
2.2.2	Urban wind profile.....	8
2.2.3	Turbulence	12
2.2.3.1	Wind Spectrum	14
2.3	Wind turbines.....	15
2.3.1	Urban wind turbines.....	16
2.3.2	Horizontal axis wind turbine (HAWT).....	16
2.3.3	Vertical axis wind turbine (VAWT).....	16
2.3.4	HAWT vs VAWT	17
2.3.5	Economics of urban wind turbines.....	21
2.4	Wind resource assessment	24
3.	Methodology	31
3.1	Location	31
3.2	Equipment.....	31
3.3	Data collection	35
3.4	Anemometers set up.....	37
3.5	Data processing.....	40
4.	Results and Discussion.....	44
4.1	Daily Mean Wind Behavior.....	44

4.2	Hourly Mean Wind Behavior.....	46
4.3	Wind Power Density.....	47
4.4	Wind Roses.....	50
4.5	Histograms and Rayleigh distributions.....	55
4.6	Turbulence Study.....	61
4.7	Autocorrelation of Wind Velocity.....	66
4.8	Tory Building 2016 Data Assessment.....	73
5.	Conclusion.....	80
5.1	Summary.....	80
5.2	Future Work.....	81
	References.....	83
	Appendix A: Anemometers Technical Information.....	88
	Appendix B: The DICE building pictures.....	92

List of Tables

Table 1 Values for roughness length z_0 , and exponent m for different surfaces (Wood, 2011).....	9
Table 2 Anemometers specifications comparison.....	34
Table 3 Arduino MEGA specifications	35
Table 4 Data logging format	36
Table 5 Canadian Wind Atlas Parameters 50m Mesoscale	49
Table 6 Wind Statistical Parameters, Rayleigh distribution	58
Table 7 Average wind power density available on February 2017, based on Rayleigh distribution.....	59
Table 8 Averaged Turbulence Intensity.....	65
Table 9 Autocorrelation Parameters 7 pm	69
Table 10 Autocorrelation Parameters 4 pm	72
Table 11 Rayleigh Parameters EAS Weather Station 2016.....	76

List of Figures

Figure 1 Canada’s energy flow in 2013 (CESAR, 2017).....	5
Figure 2 Vertical layering of the ABL over flat terrain, modified from (Emeis, 2013).....	7
Figure 3 Vertical layering in the UBL, modified from (Emeis, 2013).....	11
Figure 4 Typical turbulence intensity plot (taken from Neuman et al., 2006).....	14
Figure 5 Three bladed horizontal axis wind turbine (Ayhan & Sağlam, 2012).	17
Figure 6 Savonius wind turbine (Ayhan & Sağlam, 2012).	18
Figure 7 Darrieus wind turbine (Paraschivoiu, 2002).	19
Figure 8 Characteristics HAWT and VAWT (Natural Resources Canada, 2003).	19
Figure 9 Contours of velocity magnitude (L. Lu & Ip, 2009).....	20
Figure 10 Side view of streamlines around building (Larin et al., 2016).	21
Figure 11 The economy of scale diagram.	23
Figure 12 Basic approach for wind resource assessment (Wind Empowerment, 2017).	24
Figure 13 DICE building location (Google, 2017).	32
Figure 14 DICE building detailed view (Google, 2017).....	33
Figure 15 Anemometers.....	34
Figure 16 Overview of data acquisition system.....	36
Figure 17 Data logging system (Arduino board)	37
Figure 18 Anemometers set up on DICE rooftop	38
Figure 19 Anemometers set up on DICE rooftop (2).....	39
Figure 20 Arduino board and junction box detail	40
Figure 21 Daily Mean Wind Speed DICE building February 2017.....	44
Figure 22 Daily Wind Speed Tory Building February 2017.....	45
Figure 23 Hourly Wind Speed DICE building on Feb. 12 th	46
Figure 24 Hourly Averaged Turbulence Intensity, February 12 th 2017.....	47

Figure 25 DICE WPD based on daily averaging time, February 2017.....	48
Figure 26 Daily Averaged WPD, Tory Building February 2017.....	49
Figure 27: (a) Wind Rose Wind Monitor #1 (DICE), (b) Wind Rose Wind Monitor #2 (DICE), (c) Wind Rose Wind Monitor #3 (DICE), (d) Wind Rose 3D ultrasonic Anemometer (DICE), (e) Wind Rose TBWS.	53
Figure 28 Rayleigh distributions: (a) Wind Monitor #1, (b) Wind Monitor #2, (c) Wind Monitor #3, (d) 3D Ultrasonic Anemometer, (e) TBWS.....	57
Figure 29 Wind Frequency and Power Distributions, Wind Monitor 1.....	60
Figure 30 Turbulence Intensity 10 min. Average: (a) u component, (b) v component, (c) w component. .	62
Figure 31 Turbulence Intensity 1min. Average: (a) u component, (b) v component, (c) w component.	64
Figure 32 Autocorrelation at 7 pm: (a) u component, (b) v component, (c) w component.....	68
Figure 33 Autocorrelation at 4 pm: (a) u component, (b) v component, (c) w component.....	71
Figure 34 Daily and Hourly Wind Speed, EAS Weather Station 2016	74
Figure 35 EAS Weather Station (TBWS) 2016 Wind Rose.	75
Figure 36 Rayleigh Distribution TBWS 2016.	76
Figure 37 Wind Frequency and Power Distributions, TBWS 2016.....	78

Nomenclature

Symbols

α	Wake factor
β	Weibull shape factor
λ_f	Frontal area density
Λ_u	Integral length scale
Λ_t	Integral time scale
ρ	Air density
σ_U	Standard deviation
τ	Time lag
φ	Frequency
A	Swept area
c	Weibull and Rayleigh scale factor
c_j	Autocovariance at lag j
c_o	Sample variance of time series
C_p	Power coefficient
C	Cumulative probability
d	Displacement height for flows over cities
g	Wind power distribution
h_r	Reference height
H	Height
I	Turbulence intensity
j	Time lag
k	Von Karman's constant
M	Exponent dependent on surface roughness
P	Probability density function
P	Wind power
\bar{P}	Averaged wind power
P_{avg}	Averaged uncorrected air pressure
$r(\tau)$	Autocorrelation function
R	Ideal gas constant
$S(\varphi)$	Power spectral density

T_{avg}	Averaged air temperature
u	Longitudinal wind velocity component
u'	Fluctuation of the longitudinal component
$u(t)$	Time series of the longitudinal wind velocity component
$\overline{u(t)}$	Wind speed mean value over an average time
$u'(t)$	Fluctuation around the average
U	Wind speed
\bar{U}	Averaged wind speed
U_*	Friction velocity
U_H	Mean wind speed at height H
$U(z)$	Wind speed at height z
$U(h_r)$	Wind speed at reference height h_r
v	Lateral wind velocity component
v'	Fluctuation of the lateral component
V	Horizontal wind speed, magnitude (u,v)
$\overline{V^3}$	Mean cubed velocity
V_{mp}	Most probable wind speed, based on Rayleigh distribution
w	Vertical wind velocity component
w'	Fluctuation of the vertical component
z	Height
z_o	Roughness length

Abbreviations

ABL	Atmospheric boundary layer
AEP	Annual energy production
DICE	Donadeo Innovation Centre for Engineering building
HAWT	Horizontal axis wind turbine
KE	Kinetic energy
pdf	Probability density function

TBWS	Tory Building EAS Weather Station
UBL	Urban boundary layer
UCL	Urban canopy layer
UWL	Urban wake layer
VAWT	Vertical axis wind turbine
WPD	Wind power density

1. Introduction

The constant increase in energy demand around the world combined with the effects on climate change due to greenhouse gas (GHG) emissions produced by fossil fuels, which are the main source of energy worldwide, is pushing the world to change policies and find more sustainable ways to produce energy (ExxonMobil, 2016; Ledo, Kosasih, & Cooper, 2011; Saidur, Islam, Rahim, & Solangi, 2010; Tummala, Velamati, Sinha, Indrajaya, & Krishna, 2016). Therefore, relying on renewable resources such as wind, solar, hydro, biomass and geothermal to produce affordable sustainable energy is essential to mitigate the impacts of climate change, reduce our carbon footprint and to stop relying on depleting energy sources. Following this path, the Paris agreement was signed in December 2016 by 195 countries willing to reinforce the global response to climate change, by reducing their emissions and keeping the global temperature rise under 2 degrees Celsius (UNFCCC. Conference of the Parties (COP), 2015).

While the United States of America has withdrawn from it, many countries, like Canada, have re-confirmed their commitment to be part of the change. Many countries have started to promote substantial investment in renewable energies, especially wind power which is renewable, reduces carbon dioxide, and represents one of the fastest growing sectors in sustainable energies (Archer, 2005; Makkawi, Celik, & Muner, 2009). This trend is expected to continue as some studies performed to evaluate the available potential of global wind energy have shown that there is enough power in the Earth's winds to be a primary source of near-zero-emission electric power (Archer, 2005; X. Lu, McElroy, & Kiviluoma, 2009).

The idea of producing clean power in the main consumption areas brings attention to the application of small scale wind turbines. Urban wind power would bring different benefits to the cities, like avoiding the transport of large amounts of electrical energy from wind farms or solar plants, wind monitoring can also help with improving the efficiency of HVAC systems, building planning and help in making cities more sustainable. In the near future, urban wind energy has the potential to play a key role in the context of smart cities (Simões & Estanqueiro, 2016), and studies conducting life cycle assessments (LCA) have concluded that the use of small wind turbines benefits the environment by reducing by 93% GHG emissions compared to other sources of energy production (Fleck & Huot, 2009). However, the application of urban wind power presents many challenges that so far have not been overcome.

The wind potential in urban areas is difficult to assess and not fully understood, the amount of energy that can be extracted from the urban environment is considerable low compared to large scale wind and solar farms. Another point is that harvesting methods need the public acceptance (Karthikeya, Negi, &

Srikanth, 2016; Simões & Estanqueiro, 2016) concerning the technology itself and other factors such as how machines fit into the urban setting. In addition, the normalized cost of power production from small scale wind turbines is usually higher than medium and large scale systems (including solar), especially in poor wind conditions; and economic analyses have shown that the payback period is usually long (16-18 years) making them less appealing to investors (Grieser, Madlener, & Sunak, 2013). Maximizing the potential for urban wind by setting the turbines in areas where the local wind speed increases, may be helpful in overcoming the aforementioned disadvantages. Wind velocity is a key parameter in assessing a potential site, since the power output of a wind turbine is proportional to the cube of wind speed (Dayan, 2006; Wood, 2011). With this fact in consideration, there has been interest in studying the concentration effect created by the urban landscape, that in combination with buildings' heights could increase the power density by 3-8 times compared to rural settings (Ayhan & Sağlam, 2012; Mertens, 2006). However, urban areas present many limitations in the wind quality because in the built environment, air flows are more unsteady and the turbulent boundary layer affects the performance of the turbine by reducing its power output and fatigue life (Ayhan & Sağlam, 2012; Makkawi et al., 2009). For these reasons wind turbines should be placed in locations with high wind speeds and low turbulence intensity. Rooftops of high rise buildings are potentially a good option, especially around the edge of the building because there is often an accelerated shear layer (Ayhan & Sağlam, 2012; Mertens, 2006; Toja-Silva, Lopez-Garcia, Peralta, Navarro, & Cruz, 2016).

Urban wind energy has been studied by many researchers, however its most important barrier is the lack of information regarding the actual energy content of the wind in cities, and adequate wind data measurements (Beller, 2011; Simões & Estanqueiro, 2016). Usually CFD simulations are used to assess urban wind resource, but wind data are always necessary in order to validate these simulations. Most of the time, researchers rely on wind atlas, or wind data from airports and weather stations that are often not representative of the conditions in question due to their distance to the area of evaluation.

This thesis provides an insight of the wind energy in Canada and an experimental study on wind resource assessment by analyzing the recently constructed engineering building at the University of Alberta. Data were gathered with four different wind sensors at low height compared to the common practice, with the intention of studying the wind flow at the edge of the building in order to determine if there is an acceleration effect due to the building structure that could help with the disadvantage of having a lower energy production in cities, compared to wind farms

1.1 Thesis objective

The general objective of this research was to study the wind field around the University of Alberta North Campus, focusing on the potential for energy harvesting with small wind turbines at the edge of the Donadeo Innovation Centre for Engineering (DICE) building. In order to reach this objective the following elements were developed:

- Design and build a data logging system, able to save data simultaneously from four wind sensors at a high sampling rate.
- Study the wind field and concentration effect at the edge of DICE building. Based on wind statistical tools, assess the wind potential.
- Compare results with data obtained from Tory building EAS Weather Station (TBWS).

1.1.1 Specific objectives

In order to narrow the research, the following elements were studied:

- Compute and plot wind roses with data gathered during the month of February 2017.
- Determine the wind probability using Rayleigh distribution function.
- Study the turbulence at the edge of the building, and compare results with different approaches:
 - 10 min. turbulence intensity (I).
 - 1 min. turbulence intensity (I).
 - Autocorrelation of the three components of the wind velocity (u, v, w).
- Determine available power at the edge of the building.

1.2 Thesis format

This thesis is organized into five chapters, starting with Chapter 1 introducing the topic and importance of the thesis. Chapter 2 develops the literature review and includes fluid mechanics concepts that are important for the study of wind monitoring and wind turbine applications. Chapter 3 explains the methodology that was followed to conduct the wind resource assessment, including a description of the studied location, equipment used for wind monitoring and data processing. Results and discussions are presented in Chapter 4, including a comparison between our results and other research studies. To conclude, Chapter 5 provides a summary of the work and proposes recommendations for future work.

2 Literature and Basic Concepts

2.1 Energy in Canada

Canada is unique among nations in terms of energy resources. In its vast territory it has large potential in hydropower, oil, coal, natural gas, biomass, wind, geothermal and uranium for nuclear power (Oliver et al., 2016).

The primary resource of energy in Canada is oil followed by uranium and natural gas. However most of these resources are exported, with the United States as the primary market. In terms of electricity production, hydropower is the principal source used, followed by coal, nuclear and natural gas. The input from wind and solar is relatively small compared to the other sources, but their contribution is quickly growing (Oliver et al., 2016).

Other sources of energy like crude oil, natural gas, coal and biomass are mostly used to power industrial processes, transportation and to heat homes and buildings. As an interesting fact, two thirds of the energy sources used to provide energy services are wasted, most of the time as heat (Oliver et al., 2016).

This information can be visualized in a better way with the Sankey Diagram in Figure 1, which presents the energy flow in Canada in 2013.

As we have seen, the main electricity source in Canada is hydro power. The provinces with most of the hydro production are Quebec, Manitoba, British Columbia and, Newfoundland and Labrador (Oliver et al., 2016), while some provinces use hydro for 20% or less of their power (AB, SK, NS). These provinces use fossil fuels (mostly coal) as their primary electricity resource.

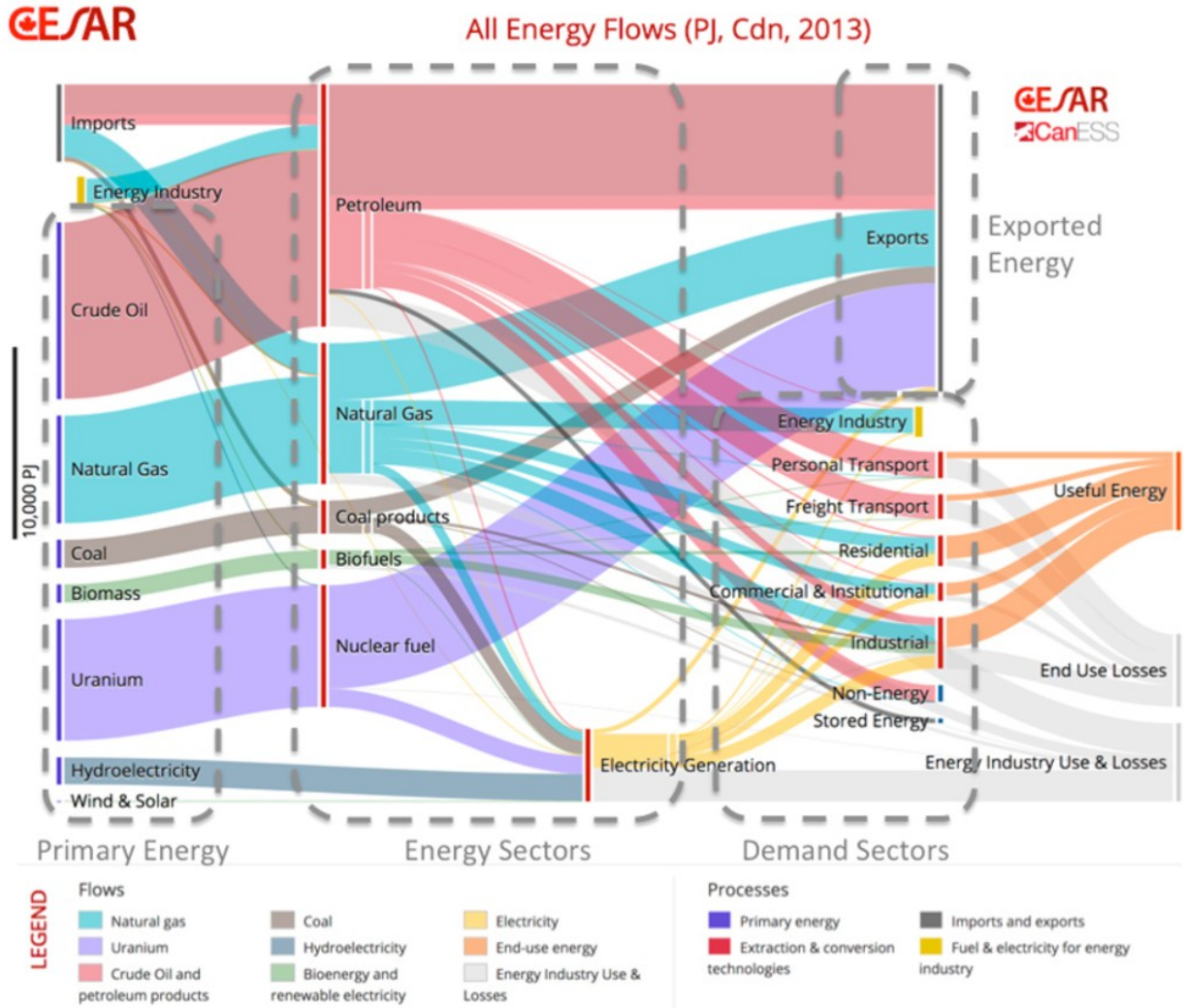


Figure 1 Canada's energy flow in 2013 (CESAR, 2017).

This is a positive aspect, especially recently where the reduction in emissions is desired. However some provinces like Ontario produce their electricity mostly from nuclear power, and others from fossil fuels like is the case of Alberta and Saskatchewan (Oliver et al., 2016).

Alberta, a province of our interest produces almost 90% of its electricity from coal and natural gas and it is the largest consumer of coal for electricity of the country, however the province has pledged to phase out coal from the power generation by 2030 (Oliver et al., 2016).

On this aspect, wind power has earned special interest in the energy sector. Canada by the end of 2016 had a wind power installed capacity of 11,900 MW (GWEC, 2017). However this refers to large scale wind power, and there is an interest of integrating small scale turbines into the urban environment to produce clean energy in the cities.

2.2 Wind speed in the built environment

In this section we will discuss the importance and characteristics of the wind flow in the built environment. Understanding the wind structure in complex terrain such as cities is a key concern in order to successfully assess urban wind resources. We will begin by studying how the wind varies in terms of height and by discussing the atmospheric boundary layer.

2.2.1 Vertical wind profile

It is important to understand the difference between the wind velocity profile over flat terrain and over the built environment. Over the earth surface, because of the no-slip condition, we have the presence of the atmospheric boundary layer (ABL). The ABL is the lower part of the troposphere, in other words, the lowest layer of the atmosphere. It is the only part of the atmosphere where frictional forces are significant; and where temperature and atmospheric stability present diurnal and annual variations. Over flat, horizontal and homogeneous terrain the ABL presents its simplest structure and it is divided in three vertical layers. The first layer, known as the roughness sublayer, is only a few millimeters deep with no relevance for wind energy applications (Emeis, 2013). The second layer it is known as the surface layer or Prandtl layer and it is assumed to occupy the lowest 10% of the ABL. The thickness of the surface layer varies between day and night. During the day it may be up to 100 m deep, however during clear nights with calm winds the layer's thickness is small, less than 10 m. In the surface layer, the influence of the Coriolis force is negligible and forces due to turbulent viscosity dominate, this means that equilibrium between the pressure force and frictional forces is often observed. The Prandtl layer is also characterized by vertical wind gradients, which means that the wind speed increases strongly with height (Dutton & Panofsky, 1984; Emeis, 2013).

The third layer is the Ekman layer, which covers the 90% of the ABL. Here the Coriolis force is important and causes a change of the wind direction with height. The balance of the forces involved in this layer present the Coriolis force, pressure gradient force and the frictional forces. The depth of the layer varies between 100m during night time with calm winds, to 2-3km at daytime with strong solar irradiance. Another characteristic of the Ekman layer is that the vertical gradients are much smaller compared to the Prandtl layer (Emeis, 2013).

It is important to mention that in the free troposphere, above the ABL, the frictional forces are negligible. The balance of forces are dominated by Coriolis and pressure force. This is the most fundamental balance of forces in wind meteorology (Emeis, 2013).

The layers described previously are shown in Figure 2, where z_o is the roughness length.

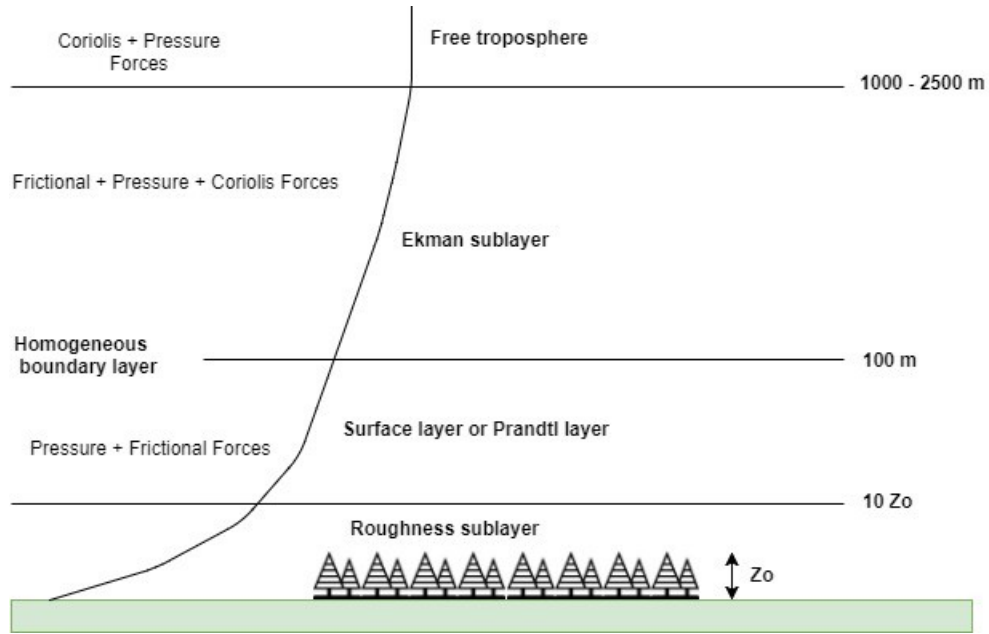


Figure 2 Vertical layering of the ABL over flat terrain, modified from (Emeis, 2013).

The ABL over flat terrain evolves mostly because of the diurnal changes in the energy balance on the earth surface. During daytime, because of solar radiation, a convective boundary layer grows because of the energy input from below, generating thermal convection. During the night, when the soil cools down, a stable boundary layer is created which is characterized by low turbulence intensity. When the clouds, rain and wind override the effect of the radiation a neutral boundary layer forms (Emeis, 2013).

As discussed before, in the surface layer the wind velocity varies respect to the height; this vertical gradient, translated into different wind speeds between neighboring heights causes mean shear stress. Under neutral conditions, the simplest expression to describe the variations of the wind speed in terms of the height $U(z)$, is the power law (Wood, 2011).

$$U(z) = U(h_r) \left(\frac{z}{h_r} \right)^m \quad 2.1$$

Where $U(z)$ is the determined wind velocity at height z , $U(h_r)$ is the wind velocity at reference height h_r , and m is an exponent that depends on the roughness of the surface.

In the surface or Prandtl layer, it is usually accepted that the logarithmic law is more accurate than the power law. The logarithmic law for flat terrain is defined as:

$$U(z) = U(h_r) \left(\frac{\ln(z/z_0)}{\ln(h_r/z_0)} \right) \quad 2.2$$

Where z_o is the roughness length and it is used to characterize the drag on the surface. Different values for roughness length z_o and m are presented in Table 1.

According to Emeis (2013) there is another way to represent the logarithmic law in the surface layer, and it is defined in equation 2.3.

$$U(z) = \frac{U_*}{k} \ln\left(\frac{z}{z_o}\right) \quad 2.3$$

Where U_* is the friction velocity and k is the Von Karman's constant, usually taken as 0.4. The friction velocity is related to the shear stress near the ground and it is the usual scaling velocity for the wind speeds and the vertical wind shear in the atmospheric surface layer (Emeis, 2013).

Values for friction velocity can be found in the literature or derived with high resolution wind measurements from an ultrasonic anemometer using equation 2.4:

$$U_* = \left(\overline{u'w'^2} + \overline{v'w'^2}\right)^{\frac{1}{4}} \quad 2.4$$

Where u' is the turbulent fluctuation of the East-West wind component, v' the fluctuation of the North-South component, and w' the fluctuation of the vertical component. All three fluctuating elements are available for data analysis when the wind is measured by an ultrasonic anemometer.

Where u , v and w are the three components of the wind velocity; u is longitudinal component East-West direction, v is the lateral component North-South and w the vertical component. Each of these components can be decomposed into a mean wind speed and a fluctuation around this mean (Emeis, 2013).

The definition of the time series of the longitudinal component of the wind velocity $u(t)$ is presented in equation 2.5.

$$u(t) = \overline{u(t)} + u'(t) \quad 2.5$$

Where $\overline{u(t)}$, is the mean value over an average time and $u'(t)$ is the fluctuation around this average. The same definition applies for the lateral component v and the vertical w .

2.2.2 Urban wind profile

As mentioned before, the continued growth of cities has resulted in an increasing energy demand in urban settlements. This has led researchers to study the potential of using wind turbines to produce energy in

cities and to try to understand why this technology is not fully applicable and able to compete with other sources of energy like urban solar, and what can be done to make urban wind power a real viable option in the future. The interest in trying to understand how to make urban wind energy harvesting more power efficient, has increased the interest in studying the structure of the urban boundary layer (UBL).

The wind field within the built environment is characterized by an urban boundary layer flow (UBL) which is a portion of the ABL over urban areas, and it is generated by frictional drag on the surface. The urban surface is characterized by different aspects: large roughness elements, reduced moisture availability at the surface, wide spread sealed areas and high heat storage. This produces higher turbulence intensity in the UBL and stronger heat fluxes from the surface into the UBL (Emeis, 2013).

In the urban environment as well as in open areas, the wind is driven by large scale atmospheric motions. However in the built environment the flow is heavily retarded because of the large roughness elements, buildings and vegetation which are considered bluff bodies since there is a presence of strong flow separation, and the drag over cities is dominated by pressure drag (Neuman, Emeis, & Illig, 2006; Oke, 1990; Plate, 1995).

Table 1 Values for roughness length z_o , and exponent m for different surfaces (Wood, 2011).

Landscape type	z_o (mm)	m
Lakes, ocean, calm open sea	0.2	0.104
Snow	3.0	0.100
Rough pasture	10.0	0.112
Crops	50.0	0.131
Scattered trees	100.0	0.160
Many trees	250.0	0.188
Forest	500.0	0.213
Suburbs	1500.0	0.257
City centre	3000.0	0.289

The UBL is usually divided in four vertical layers; a representation of this vertical structure is shown in Figure 3. The lowest part of the layers is known as the urban canopy layer (UCL), and extends from the ground to the mean top height of the buildings, referred as H in Figure 3. The following layer is the wake layer (UWL), where the influence of buildings on the flow is still notable. This layer usually extends to about three to five times the mean height H of the buildings. These two layers (urban canopy layer and the

wake layer combined are usually called the urban roughness sub-layer, where complex vertical exchange induced by vertical motions can occur (Emeis, 2013).

Beyond the urban roughness layer the constant flux layer (CFL) is present. This layer over flat terrain is known as the Prandtl layer, so the balance of forces is basically the same with pressure and frictional forces in equilibrium. Above the CFL appears the Ekman layer, where the Coriolis force is important, making the wind direction to turn into the direction of the geostrophic wind (Emeis, 2013). These two layers are often jointly addressed as the mixed layer, where the turbulence is mostly generated by convective air motions and not directly affected by the surface roughness (Romanic, Rasouli, & Hangan, 2015).

Figure 3 also shows the atmospheric pressure disturbances upstream and downstream of the buildings and it is addressed as p^+ and p^- .

Most urban wind turbines installed on the rooftops are inside the roughness layer and, because of irregularities in this surface; the wind flow incident on wind turbines is complex and multi-directional, affecting their actual power production.

For the built environment, the logarithmic wind profile needs a modification to account for the high roughness. The expression can be modified as:

$$U(z) = \frac{U_*}{k} \ln\left(\frac{z-d}{z_o}\right) \quad 2.6$$

Where d is the displacement height, relevant for flow over cities and forests.

Over areas covered with buildings or trees, the displacement height d gives the vertical displacement of the entire flow regime. z_o and d depend on the extent of the footprint (or fetch) upstream of the place where the wind profile is to be evaluated.

2.2.3 Turbulence

Turbulence is a type of fluid flow that is heavily rotational, apparently chaotic, and it is present in most of the flows in nature where forces of momentum are much greater than viscous forces. Turbulence has eddy structures ordered in a continuum spectrum of sizes and intensities. In the atmosphere, the flow near the ground is most of the time turbulent up to a height of 1km or more during the day, and about 100m at night. At larger heights, turbulence happens in cumulus clouds and in layers with strong change in the mean wind speed or direction (Dutton & Panofsky, 1984; Emeis, 2013; Tennekes & Lumley, 1999).

According to Dutton & Panofsky (1984) and Tennekes & Lumley (1999), there is no simple definition of turbulence; however, turbulence can be described by the following characteristics:

- Turbulence occurs at high Reynolds numbers.
- The fluid flow is unsteady and a stochastically function of both space and time.
- The flow is rotational and three-dimensional with gradients occurring in all directions.
- Turbulent flows are diffusive, causing rapid mixing and increasing rates of momentum, heat and mass transfer.
- Turbulent flows are dissipative. Viscous shear stresses deform the flow, increasing the internal energy (temperature) of the fluid at the expense of the kinetic energy. This characteristic explains why turbulence needs a continuous energy supply from the environment to make up for the viscous losses; if no energy is supplied turbulence decays.
- Gradients are produced in the turbulent flow by stretching of vortices, a process that moves kinetic energy to smaller wavelengths. This is known as the turbulence energy cascade.

The energy cascade is explained as the existence of energy transfer from large eddies to smaller, due to vortex stretching and leading to viscous dissipation of energy near the Kolmogorov microscale. Most of the energy across a determined wave number comes from a neighboring larger eddy and it is transferred to the next smaller one. Therefore larger and smaller eddies have no effect on the energy transfer at intermediate wave numbers (Tennekes & Lumley, 1999)

The vortex stretching mechanism may be explained as follows: when vorticity is inside a strain-rate field, it experiences stretching. Based on the conservation of angular momentum, it is expected that the vorticity in the direction of a positive strain rate is amplified, while the vorticity in the direction of a negative strain is attenuated (Tennekes & Lumley, 1999).

As discussed before, wind fluctuates randomly in magnitude and direction; and its measurement can be decomposed as shown in equation 2.5. The fluctuating part of the wind (turbulence) can be studied with

statistical tools. One common practice used in wind energy applications to quantify the turbulence at a desired location, is known as turbulence intensity I , and it is defined as (Wood, 2011):

$$I = \frac{\sigma_U}{U} = \frac{1}{U} \left[\frac{1}{T_s} \int_0^{T_s} u^2 dt \right]^{1/2} \quad 2.9$$

Where U is the mean wind velocity of the sampling period, T_s is the sampling time and σ_U is the standard deviation of the velocity defined as:

$$\sigma_U = \sqrt{\frac{1}{n-1} \sum_{i=1}^n (\bar{U}_i - U)^2} \quad 2.10$$

Equation 2.9 brings a key question, what should be the proper sampling time in order to calculate turbulence intensity? According to Wood, (2011) the sampling time (T_s) should be sufficiently large that any increase would not alter the value of I more than a small negligible amount. In practice however, this is hard to achieve, and the most common T_s used in wind turbine applications is 10 min. (Wood, 2011).

Turbulence intensity usually characterizes the high frequency of turbulence (Emeis, 2013). It is a key aspect when it comes to assess a location for power production, since it has important effects on a wind turbine performance. It affects the power output and increases fatigue loads on the turbines. According to the National Renewable Energy Laboratory (NREL), acceptable values of turbulence intensity for setting urban wind turbines in terms of power production and fatigue loads, should be under 18% (Fields, Oteri, Preus, & Baring-gould, 2016). Another characteristic of turbulence intensity is that it decreases as the wind speed increases. This means that at low wind speeds the relative turbulence is higher; this can be seen in Figure 4 which shows a typical turbulence intensity plot as function of wind speed. The turbulence intensity is over the 10% at wind speeds between 0 and 5 m/s, and then it tends to be constant below 10 % between 5 and 25 m/s, with a slow decrease over this range.

When it comes to calculate the power curve, the International Electrotechnical Commission (IEC) mandates $T_s= 10$ min. However we will discuss more about turbulence intensity and how the averaging time affects the results in section 2.4.

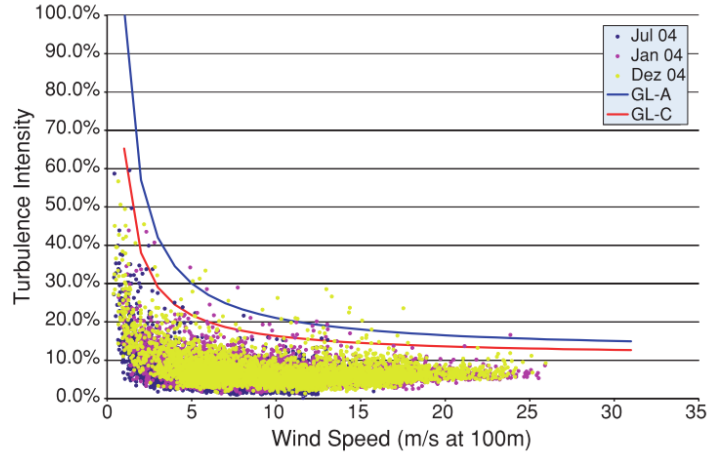


Figure 4 Typical turbulence intensity plot (taken from Neuman et al., 2006).

2.2.3.1 Wind Spectrum

The spectral analysis allows us to have an idea of how eddies of different sizes exchange energy with each other. The value of the spectrum at a given frequency is the mean energy in the turbulent fluctuation at that wave number (Tennekes & Lumley, 1999). In other words, the spectrum describes the frequency dependence of the power of turbulent fluctuations. It differs from turbulence intensity, since the standard deviations of the wind components are integral values over the entire turbulence spectrum (Emeis, 2013).

The spectra are decompositions of the measured function into different wavelengths, and it is mathematically defined as the Fourier transform of the autocorrelation of the wind velocity $u(t)$.

The autocorrelation provides information about how the values of $u(t)$ are related at different times, and it is defined by Tennekes & Lumley, (1999) as:

$$r(\tau) = \frac{\overline{u(t)u(t')}}{\overline{u^2}} \quad 2.11$$

Where $r(\tau)$ is the autocorrelation coefficient and τ is the time lag ($\tau = t' - t$). The autocorrelation is equal to one at the origin; it is also real, symmetric and it goes to zero faster than $1/\tau$. Its integral scale exists and it is defined as:

$$\Lambda_t = \int_0^{\infty} r(\tau) d\tau \quad 2.12$$

In turbulence, the integral scale it is always assumed to be finite, and its value is a rough measure of the interval over which $u(t)$ is correlated with itself.

The power spectral density or spectrum is the Fourier transform $S(\varphi)$ of $r(\tau)$, and it is defined by:

$$r(\tau) = \int_{-\infty}^{\infty} e^{i\tau\varphi} S(\varphi) d\varphi$$

2.13

$$S(\varphi) = \frac{1}{2\pi} \int_{-\infty}^{\infty} e^{-i\tau\varphi} r(\tau) d\tau$$

Where φ is frequency. $S(\varphi)$ shows how the turbulent kinetic energy is distributed with respect to frequency φ .

In the ABL, the wind speed spectrum shows a minimum is the range of 1 hour (0.0003 Hz) (Van der Hoven, 1957). Higher frequencies are referred as turbulence, which as previously discussed, is usually characterized by turbulence intensity (Emeis, 2013). However, spectral analysis gives information that it is not attainable in other ways (Tennekes & Lumley, 1999). For example, it provides the necessary information to calculate loads for wind turbines (Emeis, 2013).

On the other hand, the low frequency end of the spectrum (0.01- 0.001Hz), is usually described by the Weibull distribution (Emeis, 2013), this concept will be developed in section 2.4.

2.3 Wind turbines

Most of the time the primary purpose of wind turbines is to transform the kinetic energy of the wind into electric power. In wind energy applications, it is important to know the amount of available energy in the wind and how much power can be harvested.

In energy harvesting, the wind velocity is an extremely important parameter since the power output of a wind turbine depends on the cube of the wind speed (Wood, 2011).

The expression for power is defined as:

$$P = \frac{d(\text{KE})}{dt} = \frac{1}{2} \rho A U_o^3$$

2.14

In practice, the actual power yielded by a turbine is never greater than the one suggested by equation 2.14. It is not possible to extract all the kinetic energy from the wind; since this would mean that the wind flow is being decelerated to rest (Wood, 2011). There's a limit that wind turbines have in terms of output power, this is known as the Betz-Joukowski limit and it is independent of the turbine size. This limit sets the maximum power coefficient (C_p) at approximately 0.593.

2.3.1 Urban wind turbines

Wind turbines for the built environment are installed on the building rooftops, side-mounted to a building, integrated into the building design, or even ground mounted near buildings. They are usually designed to operate within a certain range of wind speeds, in response to the complicated aerodynamic and atmospheric wind fields. Their size and capacity are much smaller than turbines in wind farms, which is why they are usually named small scale wind turbines.

Modern small scale wind turbines vary in size and design, and according to IEC 61400-2, they have a rotor swept area less than 200 m², and a nominal power up to 20 kW (Cace et al., 2007; Tummala et al., 2016; Wood, 2011). They are generally classified into two main categories: the horizontal axis wind turbine (HAWT) and the vertical axis wind turbine (VAWT). Because of the constant exposure to winds, snow, rain, sun or salty air, modern wind turbines should be made of durable and corrosion-resistant materials and have an expectancy life of at least 20 years (Ayhan & Sağlam, 2012; Natural Resources Canada, 2003; Tummala et al., 2016)

This section gives some general information about the most used small wind turbines in the built environment. For a more complete research about small wind turbines technology, analysis and application with emphasis on HAWT systems, refer to Wood, (2011), or for VAWT systems with comparison between both Eriksson, Bernhoff, & Leijon, (2008) or Paraschivoiu, (2002). In addition, the International Energy Agency (IEA) Wind Task 27 (IEA-Wind, 2016) provides recommended practices with test results based on the IEC standards, which address the resource assessment relevant for urban areas and the special testing and design standards needed for SWTs in turbulent urban sites (IEA-Wind, 2011).

2.3.2 Horizontal axis wind turbine (HAWT)

HAWTs are the most familiar turbines in the wind industry. In order to produce power, the rotor needs to be oriented perpendicular to the wind direction by a tail or a yaw system. Small HAWTs can be installed on a tower, which does not require a large area, and generally they have a relatively high power coefficient (Sathyajith, 2006; Tummala et al., 2016). An example of a HAWT is presented in Figure 5.

2.3.3 Vertical axis wind turbine (VAWT)

The principal characteristic of VAWTs is that blades rotate about an axis perpendicular to the ground. Also, the generating equipment can be located at ground level, which makes it easier for maintenance purposes. This type of turbine tends to be used in the built environment because it can receive wind from any direction, thus avoiding more complicated automatic yawing mechanisms, which involve control

systems and drive mechanisms. There are two basic categories of VAWTs: Savonius and Darrieus turbines:

The Savonius wind turbine, shown in Figure 6, is a drag based wind turbine that can produce energy at low wind speeds (1 m/s), and the high solidity of its rotor involves a high starting torque (Ayhan & Sađlam, 2012; Sathyajith, 2006). This turbine has a relatively simple manufacturing process, making it cheaper than a HAWT.

The Darrieus wind turbine is a lift and drag driven VAWT. Basically it consists of two or more airfoil-shaped blades linked to a vertical rotating shaft (Ayhan & Sađlam, 2012). Its rotor is capable of working at high tip speed ratios, making this turbine attractive for the wind industry (Sathyajith, 2006). However, its curved or twisted blades are complicated to manufacture and to transport, and this may cause high production costs (Eriksson, Bernhoff, & Leijon, 2008). An example of a Darrieus turbine is presented in Figure 7.



Figure 5 Three bladed horizontal axis wind turbine (Ayhan & Sađlam, 2012).

2.3.4 HAWT vs VAWT

When comparing HAWT and VAWT, the horizontal system is more mature and proven product in the wind industry, and generally it produces well in rural settings or open farms where the wind flow can be relatively steady and unidirectional. However in the built environment and particularly on rooftops with

high turbulence intensity, VAWT often outperforms HAWT because of its lower sensitivity to changes in the wind direction and its capacity to produce electricity even in complex and variable wind conditions. Furthermore, with the addition of a diffuser on the design of a VAWT, it may be possible to take more advantage of high wind velocities created by accelerated flow at building's rooftops, and so increasing the power production (Krishnan & Paraschivoiu, 2015).



Figure 6 Savonius wind turbine (Ayhan & Sağlam, 2012).

Other drawbacks of HAWT are the high tip noise, which can affect urban residents, and their low generating capacity from wind speeds less than 6 m/s (Islam, Mekhilef, & Saidur, 2013). VAWTs produce less noise, especially the drag vertical system which is quite silent, and can generate power in winds as low as 1 m/s (Islam et al., 2013).

However, despite all these advantages for urban settings, there are still several researchers (Cace et al., 2007; Pagnini, Burlando, & Repetto, 2015) who have found that for low turbulence conditions, HAWTs can be more efficient than VAWTs in the urban environment. VAWTs have poor starting performance and some, like the Darrieus model need energy before starting to turn, contrary to HAWTs. In addition, they are usually more expensive because they require larger generators and brakes for the same rated power. A visual comparison between the two types of turbines is presented in Figure 8.



Figure 7 Darrieus wind turbine (Paraschivoiu, 2002).

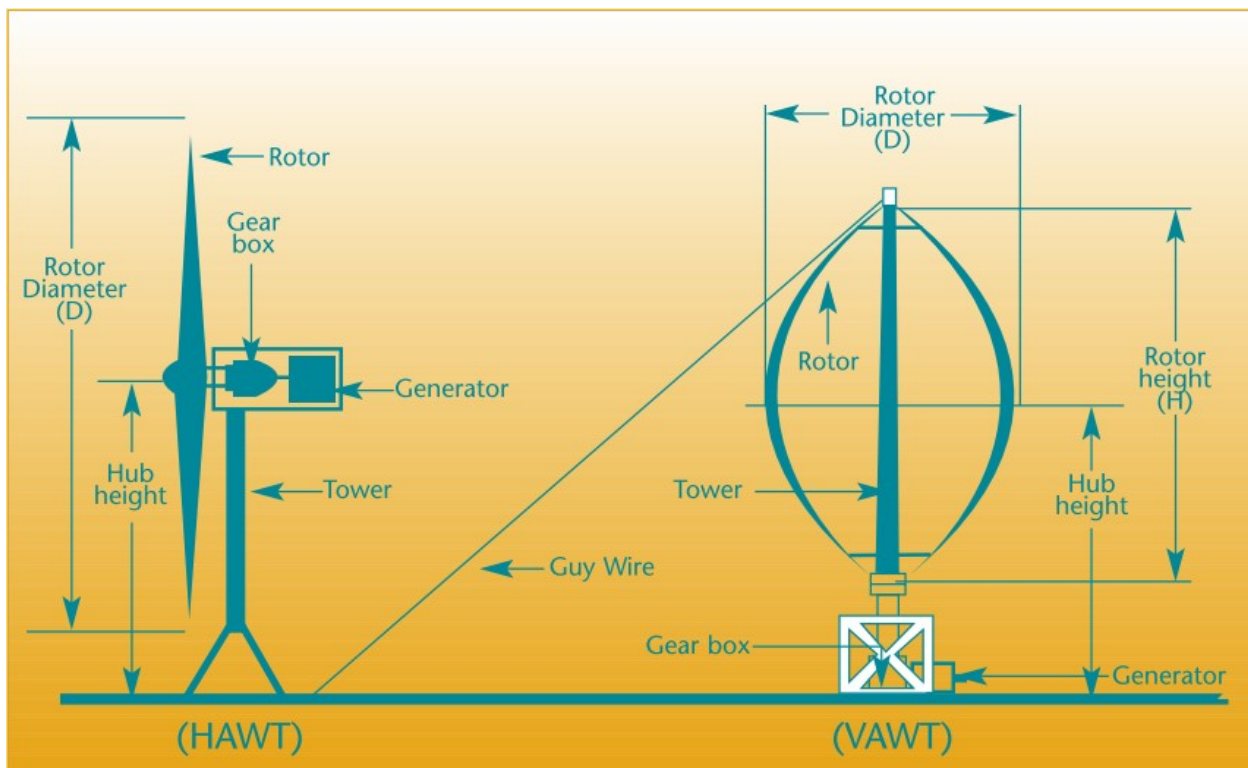


Figure 8 Characteristics HAWT and VAWT (Natural Resources Canada, 2003).

As it has been pointed out in the previous section, current wind turbines are not specifically designed for the urban environment. They are adaptations of wind turbines that are usually deployed in rural settlements. Adapting these turbines to the complex urban wind environment is in fact a major challenge;

not only in terms of performance but additional building related requirements like noise restrictions and matching with the structural and esthetic integrity of the building (Ayhan & Sağlam, 2012).

With this fact, some researchers (Krishnan & Paraschivoiu, 2015; Larin, Paraschivoiu, & Aygun, 2016) have studied ways to improve the efficiency of innovative urban wind turbines, that take advantage of the accelerated flow developed at the edge of the building. This concentration effect also has been discussed by L. Lu & Ip (2009), which by conducting computational simulations, found that at high rise buildings, the wind flow over the roof increased its velocity by 2 compared to ground level and by 1.5 compared to the wind speed at the same height in open area. However, there is no specification of how thick this concentration area is, and if it is actually viable to set turbines near this area. Their results showing an increase in the wind speed on top of the buildings can be seen in Figure 9.

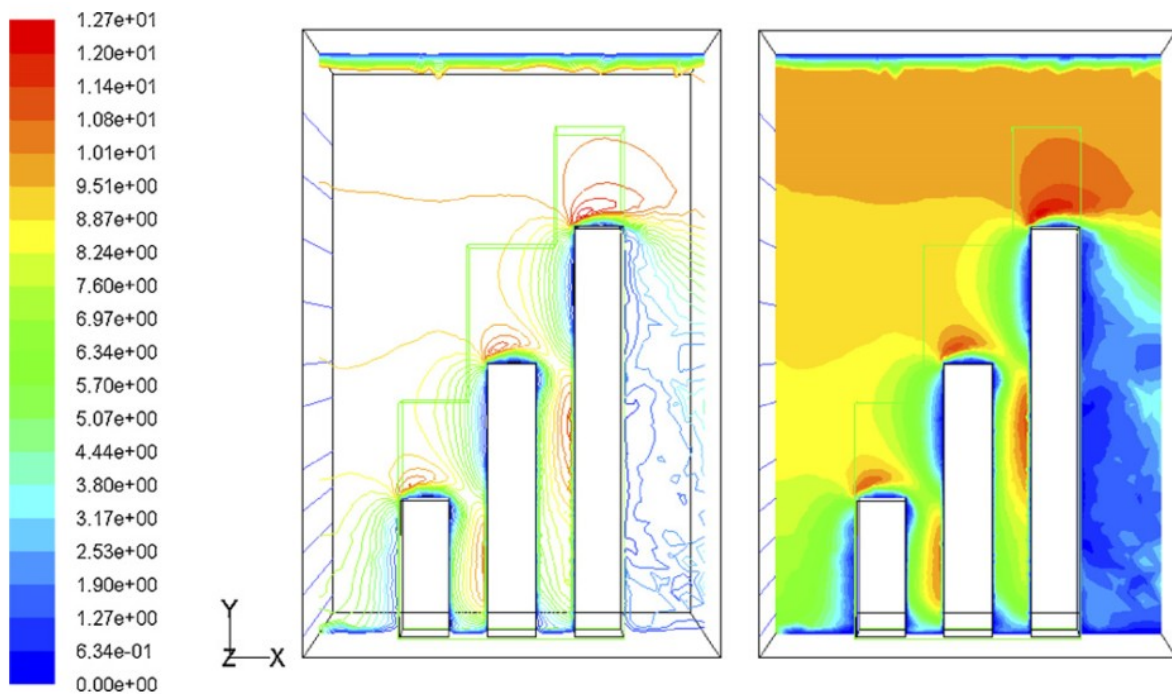


Figure 9 Contours of velocity magnitude (L. Lu & Ip, 2009).

Abohela et al. (2013) also studied the wind flow around buildings and the concentrations effect created by rooftops. They concluded that for all investigated types of roofs, there is an acceleration of wind; and that a roof mounted turbine may produce 56% more energy than an open field wind turbine.

Another study in the concentration effect of buildings and wind turbines, found that because of the concentration effect around buildings, there is a higher energy yield if turbines are installed on buildings compared to open ground. They also found that the Darrieus wind turbine would be preferable for the

urban environment, especially in the skewed flow above the roof of sharp edges of the buildings (Mertens, 2006).

In the Larin, Paraschivoiu, & Aygun, (2016) study, the positioning of the wind turbine in the rooftop came from the hypothesis that the acceleration of the flow at the edge would increase the performance. They found that when the turbine was placed near the edge, there was a noticeable acceleration between the turbine and the corner.

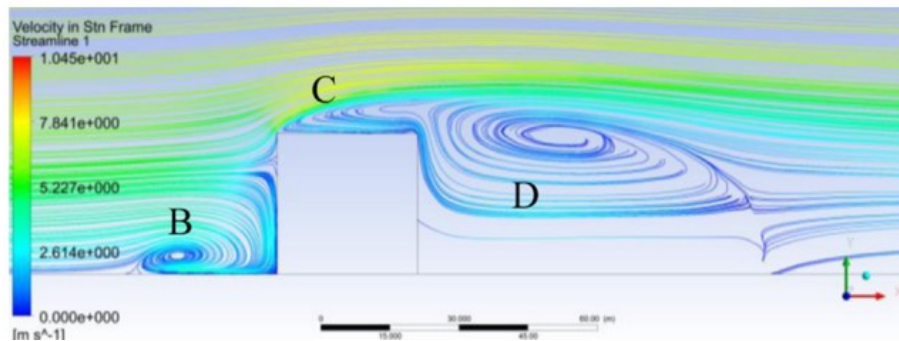


Figure 10 Side view of streamlines around building (Larin et al., 2016).

Figure 10 shows the accelerated zone “C” at the edge of the building where the wind turbine was studied (Krishnan & Paraschivoiu, 2015; Larin et al., 2016).

Because of the need of designing wind turbines for the urban environment that may take advantage of the concentration effects, one of the objectives developed in this thesis, is the experimental study of the wind flow at the edge of a high rise building. The novelty of this study comes from the fact that most of the studies are based on computational simulation (CFD) or wind tunnel testing (Abohela, Hamza, & Dudek, 2013; Emeis, 2013; L. Lu & Ip, 2009; Mertens, 2006). Many simulations have been done to study this wind pattern, but as it was stated by (Simões & Estanqueiro, 2016) there is a lack of wind measurement data that indeed may improve the understanding of the concentration and acceleration effect of the wind around the urban environment and how small wind turbines can be redesigned to be more competitive and have a real place in urban power harvesting.

2.3.5 Economics of urban wind turbines

According to IRENA, (2012), from the total global wind power market in 2010, the small wind turbines share was estimated to be around 0.14% and expected to grow to 0.48% by 2020. Gsänger & Pitteloud, (2015), presented a similar forecast for 2020, showing a growth rate of 20% from 2015 to 2020. This means that the small wind turbine sector should reach a global installed capacity of 2 GW by 2020, so the market is expected grow steadily through the years to come.

The deployment of small wind turbines have shown a fast expansion as the technology is finally appearing to be becoming more accessible. The development of small wind turbine technology has copied the large turbines, with a variety of sizes and style, although horizontal axis wind turbines dominate the market (IRENA, 2012).

In 2007 Cace et al., (2007) noted that the capital investment of a small scale wind turbine was between 3,280 and 12,400\$/kW. Large scale wind turbine prices were around 1,360\$/kW for on-shore and 2,725\$/kW for off-shore facilities (Cace et al., 2007). These numbers has changed during the years, but the capital cost of the energy produced by a small wind turbines remains higher than large scale wind turbines (IRENA, 2012).

The cost of small wind turbines varies depending on the competitiveness of the market and factors affecting installation. However, costs for a well sited wind turbine tend to range between 3,000 and 6,000\$/kW; and the average installed price of a small wind turbine system in the United States is 4,400\$/kW and 5,430\$/kW in Canada (IRENA, 2012). It is notable how costs have change since 2007, costs are significantly lower in China, ranging between 1,500 and 3,000\$/kW.

Comparing more recent capital costs of small wind turbines with onshore large scale, it is noticeable how the cost of small scale still higher since the capital cost for onshore turbines ranged between 1,300\$/kW and 1,384\$/kW in 2010 (IRENA, 2012). The capital cost of offshore wind power is higher than onshore wind energy. This higher cost is due to the large investment needed in offshore projects in terms of laying submarine cables, constructing expensive foundations at sea, transporting materials and turbines to the wind farm, and installing equipment. Offshore turbines are also more expensive, they need to be designed with additional protection against corrosion and the harsh marine environment to help reduce maintenance costs, which are also higher (IRENA, 2012). Capital costs however, present only half of the costs involved in wind projects. The yield capacity factor is much higher for large scale projects and this presents an advantage against small scale.

The difference in cost between small scale and large scale turbines comes from the fact that large and small scale wind turbines have different levels of sophistication that affect their technology, technology and yield capacity. Another point is the economy of scale, which is applicable to renewable energies. The concept of economy of scale appears in areas where the average cost declines as the quantity of output increases. In wind energy there two aspects, the first one is that wind turbines are getting bigger and bigger in term of size and capacity. The second aspect is the creation of wind farms, where a group of wind turbines are deployed all together under a common ownership (Loomis, 2011). A diagram showing the concept of the economy of scale is shown in Figure 11.

It is possible to compare the economy of scale of a small wind turbine with a large turbine with an example. A small wind turbine rated with a 10kW capacity, can be installed on a 30m pole and has a relatively small swept area compared to a large scale wind turbine. As mentioned before, the amount of energy that a turbine is able to extract from the wind depends on the area, so this is a key factor in the comparison. A large scale wind turbine, rated with a 1.5MW capacity, has a larger swept area and it is commonly installed at 80 meters over the ground. The swept area of the second turbine is much larger than the small scale, therefore it can harvest much more of the energy that is contained within the wind. There is a second factor that affects the economy of scale, and it is related to the height of the turbines. Wind speed increases with height, so in this case the large scale wind turbine would be in a higher wind speed zone, and the energy output is proportional to the cubic of the wind speed. In other words the higher and larger the swept area is, more power can be produced by a single turbine, increasing the output power and therefore reducing costs compared to smaller turbines. A similar analysis can be made with wind farms. Having a group of turbines together attached into a single substation and tied to the transmission grid creates great economies of scale not only in the area of construction but also in operations and maintenance (Loomis, 2011).

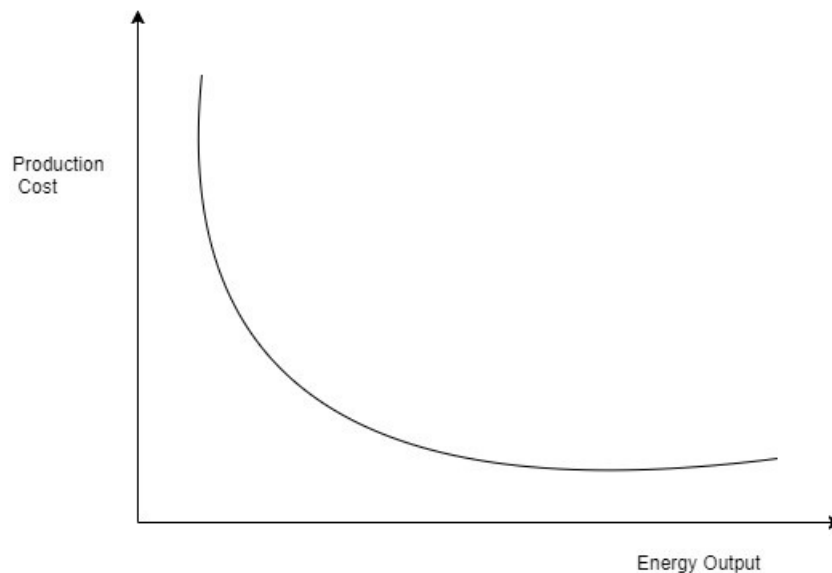


Figure 11 The economy of scale diagram.

To conclude, the fact that the capital costs of small scale turbines still higher shouldn't be discouraging because urban wind turbines are in constant development, getting more efficient and how it happened before with PV technologies, prices has been dropping for urban wind turbines (Cace et al., 2007).

2.4 Wind resource assessment

As mentioned before, wind is a variable resource. There are periods with high wind speeds, calm periods that last for days, wind gusts that last for seconds and irregular shapes on the terrain that affect the wind field in many ways. In conclusion, assessing the wind resource is not an easy task.

However, every wind power project needs a wind resource assessment, to conclude if the location is suitable for energy harvesting. There are some basic steps that can be followed when conducting a wind resource assessment. The first step is to consult the desired location in a wind map, get the annual mean wind speed and extrapolate it to the desired height. If the annual mean wind speed is higher than 4m/s, a more exhaustive assessment should be done. A basic overview of a wind resource assessment is presented in Figure 12.

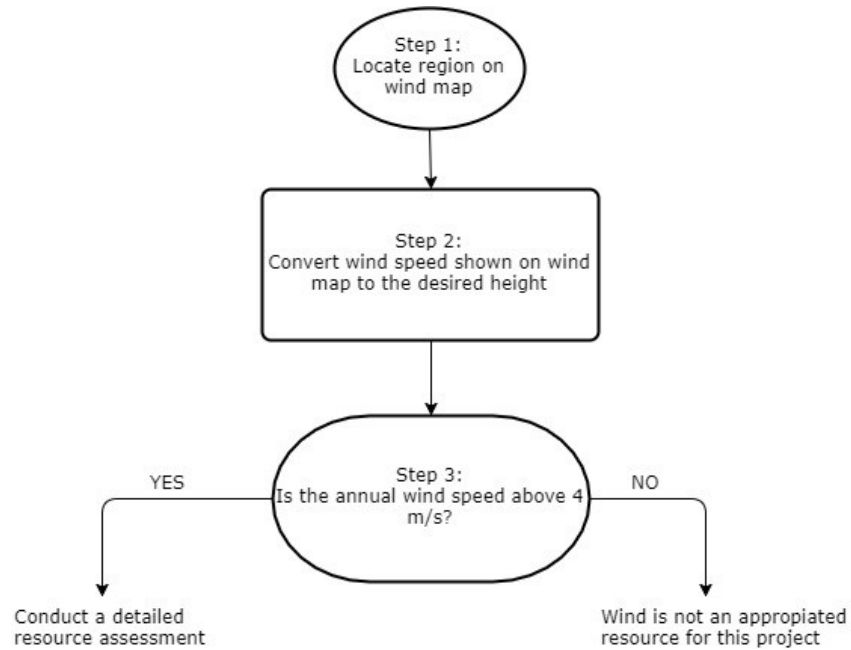


Figure 12 Basic approach for wind resource assessment (Wind Empowerment, 2017).

When it comes to the urban environment, conducting a thorough wind assessment is the most challenging and critical stage of the project (Fields et al., 2016). In addition, the National Renewable Energy Laboratory (NREL) recommends taking in situ measurements as the best method for conducting a wind resource assessment, and Emeis, (2013) agrees that a realistic understanding of the flow field above buildings and within street canyons is essential for the deployment of urban turbines in built-up areas. However, this approach is clearly more expensive than predicting or simulating wind flows around the built environment.

As we have seen, analyzing the wind velocity is a key aspect in every wind assessment. The behavior of the wind at a given site can be specified as a probability distribution function (pdf). These probabilities range from zero to one, with zero meaning no chance of occurring and one, certain to occur. The probability distributions can be divided as the probability density function $p(U)$, or the cumulative probability $C(U)$. Where $p(U)$ measures the occurrence of a particular wind speed, and $C(U)$ gives the probability that the wind speed is less than U ; they are related by equation 2.15 (Caretto, 2010; Wood, 2011).

$$\frac{dC}{dU} = p \quad 2.15$$

There are two commonly used probability distribution functions for wind energy applications; these are Weibull and Rayleigh distribution. Weibull probability distribution is described by the following equation:

$$p(U) = \left(\frac{\beta}{c}\right) \left(\frac{U}{c}\right)^{\beta-1} \exp\left[-\left(\frac{U}{c}\right)^\beta\right] \quad 2.16$$

And the cumulative distribution is given by:

$$C(U) = 1 - \exp\left[-\left(\frac{U}{c}\right)^\beta\right] \quad 2.17$$

Where U is wind speed, β is the shape factor, which is dimensionless and describes the shape of the distribution; and c is the scale factor in m/s, proportional to the mean wind speed of the whole time series.

The Rayleigh distribution is a simplified version of Weibull used for wind assessment and described in IEC-61400-2 (IEC, 2013). It assumes a constant shape factor β of 2. This simplification modifies equation 2.16 and 2.17, and they are described as:

$$p(U) = \left(\frac{\pi U}{2\bar{U}^2}\right) \exp\left[-\pi\left(\frac{U}{2\bar{U}}\right)^2\right] \quad 2.18$$

$$C(U) = 1 - \exp\left[-\pi\left(\frac{U}{2\bar{U}}\right)^2\right] \quad 2.19$$

Where \bar{U} is the average of wind speed U .

The probability of the wind is also used to calculate the averaged power output of a wind turbine for a particular site. As shown in equations 2.18 and 2.19, an averaged wind speed is needed. The most typical averaging time used to determine the averaged power production is 10 minutes, this is based on the IEC-61400-12 standard (Measnet, 2009; Wood, 2011). A free summary of the IEC standard procedure is available at Measnet, (2009).

Small wind turbines are more susceptible to wind changes and expected to react faster than large size turbines. For this reason the IEC 61400-12-1 (IEC, 2005a), allows the use of 1 minute averaging time for the calculation of the power performance. However, Pagnini et al. (2015) studied the effect of averaging time in power performance. Based on the IEC 61400-12-1, they determined the power curve of two different wind turbines with 10 minute and 1 minute averaging time, finding that the two curves almost overlapped for wind speeds within the range 0 to 12m/s. Above this range, minor differences appeared in the power curves, which did not affected the overall energy production. Pagnini et al. (2015) concluded that for both turbines, the overall power production is not affected by the averaging time, showing that time averaging is irrelevant when determining the real performance of a wind turbine.

With the probability distribution function and the power curve of the turbines, it is possible to determine the annual energy production (AEP). The standard IEC 61400-12-1 presents a systematic procedure for the calculation of AEP. A summary of this procedure is available from Measnet, (2014). One key step in the determination of AEP is that the averaging time and bin width of the probability distribution needs to coincide with the power curve. If the power curve doesn't coincide with the distribution of the site, a correction of the power curve must be calculated in order to obtain a power curve whose wind speed bin centre match the site specific wind distribution bin centre. This is necessary in order to obtain a value of power for each bin which can be directly multiplied by the number of hours occurring in its respective bin (Measnet, 2014).

As well as wind speed distribution, wind direction frequency and distribution is important. This parameter is analyzed with wind roses, which include the wind direction distribution as well as the most frequent wind speed in that direction.

Numerous studies have been undertaken in urban wind measurements. As mentioned in section 2.2.3, one of the key parameters besides wind speed and direction, when it comes to urban wind power generation, is the turbulence intensity (I). Acceptable values of I depending of wind turbines classes and wind turbulence classification can be found in the standards IEC 61400-1 (IEC, 2005b).

In a wind resource assessment conducted in Singapore, the researchers (Karthikeya et al., 2016) studied the wind pattern in built-up areas, determined the best location and assessed feasibility producing energy from wind in Singapore. In their study, wind data were gathered from five different sites with a combination of wind sensors. Some measurement sites had 3D sonic anemometers as primary sensors combined with cup anemometers that were used as backup. In other locations the researchers deployed a LiDAR system for short term measurements. Wind data were collected for a period of two years (2012-2014) with a frequency of 4Hz. Later on, the raw data were processed in 10 minute averages for the data analysis.

In their statistical analysis, the researchers Karthikeya et al. (2016) calculated a 10 minute Weibull probability function to describe the distribution of wind speeds, a 10 minute average turbulence intensity, wind roses for direction distribution, and also conducted a brief techno-economic analysis. Their results indicated that the southern coast of Singapore presented better wind resources, with January being the month with the highest wind velocities. The maximum power density found was 45W/m^2 ; and the highest turbulence intensity was 0.25 at a wind speed of 15m/s. It is noted that this I is higher than the value recommended by NREL. Karthikeya et al. (2016) also found that the turbulence intensity decreased as the wind speed increased in all of their studied sites, which is expected. The higher potential in the southern location is explained by the coastal geography, since in coastal areas the wind is smoother and wind speeds are higher. They also found that it is possible to get a payback period of less than 20 years and recommend that in order to fully understand the wind structure in the urban environment and choose the best location for energy harvesting, computational simulation (CFD) would be beneficial.

In another study conducted in France (Ramenah & Tanougast, 2016), the researchers evaluated the performance of a micro-wind turbine in an urban environment. To run the assessment, they gathered wind data with a cup anemometer and data from the wind turbine, both installed at 12m above the ground in a meteorological station. The wind data were used to plot wind roses and to determine the wind probability density by using the Weibull probability function. With these results, the power output was calculated and compared with the actual power measurements of the same turbine.

Their results showed that it is possible to accurately determine the annual energy production (AEP) of a wind turbine in the urban environment by using the annual average wind speed (Ramenah & Tanougast, 2016). They draw this conclusion since the difference between the energy output measured directly from the turbine, and the one estimated with the probability density function, was less than 0.5%. Another point to be considered is that before installing any turbine, the actual wind speed and turbulence characteristics must be known at the corresponding height (Ramenah & Tanougast, 2016).

In a similar study, Pagnini et al (2015) conducted in situ experimental analysis of two 20kW wind turbines (HAWT and VAWT) in the coasts of northern Italy. The researchers gathered wind data using a 3D ultrasonic anemometer with a sample rate of 10Hz, and the chosen site was particularly interesting since it presented two different wind regimes, low and high turbulence.

The raw data were processed into a 10 minute mean wind speed, which allowed them to plot wind roses, getting the main direction of the wind coming from the North-West; the Weibull distribution which was used later to calculate the 10 minute mean power produced by each turbine, and 10 minute turbulence intensity.

Pagnini et al. (2015) also determined the Power Spectral density (PSDF) on the wind in two different directions, from the sea and from land. Both spectral results and the turbulence intensity showed that the wind coming from the sea side had lower turbulence than the one coming from inland. This result is expected since the land zone has higher roughness and thermal convection than the sea.

Pagnini et al. (2015) calculated the real power production of the each turbine, showing that overall the HAWT produced more power than the VAWT, however, when the wind blows from land and the turbulence grows, the VAWT behave more efficient than HAWT and produced more power. The researchers also determined the measured power curve for each turbine and compared it to the curve supplied by the manufacturers. In their results it can be noted that the measured power curves are lower than the one provided by the manufacturers for wind speeds over 6m/s. It can also be noted that the two turbines are quite sensitive to wind gusts and turbulent conditions, especially the HAWT which power output was more affected.

Another finding was that the power curve increased inversely proportional to the turbulence intensity (Pagnini et al., 2015); this is important since picking sites with low turbulence intensity can be better for turbine performance. To get a better idea of the effect of turbulence in the power curve, Pagnini et al. (2015) determined equivalent power curves with two different approaches, accounting for the turbulence intensity. The results showed again high discrepancies with the manufacturers' curves for velocities higher than 6m/s, leading to the conclusion that ambient turbulence is not the only factor responsible for turbine performance. The turbine control systems or technical issues may have a bigger impact on the low actual return. These results were in agreement with other studies where the low efficiency of SWT in complex wind conditions was not only attributed to the ambient turbulence but also to the turbine characteristics (Albers, Jakobi, Rohden, & Stoltenjohannes, 2007; Lubitz, 2014).

Bai et al. (2016) reported that the power curve calculated with empirical wind data and direct power output under real meteorological conditions had a large variability. By studying four influential factors (wind azimuth, solar radiation, wind elevation and air density), they developed a stochastic power curve with reduced variability. The methodology described in their work can be used to create stochastic power curves that may help to estimate more accurate power forecasting under real meteorological conditions.

In an assessment of the sea breeze energy potential in Barcelona, Spain, Mazon et al. (2015) processed and computed wind speed distributions at 10m high for a whole year of wind data. Weibull probability density functions were used to assess the performance of two off grid small wind turbines. Their Weibull results showed scale factors ranging from 3.01 to 4.23m/s, with 60% and 40% probabilities of wind speeds higher than 3m/s. In terms of the main wind direction, during the year, 45% of the time the wind direction ranged from NW to NE and wind directions ranging from SW to SE represented 38%.

Based on manufacturer's power curve and the Weibull pdf, Mazon et al. (2015) determined the potential power output of each turbine, obtaining 132 and 155kWh during the whole year. This result showed that the sea breeze is a potential energy resource, not only applicable for the Mediterranean coast but to other peri-urban coastal areas (Mazon et al., 2015).

As part of the wind assessment, other researchers have been more interested in studying the effect of different wind speed sampling intervals and averaging periods on the turbulence intensity (Tabrizi, Whale, Lyons, & Urmee, 2015b). Concerning the averaging time, choosing 10 minute averages is a common practice for wind resource assessment based on Van der Hoven (1957) and described in the standard IEC 61400-12-1 (2005a). Tabrizi et al. (2015b) calculated the turbulence intensity under slightly unstable and neutral conditions based on 2 year period data, further processed in different ways: first, with 3 sampling rates: 1, 4 and 10 Hz averaged on 10 minute, and second with 3 averaging periods: 10, 5 and 1 minute, sampled at 10 Hz. The effect of sampling periods appeared to be minor: only slight differences are found in the mean turbulence intensity for the wind components, with a maximum relative percentage difference equal to 4.34% observed between 10 and 1 Hz datasets (under slightly unstable conditions).

In contrast, decreasing the averaging periods led to a decrease in the value of the calculated turbulence intensity; Tabrizi et al. (2015b) reported that the vertical component was less affected by the averaging time reduction, showing a relative percentage difference of 11% when using 10 minute compared to 1 minute averaging time. In contrast, the lateral component showed a turbulence intensity reduction from 27% to 20% under neutral conditions, when using 10 minute and 1 minute averaging time. Similar results were found for the longitudinal component, presenting a turbulence intensity reduction from 29% to 22% when using 10 minute compared to 1 minute averaging time. These results showed that the lateral and

longitudinal wind components are more sensitive to averaging time than the vertical component, possibly because of the horizontal scale of the local environment (Tabrizi et al., 2015b).

A decrease of the turbulence intensity was also observed by Elliot & Infield (2014) in their analysis of wind data recorded using a 15kW wind turbine, but with an intensity 22% higher for 10 minute averaging time compared to 1 minute.

Another study performed in Australia by Tabrizi et al. (2015a) questioned to which extent the current IEC 61400-2 (2013) design standard is suitable for urban applications. This problem arises from the fact that the typically used turbulence models are based on observations in the atmospheric surface layer developed over flat, and smooth terrain and do not offer any modifications for complex terrain like urban settlements (Tabrizi, Whale, Lyons, & Urmee, 2015a).

This study deployed a 3D ultrasonic anemometer on the rooftop of a warehouse to measure the three components of the turbulence power spectral density. Then, the measurements were compared with power spectral densities calculated with Kaimal and Von Karman models to assess how well these models predicted turbulence spectra in urban settlements. Wind data at a rate of 10Hz were gathered for almost a year, and analyzed in groups of 10 days with 10 minute averaging times. The results showed that the longitudinal and lateral components of the spectra of the measured data were underestimated by both models on frequencies larger than 0.1Hz and 0.2Hz respectively. In terms of the vertical component, the values obtained by the Von Karman model were inaccurate; while the Kaimal model underestimated the measured data close to the roof at frequencies larger than 0.5Hz.

Overall, the Kaimal spectra predicted the trends of wind velocity better than the Von Karman model. After conducting a sensitivity analysis with respect to the length scale, the researchers found that the prediction of the spectra could be improved by choosing smaller length scales in the current models. This is consistent with the fact that in the urban environment smaller eddies are formed because of the obstacles, having an effect on the atmospheric turbulence (Tabrizi et al., 2015a). These results may have an impact at the moment of assessing a site for SWT's deployment, since if the modeled turbulence intensity is not accurate it can lead to wrong decisions in specifying SWT's optimum location. As previously mentioned, high turbulence intensity affect the performance of the turbine by working under the manufacturer power curve, suffering higher loads on the structure and adding additional maintenance costs.

3. Methodology

This section explains the steps followed to install the anemometers and collect the wind data. It also explains how the data were processed in order to study the wind field at the Donadeo Innovation Centre for Engineering (DICE) building.

3.1 Location

Data were collected at the new engineering building at the University of Alberta. The DICE building is located in the North Campus, at the coordinates: 53°31'41.7"N - 113°31'46.9"W (Google, 2017). Its dimensions are 62.9m tall, 99.5m long and 64.3m wide; making it the tallest building in North Campus.

This building is ideal to conduct our wind field study at the edge of the rooftop; specially the North-West side, which faces the river valley, William Hawrelak Park and a small neighborhood with no major obstacles. On the other hand, the East and South side faces other campus buildings; having a higher roughness length on this side we would expect the wind field from this direction to be more disturbed than the one coming from North-West.

The anemometers were installed in the North-West face of the building. A satellite view of the location of the building, taken from Google My Maps (Google, 2017), is shown in Figure 13. In this figure, the blue pointer identifies the DICE building, and by analyzing the figure we see the geographic limits described in the previous paragraph. A detailed view of DICE building showing the location of the anemometers is presented in Figure 14.

3.2 Equipment

Four anemometers were used to gather the wind data: one 3D ultrasonic R. M. Young USA 81000 wind anemometer and three R. M. Young USA 09101 wind monitors.

The ultrasonic anemometer operates by measuring the time that takes for a pulse of ultrasonic sound to travel between two transducers. The time depends on the distance between the transducers, the speed of sound and the air speed along the axis of the transducers. In order to determine the velocity of the air between the transducers, each transducer alternates as transmitter and receiver so that the ultrasonic pulses travel in both directions between them. A microprocessor determines the time that the pulse takes to travel from one transducer to the opposite one, and based on the Doppler shift it calculates the wind velocity (Centre for Atmospheric Science The University of Manchester, 2017).

Ultrasonic anemometers are highly sensitive and their measurements may be affected by small distortions past the transducers. However, they are widely used by atmospheric centers to make routine and detailed

turbulence measurements. They provide fast and accurate measurements of three dimensional wind speeds. These anemometers can operate in most conditions experienced in the atmosphere, but heavy rain and icing conditions may affect the data quality.

Ultrasonic anemometers are the first option when it comes to studying turbulence in the urban environment, they have a higher response rate and resolution in term of sensing wind speed and direction; making them better than mechanical anemometers. Another advantage of using an ultrasonic anemometer is the possibility of determining the size of the eddies that pass through the sensing volume zone. By considering a short period of time and following Taylor’s hypothesis, the size of the eddies may be approximated. This hypothesis says that it can be assume that the turbulent eddies are “frozen” as they move through the sensor and thus the local change within each eddy is negligible. For these reasons and advantages mentioned before, the ultrasonic anemometer was set as the main sensor, reporting the three components of the wind velocity (u , v and w), temperature and speed of sound.

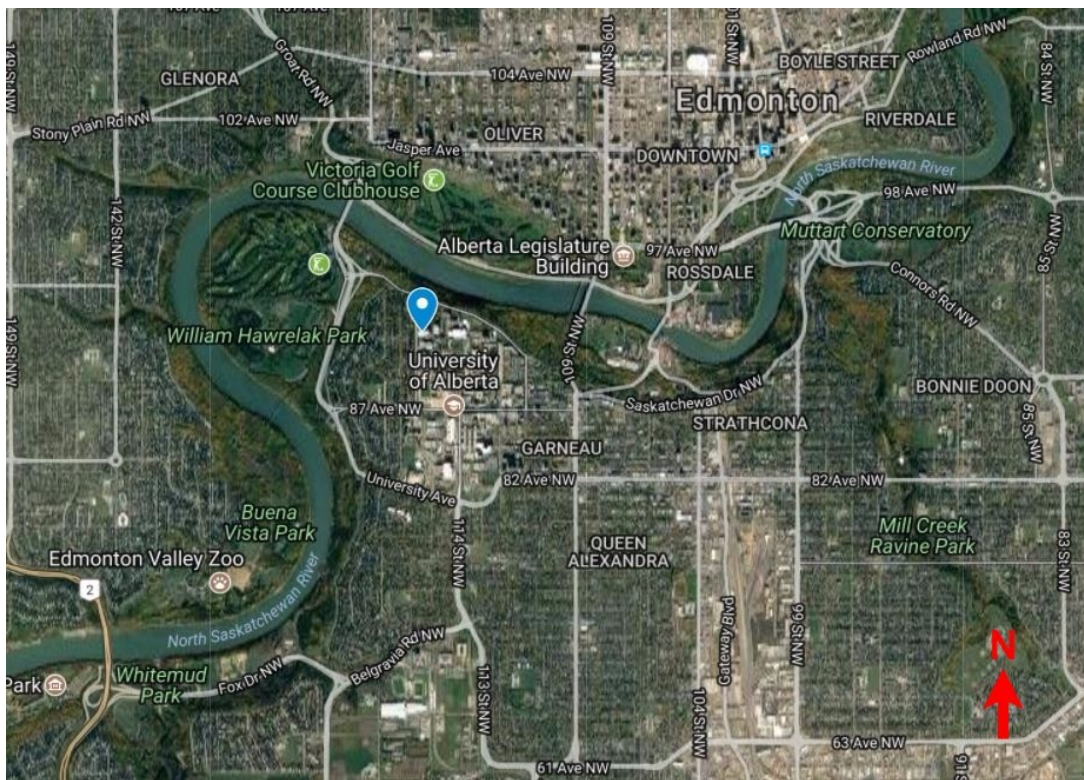


Figure 13 DICE building location (Google, 2017).



Figure 14 DICE building detailed view (Google, 2017).

The wind monitor, are mechanical anemometers that measure wind speed and direction. These anemometers are more accurate than the typical cup anemometers, and the 09101 model has the advantage of having serial output. However, as it will be explained, the wind monitors were set to voltage output for logging purposes.

The wind speed sensor of the wind monitor consists in a propeller that turns a multipole magnet. This rotation induces a variable frequency signal in a stationary coil. The raw transducer signals are processed by onboard electronics; however a conventional calibrated voltage output can be selected and processed by an external board. In our case we decided to use an external board to process the voltage output. With the use of an Arduino board the voltage output can be processed using the following conversion for wind speed, 0 – 5 VDC for 0 -100 m/s. And for wind direction, 0 – 5 VDC for 0 – 540 degrees.

The use of the voltage output allowed us to match the output rate of the wind monitors to the ultrasonic anemometer, by programming the Arduino board to read and process the information of all the sensors at a rate of 10 Hz. The board reads the voltage, performs the conversion while at the same time is reading the digital output of the ultrasonic anemometer and saving all the information in a single line of data that was stored continuously in the SD card.

Both type of anemometers are shown in Figure 15, where (a) shows the 3D ultrasonic anemometer, and (b) the wind monitor.

Table 2 presents a brief comparison between both sensors, this table presents the maximum sampling rate for serial output data. It can be seen how the ultrasonic has a higher resolution and a lower threshold. Datasheets and manuals of the anemometers with more technical information are attached in appendix A.



(a) 3D ultrasonic anemometer



(b) Mechanical anemometer (wind monitor)

Figure 15 Anemometers

Figure 15 shows one of the main differences between the two anemometers; the sonic anemometer (a) does not have moving parts. The image also shows the six transducers used to send the ultrasonic pulses.

Table 2 Anemometers specifications comparison

Specification	3D ultrasonic anemometer	Wind monitor (Analog setting)
Wind speed range (m/s)	0 to 40	0 to 100
Accuracy (m/s)	± 0.05	± 0.03
Wind direction range (deg)	0 – 359.9	0 - 360
Accuracy (deg)	± 2	± 2
Threshold (m/s)	0.01	1
Output rate (Hz)	4 - 32	1 -10
Weight (kg)	1.7	1
Temperature range (°C)	-50 to 50	-50 to 50

3.3 Data collection

To record the wind data, a data logging system was designed with an Arduino MEGA 2560 board, and a logging shield, which saves the data in an SD card. A datalogger was constructed in order to innovate by developing a low cost system capable of recording data simultaneously from multiple anemometers. This approach helped to reduce equipment cost.

A Campbell Scientific datalogger, able to record data from our four anemometers, cost approximately 4,000CAD. An Arduino MEGA cost 50CAD and the datalogging shield around 20CAD. With added miscellaneous expenses the cost would reach 100CAD. The specifications of the Arduino MEGA are presented in the next Table 3.

Table 3 Arduino MEGA specifications

Input voltage	5- 12 V
Operating voltage	5 V
Power consumption	38 mA
Flash memory	256 KB
SRAM	8 KB
Digital I/O pins	54
Analog I/O pins	16
Clock speed	16 MHz

The design and construction of the datalogging system was done during the summer of 2016. This piece of hardware is fully programmable and the code can be modified to satisfy any need of the measurement campaign.

The board was programmed to read and record the measurements of all of the 4 anemometers at a rate of 10Hz. The recorded data were saved daily in an SD card in a .txt file, named with the format “year, month, date”.

The data were saved in thirteen columns; Table 4 presents how the data were saved in the .txt file.

Table 4 Data logging format

Date	Time	Wind Monitor 1		Wind Monitor 2		Wind monitor 3		U	V	W	Temperature	Speed of Sound
		Wind speed (m/s)	Wind direction (deg)	Wind speed (m/s)	Wind direction (deg)	Wind speed (m/s)	Wind direction (deg)	(m/s)	(m/s)	(m/s)	(°C)	(m/s)

The three wind monitors were set to analog output and thus connected to the analog ports of the Arduino board. This option brings the benefit of being able to program the Arduino board to read their voltage output at a higher sampling rate compared to serial output that it is fixed at 1 Hz. The Arduino reads the voltage of the instruments at a 10 Hz rate, process the proper conversion and saves the data in the SD card. The 3D sonic anemometer was set to serial output with a 10 Hz sampling rate, and it was connected to one of the digital ports of the board. An overview of the data acquisition system is presented in Figure 16.

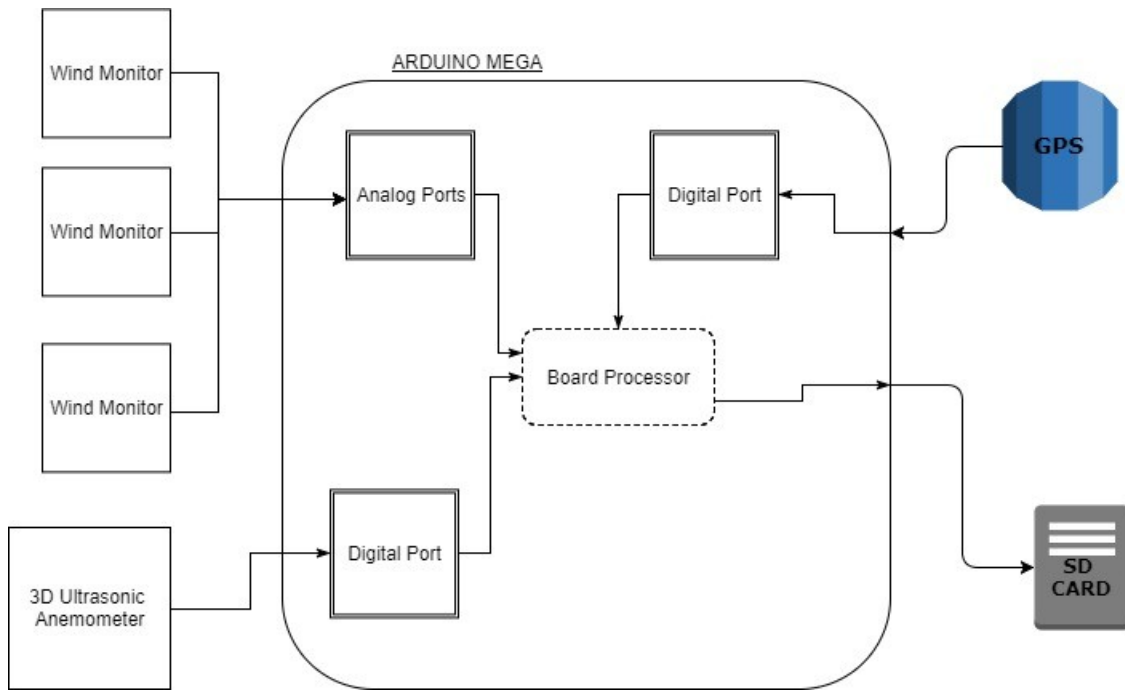


Figure 16 Overview of data acquisition system

Figure 16 shows the GPS that was added to the datalogger with the purpose of recording date and time. This modification works better than the real-time clock (RTC) that is built-in with the logging shield. Additionally, the GPS can be programmed to record location (latitude and longitude), if it is desired.

Figure 17 shows the Arduino board assembled. The GPS, SD card and the wiring system designed to log the data from the four anemometers are visible.

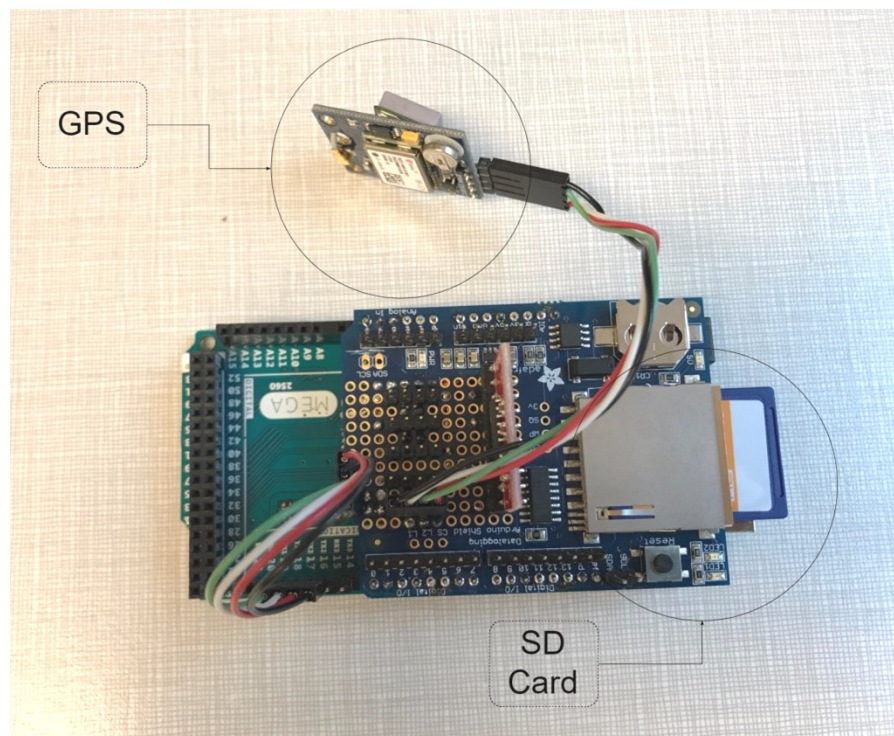


Figure 17 Data logging system (Arduino board)

The data acquisition system was tested for the first time during November 2016 at the Mechanical Engineering building rooftop. After test running the system satisfactorily for a week, it was decided that the logging system was cleared to be installed at DICE rooftop.

3.4 Anemometers set up

The four anemometers were deployed on the DICE building rooftop in the month of January 2017. All the sensors were set at 60 cm from the edge of the building; for safety reasons this was the closest distance to the edge that the anemometers were allowed to be installed.

In terms of height, two of the wind monitors were set at 80 cm over the rooftop and the third wind monitor at 140 cm. The ultrasonic anemometer was set at 96 cm over the rooftop.

As mentioned before, the sensors were set at low heights compared to other wind studies and the standard IEC 61400- Part 2 (Karthikeya et al., 2016; Pagnini et al., 2015). This was done because we are focused on studying the wind field at the edge of the building. With these different heights we compared the results from the sensors, and analyzed how the wind pattern changed along the edge.

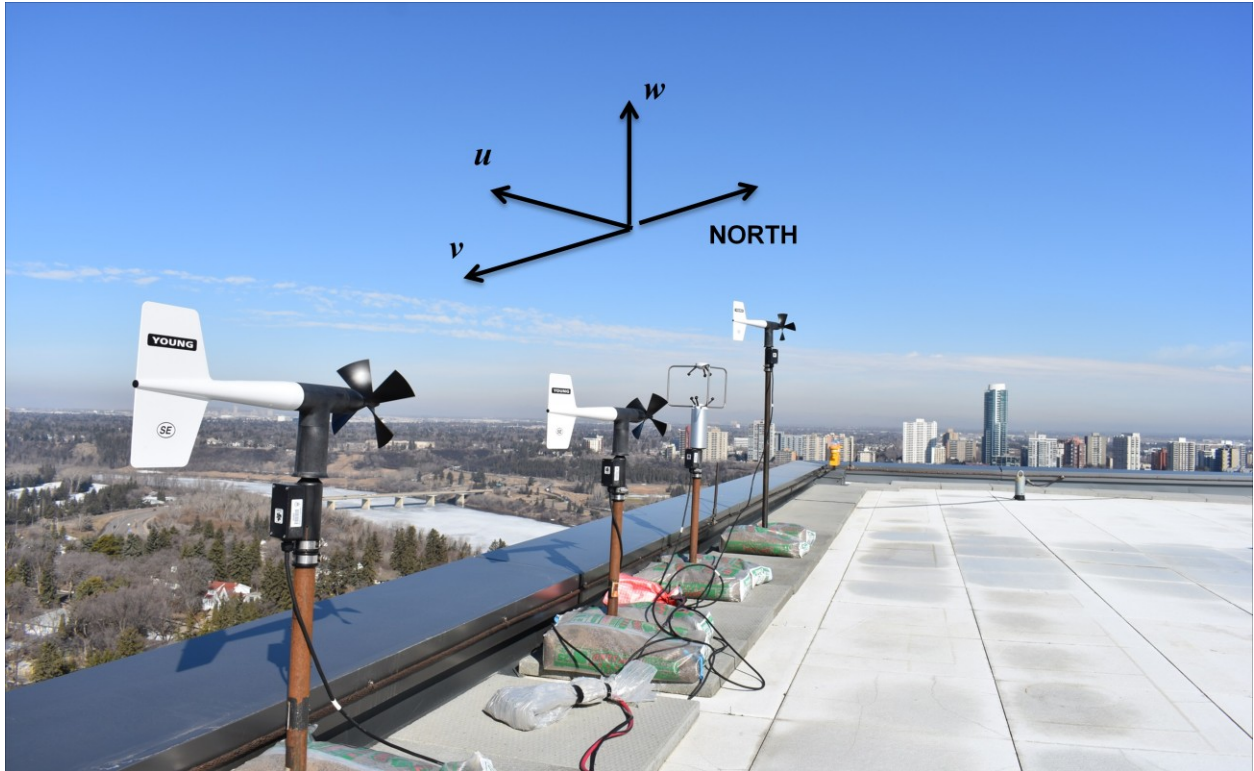


Figure 18 Anemometers set up on DICE rooftop

Figure 18 shows the distribution of the anemometers on top of DICE building. It can be seen the difference in heights and how close the equipment was installed from the edge of the building. The North direction is represented by an arrow pointing up in an angle with the caption “NORTH”. The arrow points up in an angle because the figure is a representation of a 3D environment; it is basically an isometric view of the DICE rooftop. The directions of the u , v , and w components measured by the 3D sonic anemometer are represented by arrows with their respective caption. We have u being positive with direction coming East to West, v positive from North to South, and w positive, vertically going up. This nomenclature is defined by the equipment manual.

The wind monitors were named: Wind Monitor 1, Wind Monitor 2, and Wind Monitor 3; going from left to right. This can be appreciated in Figure 19, which also shows the separation distance between every sensor. Wind Monitor #1 and #2 were separated by 166cm; the Wind Monitor #2 and the 3D ultrasonic anemometer were separated by 135 cm. The 3D sonic anemometer was separated from the Wind Monitor #3 by 130 cm.

All the sensors were installed following the manual instructions for set up. The wind monitors were aligned with the true North, with 0 degrees pointing towards true north. The North side of the ultrasonic anemometer was set to the true North as well.

The true North was set by using an electronic compass. To verify the veracity of the compass, the magnetic declination at the DICE building was determined by using a magnetic declination calculator provided by Natural Resources Canada (Natural Resources Canada, 2017). The calculator presented a magnetic declination of 14°22.02' East, which coincides with the difference between the magnetic North and true North obtained with the electronic compass.



Figure 19 Anemometers set up on DICE rooftop (2)

Figure 20 shows the wiring and how the sensors were plugged to a junction box, where the Arduino board was safely installed. Figure 20 (a) shows how the junction box was protected and insulated during the winter to keep all the electronics working, even at below freezing temperatures (the Arduino MEGA board operates at temperatures between -20 and 40°C).

Figure 20 (b), shows how the inside of the box looks. It can be noticed how the wires from the sensors are plugged into the board and the addition of two light bulbs that provided heat during the winter.

Appendix B includes other pictures showing the DICE building rooftop, equipment and details that help to visualize its location in Edmonton.



(a) Junction box and insulation



(b) Inside of junction box

Figure 20 Arduino board and junction box detail

3.5 Data processing

Data were collected from January 19th to April 20th 2017 at a rate of 10 Hz. However, due to technical issues, data between the end of February and mid-May were not saved into the SD card. Besides these issues, during a week in January, when the relative humidity of the environment was high (over 90%), the ultrasonic anemometer malfunctioned because of the icing of the transducers. The blades of the wind monitor were also iced, compromising the readings from those days. This phenomenon is mentioned by Measnet (2009), where they suggest to discard data collected with air temperatures under 2°C with relative humidity over 80%.

Because of these issues, the data of the month February were selected to be processed and analyzed. 23 days of continuous data at 10 Hz was processed using MATLAB software, which counts with a statistical toolbox, and other functions designed for wind energy applications.

The raw wind speed data of the wind monitors were averaged to 10 minutes in order to determine the wind roses and Rayleigh distributions. The wind monitors output data is wind speed, so we determined the mean wind speed average by averaging the data every 10 minutes using MATLAB averaging function.

The averaging of the direction was done with the function MEANANGLE available for MATLAB. When it comes to averaging angles, the arithmetic approach does not work properly. Because of this the function determines the mean value of the angles based on polar considerations. Then the averaged angles and wind speed were used to determine the wind roses.

The ultrasonic anemometer needs a different approach. Its output is velocity, a vector with three components (u, v, w). We can't compare this data with the data of the wind monitors unless we transform the velocity into wind speed. This was done using equation 3.5, determining the magnitude of the horizontal wind velocity and then calculating the 10 minute average.

The wind direction was determined by using the vectors u and v . Based on trigonometry we determined the angle of the resultant between these two components. These angles in degrees were later averaged every 10 minutes using MEANANGLE function for MATLAB as it was done previously for the wind monitors.

When comparing the data from these two anemometers, we need to be aware of the difference between mean wind speed and mean wind velocity. For the calculation of turbulence intensity and wind distributions we need wind speed, and in the case of determining the wind direction distribution we need the wind velocity, but in the vector format of magnitude and an angle for direction.

Daily and hourly data were studied to determine the windiest day and hour in February 2017. Autocorrelation of one minute interval of the u, v and w components of the wind velocity were computed to study the size of the turbulent elements in that particular day. For this study two hours were chosen, the hour with the highest wind speeds and the hour with the highest turbulence intensity.

The autocorrelation function used for the study, and that is included in MATLAB, is defined as:

$$r_j = \frac{c_j}{c_0} \quad 3.1$$

Where j is the time lag, c_0 is the sample variance of the time series, and c_j is defined as follows:

$$c_j = \frac{1}{n-1} \sum_{t=1}^{n-j} (u_t - \bar{u}) (u_{t+j} - \bar{u}) \quad 3.2$$

Where u_t is a time series $\{u_t : \{1 \leq t \leq n\}$, consisting of n observations of the variable U .

\bar{u} is the mean of the series, j is the lag, and c_j is known as the autocovariance at lag j .

From the autocorrelation, the integral time scale Λ_t was determined by equating the area under the autocorrelation curve to a rectangle of unity height and duration. Λ_t . The integral time scale was mathematically defined previously by equation 2.12.

The integral time scale is the most important time scale in turbulence. And it is a generic specification of the time over which a turbulent fluctuation is correlated with itself. In other words, it can be seen as measurement of the memory of the turbulence (Kundu, Cohen, & Dowling, 2012).

Assuming Taylor's frozen turbulence hypothesis, the spatial dimension Λ_u of the turbulence was calculated by multiplying the integral time scale by one minute mean wind speed.

The wind power density (WPD), defined as the kinetic energy available in the wind per unit of area (W/m^2), is often used to classify locations in terms of their potential to harvest energy, going from class 1 (poor) to class 7 (superb) (Wind Empowerment, 2017). This variable was computed using a modification of equation 2.14:

$$\text{WPD} = \frac{1}{2} \rho U^3 \quad 3.3$$

The averaged air density at DICE building was calculated from measured temperature and pressure readings taken from the TBWS, and using the ideal gas equation.

$$\rho_{avg} = \frac{1 P_{avg}}{R T_{avg}} \quad 3.4$$

Where ρ_{avg} is the air density averaged with units' kg/m^3 . P_{avg} is the uncorrected air pressure averaged for the time step, and with units in Pascals (Pa). T_{avg} is the measured air temperature in Kelvin (K) and averaged for the time step, and R is the gas constant of dry air, 287 J/kg K.

In order to compare the wind measurements of the ultrasonic anemometer with the wind monitors, the magnitude of the horizontal component of the wind velocity was defined for our convenience with the letter V (m/s).

$$V = \sqrt{u^2 + v^2} \quad 3.5$$

Where u is the longitudinal component of wind velocity East to West direction; and v is the lateral component North to South direction.

This magnitude was used at first to determine a general WPD and turbulence intensity of the 23 days of February.

Turbulence intensity of the three components of the wind velocity (u , v and w) was computed with 1 min. and 10 min. averaging time using equations 2.9 and 2.10.

Wind roses from the DICE building were plotted using 23 days of data, and compared to wind roses plotted with data from the TBWS, located at the University of Alberta North Campus.

Histograms and Rayleigh distributions fitting were also plotted for each of the data sets described previously. The probability density function plots were used to determine a more accurate WPD based on the scale factor from the Rayleigh distribution.

The results obtained from the four anemometers were compared to analyze how the positioning affected wind speed and direction; and to determine if there was a concentration effect at the edge of DICE building.

A wind resource assessment of one year (2016) of data with a sampling rate of 1 hour was done with data obtained from the TBWS. This assessment included wind roses, Rayleigh pdf and WPD calculation. Let's note that turbulence intensity was not possible to calculate for the TBWS because the maximum sampling rate available was 1 hour, making it unviable to compute because of the lack of more detailed wind speed data.

4. Results and Discussion

4.1 Daily Mean Wind Behavior

The daily wind speed recorded by the four anemometers installed at the DICE building rooftop for 23 days during the month of February of 2017 are presented in Figure 21. Figures 18 and 19 shows the location of each wind monitor and the ultrasonic anemometer on the DICE building.

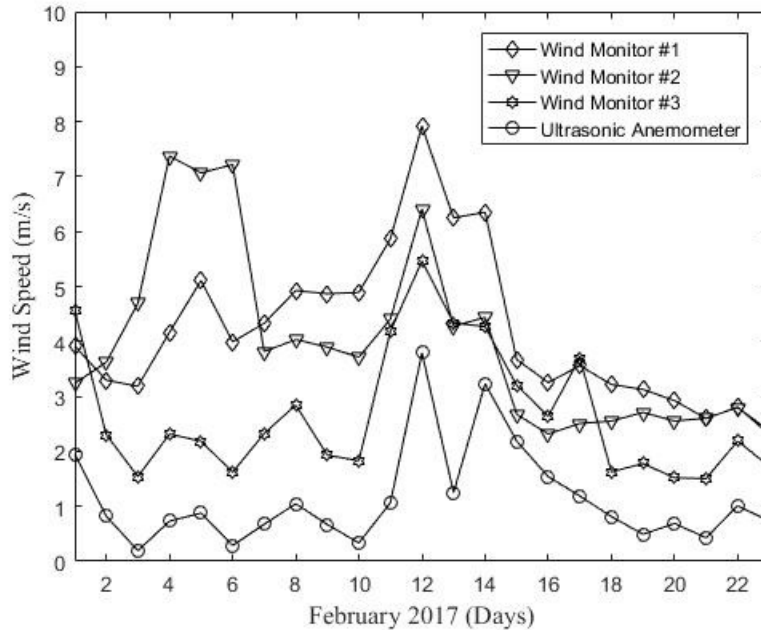


Figure 21 Daily Mean Wind Speed DICE building February 2017.

Figure 21 shows the 12th as the windiest day in February 2016. It also shows the difference in wind speed readings depending on the anemometer. Most of the sensors presented a peak on the 12th. However, the Wind Monitor #2 recorded its highest reading on February 4th.

The Wind Monitor #1 recorded the highest daily wind speed, 8m/s. This wind monitor was located closest to the southern side of the building, and the Wind Monitor #2 which was installed 166 cm beside #1 recorded the second highest daily readings, 7.5m/s.

Wind Monitor #3 and the 3D ultrasonic anemometer also presented different wind speed readings, showing that the wind speed varies depending on the position. Considering that the Wind Monitor #1 and #2 are the closest to the edge of the building in terms of height, it may suggest a tendency of higher wind speeds at closer distance from the edge.

The difference between the readings from Wind Monitor #1 and #2 could depend on the direction of the wind. If the wind flow reached one sensor before the other, the second sensor (located downstream) would be affected by the wake of the first sensor.

In order to compare the daily mean wind speed reading from the DICE building to the TBWS, daily mean wind speed from February 2017 was plotted. This plot is presented in Figure 22.

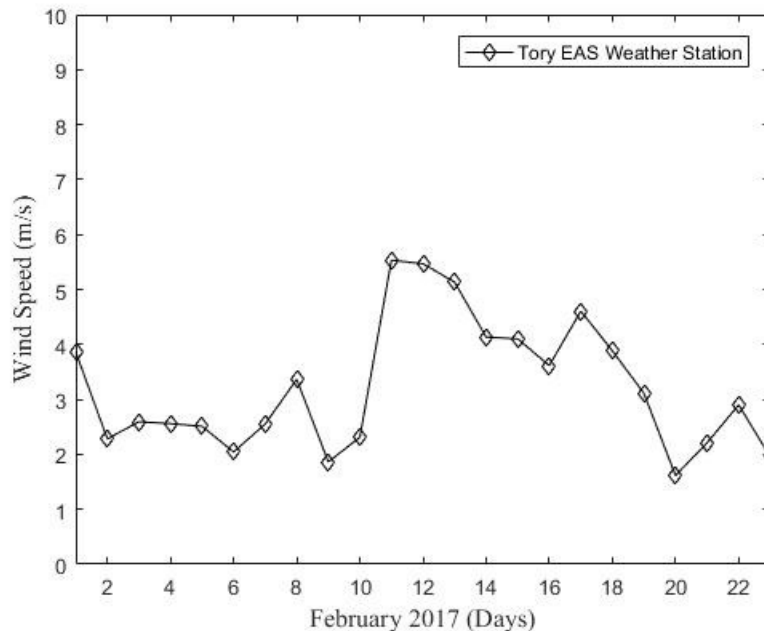


Figure 22 Daily Wind Speed Tory Building February 2017.

There is a similar mean wind speed behavior when comparing the DICE building to the TBWS. However the windiest day according to the TBWS data was the 11th and not the 12th.

Considering that the TBWS measurement system consists in a mechanical wind monitor, it is fair to compare its reading to the wind monitors from the DICE. Wind speeds from the wind monitors are in the same range of magnitude, between 8 and 2 m/s.

It is interesting to notice that the readings from Wind Monitor #1 and #2 are higher than the TBWS, which it is set in the free stream flow. Free stream flow is the upstream air flow that has not been affected by bluff or aerodynamics bodies, in this case a flow of air that is not extremely disturbed by the roughness scale of the location. The wind monitor from TBWS is supposed to be installed out of the recirculation zone of the building, measuring undisturbed wind speed. The wind monitors from the DICE were

installed close to the edge of the building in order to study if this location would present an accelerated flow, producing higher wind speeds.

Comparison between Figure 21 and Figure 22, suggests that there are higher wind speeds closer to the edge of the building. However, a turbulence study of the flow is a key aspect before deciding if this would be an optimal location for wind turbines.

4.2 Hourly Mean Wind Behavior

The windiest day of February was the 12th. Hourly mean wind speed readings are presented in Figure 23.

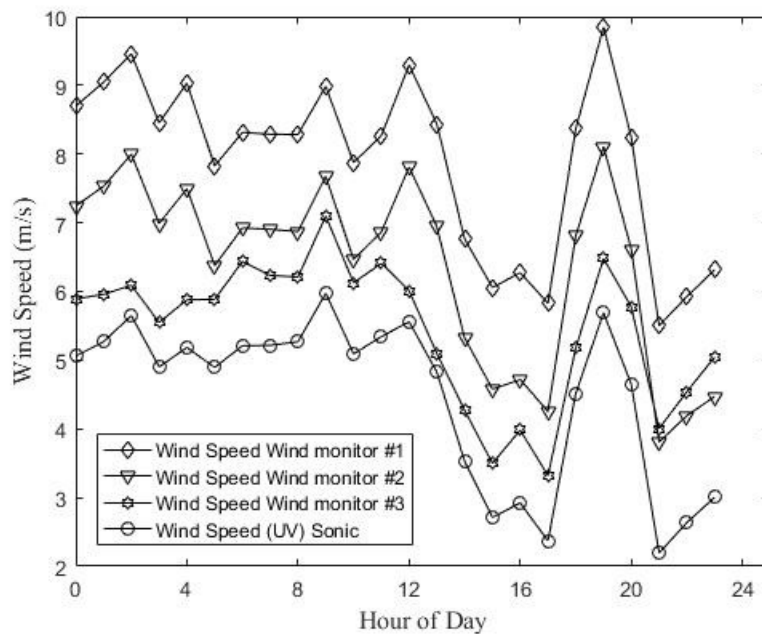


Figure 23 Hourly Wind Speed DICE building on Feb. 12th

Figure 23 shows 7 pm (19hrs.) as the hour with the highest wind speeds (10m/s) during February 12th. All the sensors recorded the same peak on that day and their readings have a similar behavior. The difference in magnitude could be attributed to the difference in the positioning of the sensors. The wind speed readings are influenced by the building, which produces a complex wind field on the rooftop.

The hourly turbulence intensity, based on the magnitude U , determined with equation 3.5 is presented in Figure 24. It shows that the highest hourly averaged turbulence intensity (0.7) was corresponds to February 12th at 4 pm (16hrs.). It can also be seen how the lowest turbulence intensity present at 7 pm (19hrs.) corresponds to the windiest hour of the day suggested in Figure 23.

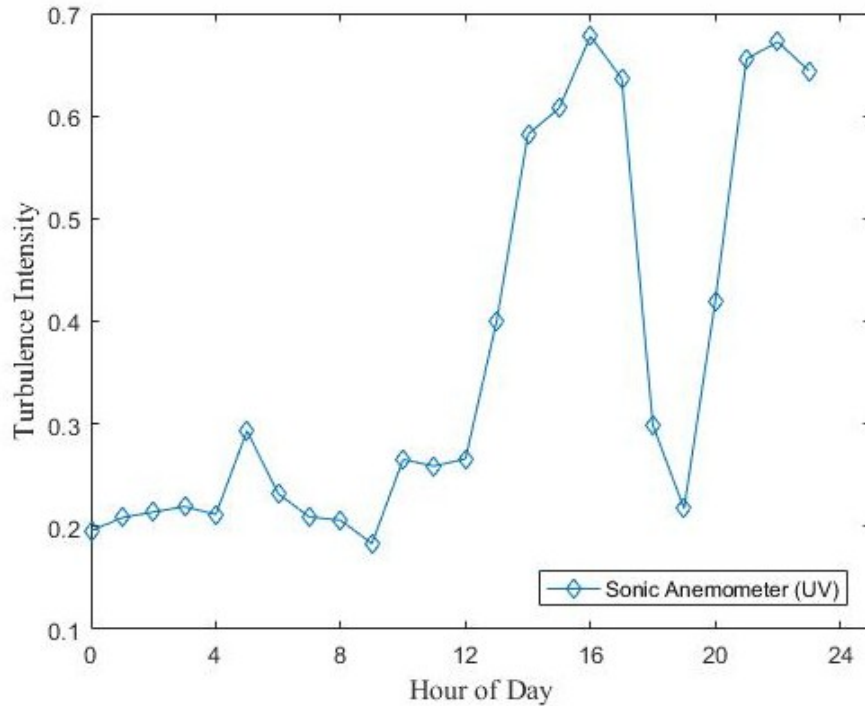


Figure 24 Hourly Averaged Turbulence Intensity, February 12th 2017

This relation between the turbulence intensity and wind speed will be discussed with more details in the next sections. However, Figure 23 and Figure 24 suggest that at lower wind speed there is a higher turbulence intensity and vice versa. Turbulence intensity in terms of wind speed will be presented and the inverse relationship discussed.

The one-minute autocorrelation of the u , v and w components of wind velocity at 4 and 7 pm. are discussed in the turbulence section of the results.

4.3 Wind Power Density

The average air density over the month of February was 1.22 kg/m^3 , with a standard deviation of 0.05 kg/m^3 . The average pressure at EAS weather station was 93.71 kPa , with a standard deviation of 0.97 kPa . The average temperature for the month of February was -5.73°C , with a standard deviation of 9.02°C .

With the averaged air density and the wind speed from the sensors, WPD was plotted for the month of February and for the 12th.

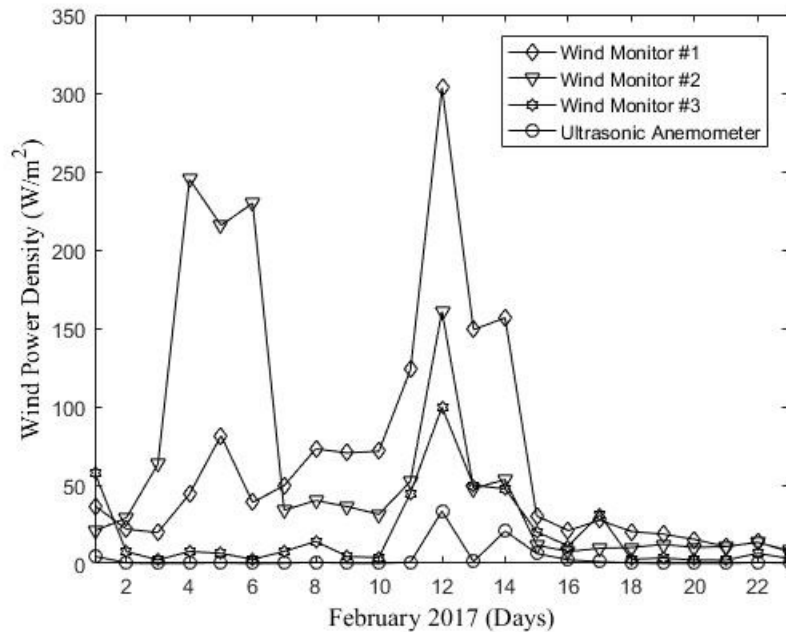


Figure 25 DICE WPD based on daily averaging time, February 2017

Figure 25 shows WPD for the month of February 2017 based on daily mean wind speed. By analyzing the figure, it can be noted that the maximum power density is slightly over 300 W/m^2 . This calculation is based on daily mean wind speed and not on a distribution fit, so the results are overestimating the most probable power density. However, at 50 m high, a 350 W/m^2 corresponds to a wind power class of 3. This power class is considered to be fair. The averaged power density of the month is much lower; with Wind Monitor #1 having 61.08 W/m^2 and Wind Monitor #2, 58.81 W/m^2 .

The fact that there is a peak on February 12th makes sense since, the available power and the power output of a wind turbine is proportional to the cubic of the wind speed.

Figure 26 shows WPD determined from the TBWS data for the month of February 2017. The maximum daily averaged power density is slightly over 100 W/m^2 , being lower than the one determined from Wind Monitor #1 and #2 at the DICE building. However, it is comparable to the power density calculated with the Wind Monitor #3 and the ultrasonic anemometer.

According to the TBWS data, only two days in February were over the 100 W/m^2 , the rest of the days were fluctuating between 0 and 50 W/m^2 . The DICE building data however, show 7 days over the 100 W/m^2 mark and the rest of the days fluctuating between 0 and 60 W/m^2 .

At a 50m hub height, 100 W/m^2 is considered to be the lowest wind power class (1).

Table 5 presents the power density and other parameters extracted from the Canadian Wind Atlas at the DICE building location (Latitude= 53.538, Longitude= -113.550) for annual and winter season (December–February).

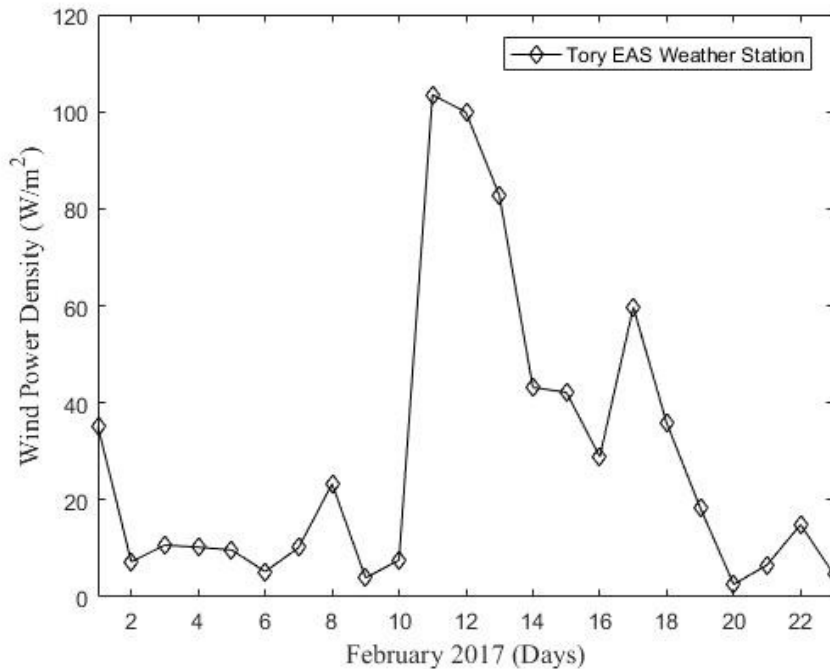


Figure 26 Daily Averaged WPD, Tory Building February 2017.

Comparing the Canadian Wind Atlas values for WPD with the TBWS, they present different values considering that for winter the Atlas shows an average of 145.50 W/m² and the TBWS monthly average over February was 28.13 W/m².

Table 5 Canadian Wind Atlas Parameters 50m Mesoscale

Period	Mean Wind Speed (m/s)	Mean Wind Energy “WPD” (W/m ²)	Weibull shape parameter “k”	Weibull scale parameter “A” (m/s)
Annual	4.70	112.50	1.78	5.28
Winter (DJF)	5.38	145.50	2.04	6.07

Comparing the measured data results with the mesoscale simulations from the Wind Atlas shows a difference in the wind potential. This is expected since the Canadian Wind Atlas is based on numerical simulations with weighted wind velocity data that gives a rough approximation of the wind behavior in a desired location. This is why when conducting a wind resource assessment, a more detailed study including wind measurements is advised to determine a more accurate wind energy potential of the site.

However, the overestimated wind power density of the Wind Atlas should not affect much the decision of producing power on this site, since a 145.50 W/m^2 wind power density at 50 m hub height is still considered to be wind power class 1, the same class obtained with the DICE and the TBWS results.

These results don't suggest any substantial increase in the available power closer to the edge of the building as discussed by Lu & Ip (2009), where they simulated a 70 m tall building and obtained a theoretical improvement of 3 to 4 times in the energy density, compared to open grounds.

In his work, Mertens (2006) discussed that the wind speed on the built environment is certainly low, however in zone regions near the buildings the wind speed can be an appreciable source of energy. This idea could be reflected with the fact that near the edge of the DICE building roof, the wind speed and power density was higher than the TBWS.

However, the work of these researchers (Ayhan & Sağlam, 2012; L. Lu & Ip, 2009; Mertens, 2006) suggests that the main concentrator effect is present between buildings rather than in flat rooftops.

The wind behavior, in terms of distributions is discussed in the following section, where wind roses and Rayleigh distributions from the DICE and the TBWS data are presented.

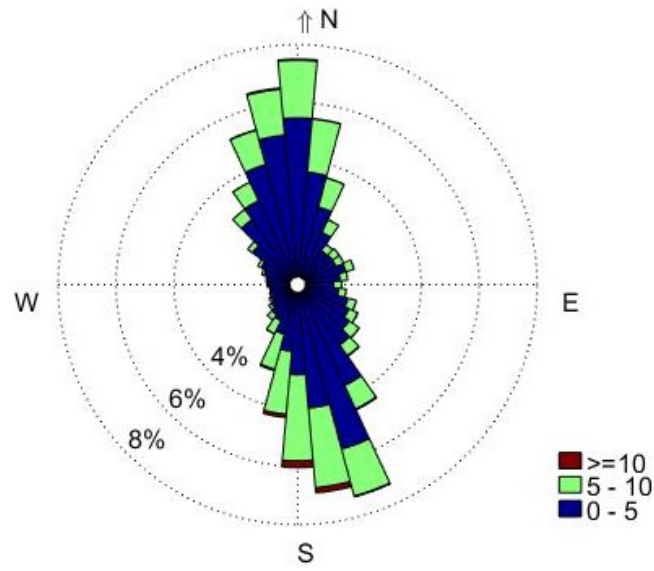
4.4 Wind Roses

Wind roses from the anemometers installed at the DICE building were compared to an hourly wind rose plotted with the TBWS wind data.

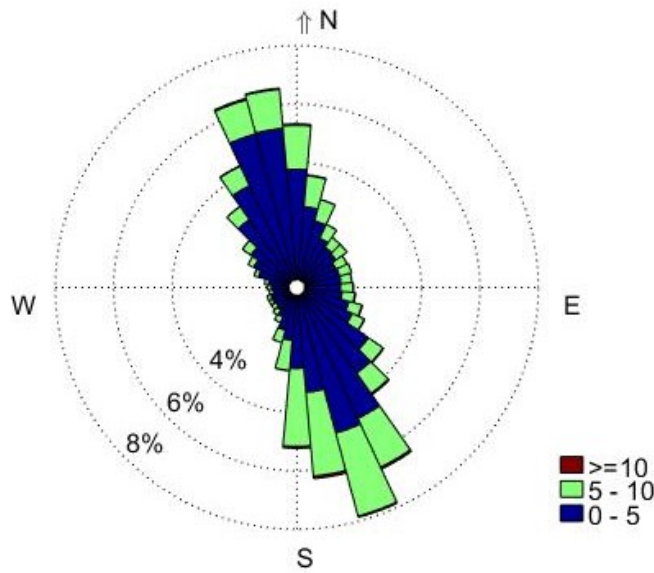
The inputs for the wind rose code used in MATLAB were: wind speed and wind direction. Some other parameters were added in order to customize the plots.

The wind roses are shown in Figure 27. As seen in the Figure, the radial direction of the wind roses represents the frequency of the wind direction; and the color gradient the magnitude of the wind velocity in m/s.

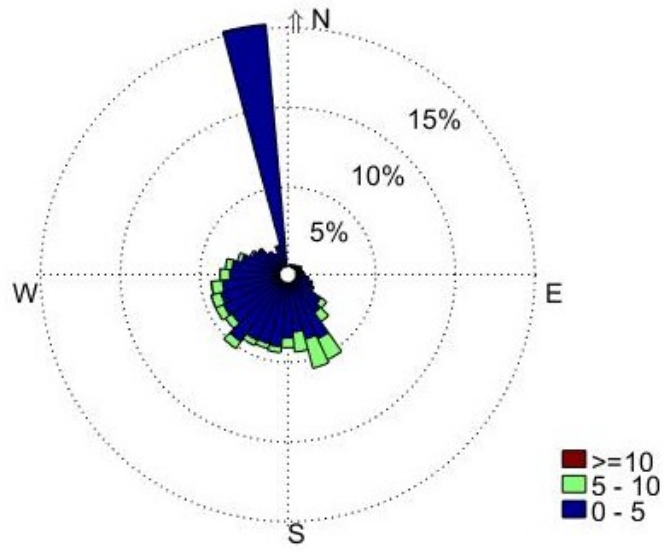
(a)



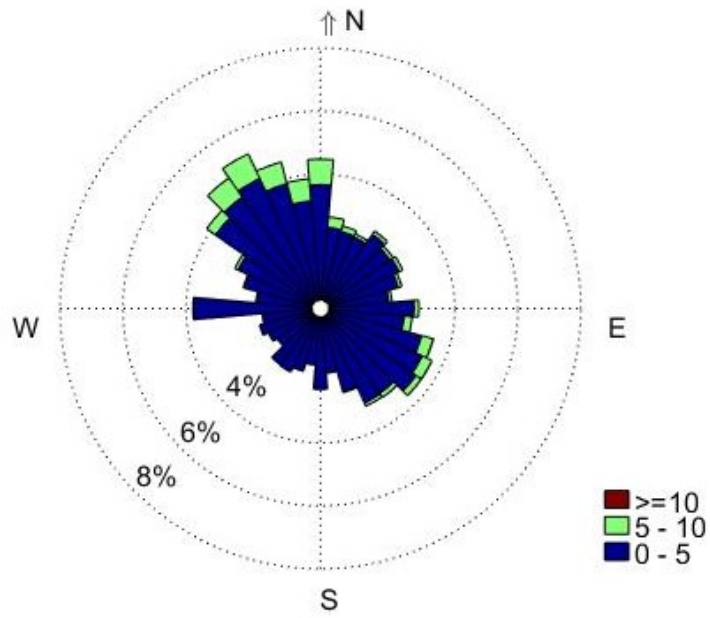
(b)



(c)



(d)



(e)

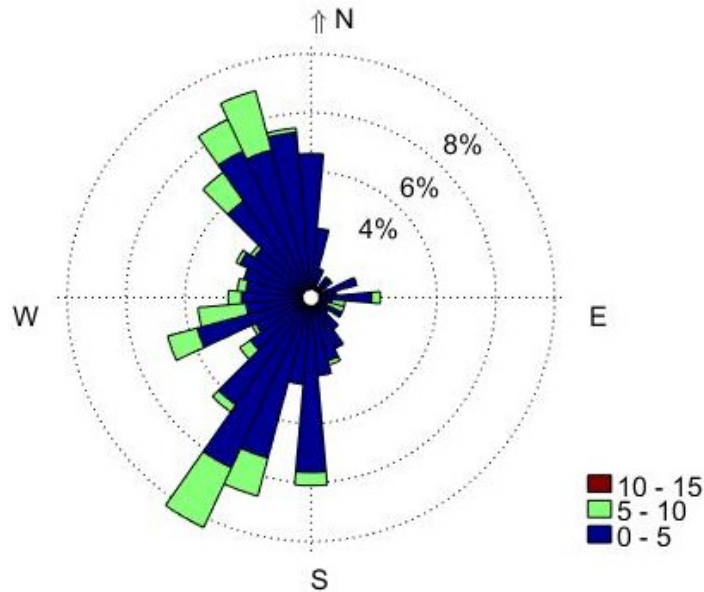


Figure 27: (a) Wind Rose Wind Monitor #1 (DICE), (b) Wind Rose Wind Monitor #2 (DICE), (c) Wind Rose Wind Monitor #3 (DICE), (d) Wind Rose 3D ultrasonic Anemometer (DICE), (e) Wind Rose TBWS.

The wind roses shown in Figure 27 present a similar behavior with the Wind Monitor #1 and #2 being the closest in terms of intensities and predominant direction. However, from the DICE building it can be seen that the predominant wind directions are Northwest and Southeast.

The frequency of the wind speed varies, showing the predominant wind speed ranging between 0-5m/s. Wind speeds higher than 5 m/s are less frequent, corresponding to less than 2%.

Wind rose (c) presents an unusual predominant wind direction (NW) with an extreme high frequency of 15%. It is basically twice of the highest frequencies shown by the other wind roses (>8%). The predominant wind speed again range between 0-5 m/s, however it also shows less wind speed over 5 m/s.

These differences could be evidence that the Wind Monitor #3 was installed inside a zone with a complex wind behavior, or a recirculation zone, and the instrument indicated wind changing direction constantly recording the erratic behavior.

Wind rose (d) which corresponds to the ultrasonic anemometer shows a similar behavior compared to (a) and (b). However it presents a peak of 4% frequency of wind coming from the West which is not shown by (a) and (b).

Wind coming from the West with a 4% frequency is shown in wind rose (c), which could mean that the ultrasonic anemometer was also sensing some of recirculation. Let's note that Wind Monitor #3 and the ultrasonic anemometer were installed higher than Wind Monitor #1 and #2. However, the readings from the ultrasonic anemometer are more reliable since the equipment is designed to record multidirectional flow, has a lower wind velocity threshold and because of how it operates, its response time is faster than the mechanical anemometers. This aspect allows the ultrasonic anemometer to record wind fluctuations faster since it has no moving parts and it does not need to change direction to be able to measure wind speed like the wind monitor.

Having the ultrasonic anemometer installed near the edge of the building and in the presence of a complex flow with recirculation, it is beneficial since the data could give an idea of the turbulent structure of the flow in that region.

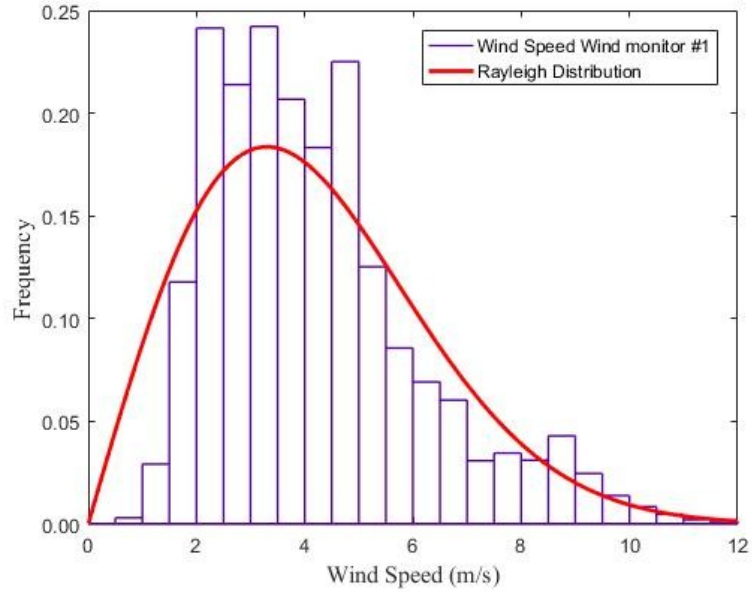
Wind rose (e) shows predominant wind directions from Northwest and Southwest. This is a different location so the difference is not surprising, however it shows NW as predominant and wind speeds in the same range as the other wind roses.

The wind roses plotted correspond to only 23 days of data from the month of February 2017. When plotting wind roses with at least one year of data, discontinuities or jumps in the directions bins are less frequent since these gaps are filled with data.

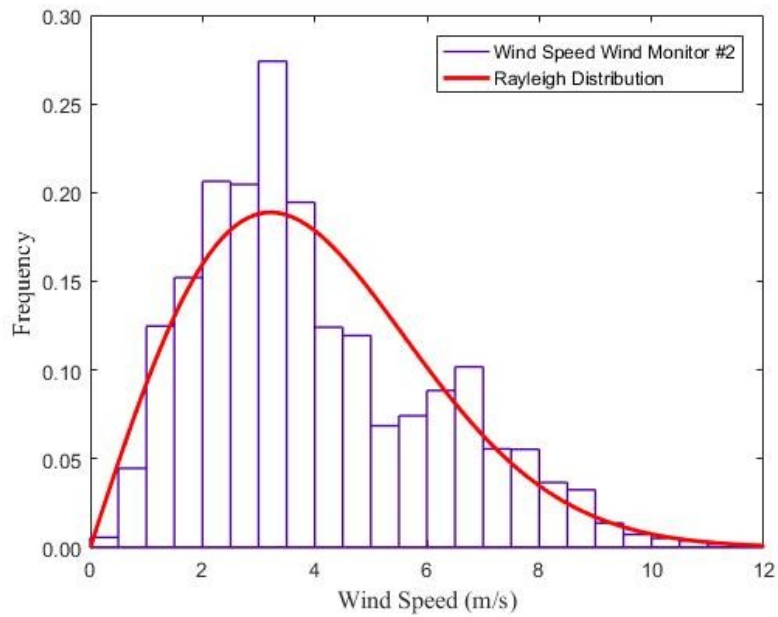
4.5 Histograms and Rayleigh distributions

Histograms from the DICE building and TBWS are presented in Figure 28.

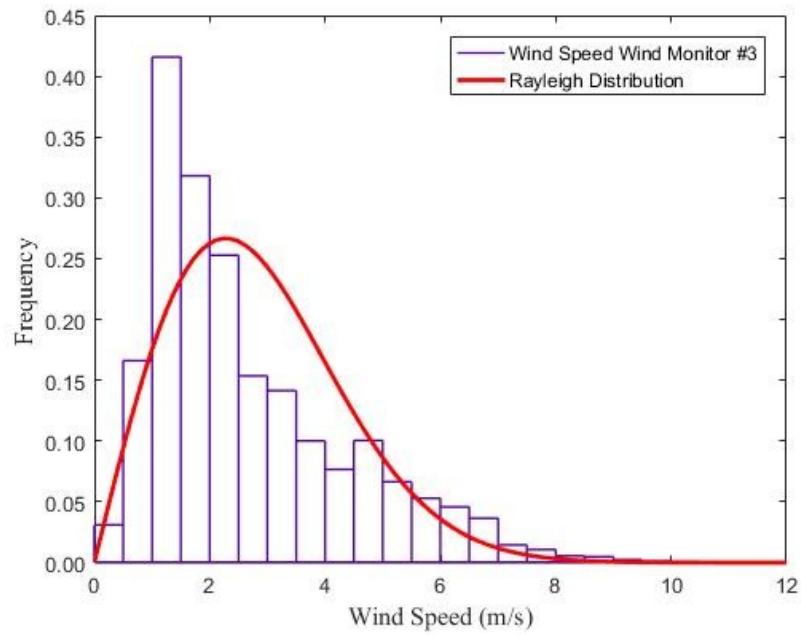
(a)



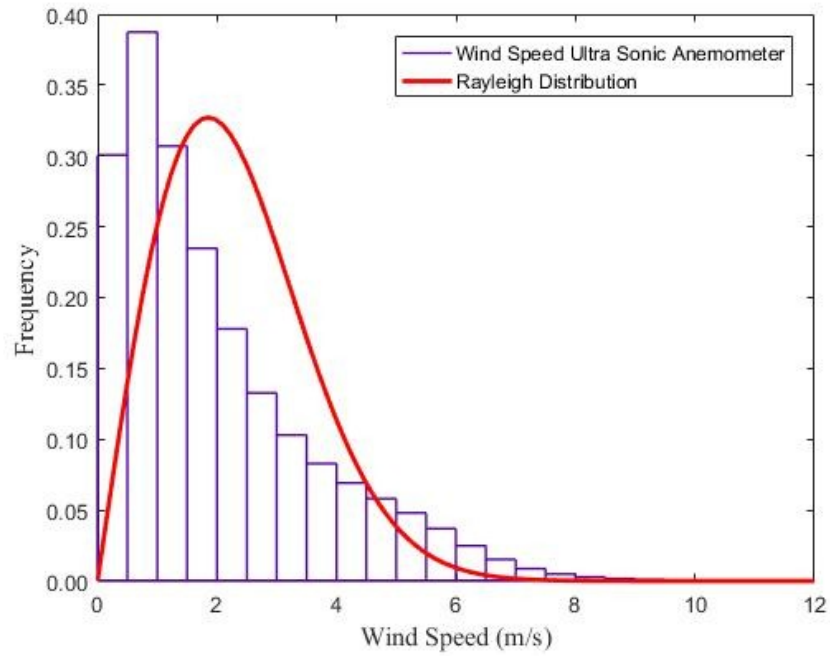
(b)



(c)



(d)



(e)

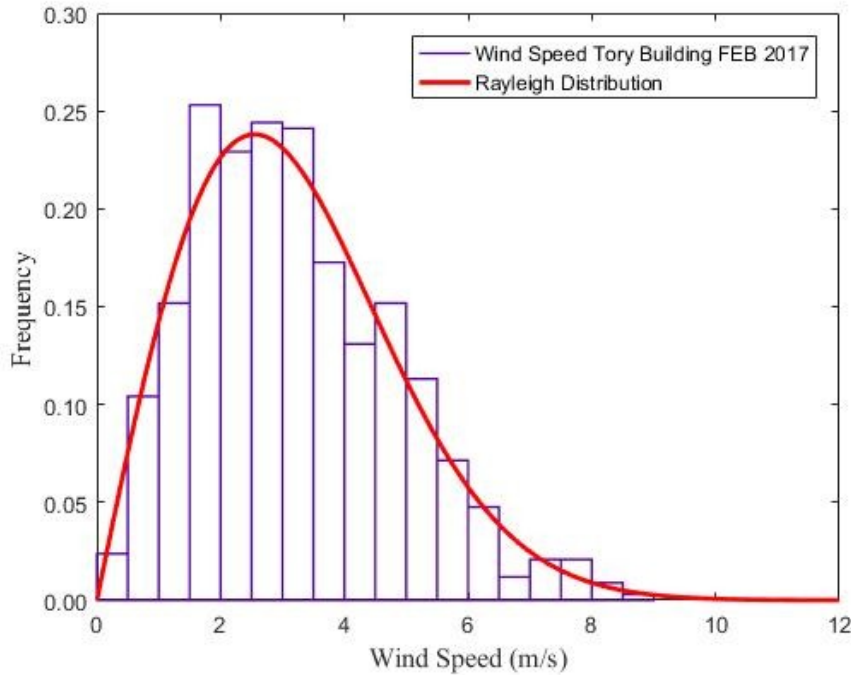


Figure 28 Rayleigh distributions: (a) Wind Monitor #1, (b) Wind Monitor #2, (c) Wind Monitor #3, (d) 3D Ultrasonic Anemometer, (e) TBWS.

It is observed in Figure 28 that the Rayleigh distributions fit well the wind speed data from wind monitors #1, #2 and TBWS. Looking at the relation between the histograms of the Wind Monitor #3 and the ultrasonic anemometer, with the Rayleigh distribution fit, it is noted a difference between the heights of the bars and the distribution fit. This shows the complexity of fitting a curve to a histogram; however, the results obtained from the fitting are still useful for analyzing the wind behavior. It is possible to fit a Weibull or Rayleigh curve to the bar heights, but this process implies constraining the curve to be properly normalized. For continues data, the bar heights are strongly dependent on the choice of the bin edges and width, and while it is possible to fit distribution in based on this, it is usually not the best way because it throws away information (MATLAB, 2017).

Figure 28 (a), (b) and (e) have their maximum wind frequencies reflecting wind speeds between of 2.5 and 3.5 m/s, corresponding to the most frequent velocities according to the distribution fit. These distributions also show an approximated 60% probability of having wind speeds higher than 4m/s for the month of February. This number is based on the area under the curve, since the whole area should be equal to 1. The two sensors, shown in Figure 28 as (c) and (d), show their highest velocity frequency with the lowest wind speed compared to the other sensors (wind speeds of 1 and 1.5 m/s).

In order to get a value of the most probable wind velocity, the following equation is defined:

$$V_{mp, Rayleigh} = \frac{c}{\sqrt{2}} \quad 4.1$$

Where c is the scale factor of the Rayleigh distribution.

Table 6 shows the parameters from the Rayleigh distribution fit including the most probable wind velocity, calculated with equation 4.1.

Table 6 Wind Statistical Parameters, Rayleigh distribution

	Mean Wind Speed (m/s)	Rayleigh Scale Parameter (m/s)	Most Probable Wind Velocity (m/s)
Wind Monitor #1	4.14	3.30	2.33
Wind Monitor #2	4.03	3.21	2.27
Wind Monitor #3	2.85	2.27	1.61
Ultrasonic Anemometer	2.34	1.85	1.31
Tory EAS Weather Station	3.19	2.55	1.80

In Table 6 it is observed that the highest most probable wind speeds were captured by Wind Monitor #1 and #2. Showing that higher wind speed, are more frequent and probable in locations closer to the edge of the building.

The average wind power in the wind can be computed in terms of Rayleigh's scale factor, and it is defined as:

$$\overline{P(V)} = \frac{\rho A \overline{V^3}}{2} \quad 4.2$$

Where $\overline{V^3}$ is the mean of the cubed velocity, defined as:

$$\overline{V^3} = c^3 \frac{3\sqrt{\pi}}{4} \quad 4.3$$

The distribution of wind power as a function of the velocity, for the Rayleigh distribution is defined as:

$$g = \frac{8V^4}{\sqrt{\pi}c^5} e^{-(V/c)^2} \quad 4.4$$

Where g is the distribution of wind power as a function of the wind velocity V .

Table 7 presents the wind power density (WPD) computed using equation 4.2 for all the anemometers, including TBWS.

This calculation provides a more accurate estimation of the available energy in the wind for the month of February 2017, since it is based on the Rayleigh distribution fit and not on daily wind speed average.

Table 7 Average wind power density available on February 2017, based on Rayleigh distribution

Anemometers	Wind Power Density (W/m ²)
Wind Monitor #1	29.20
Wind Monitor #2	26.87
Wind Monitor #3	9.50
Ultrasonic Anemometer	5.14
Tory EAS Weather Station	13.47

As observed in Table 7, the averaged wind power density based on the Rayleigh distribution is basically half of the values calculated before using the mean wind speed. The use of mean wind speed overestimates the wind power availability, which is why in order to conduct a wind assessment a probability density function must be calculated.

When comparing Table 5 and Table 7, it is observed that the Canadian Wind Atlas estimates a wind power density of 145.5 W/m² for the winter season at 50 m high. The power density estimated for the month of February is 78% lower than the one provided by the Canadian Wind Atlas. The atlas is based on data collected every 6 hours over 43 years, from 1958 until 2000. When comparing their estimation with our data, it is fair to say that this big difference could be caused by the type of location that we are studying. We are analyzing wind behavior in the urban environment, which makes the wind difficult to simulate, even with a long term database. As a conclusion, the Canadian Wind Atlas it is not designed for assessing urban environments but open field locations, like rural zones and the prairies.

Since only February's data were analyzed, we are missing much of the atmospheric information that affects the overall wind energy estimation for this location. Nevertheless, we have seen higher wind speeds recorded by the two anemometers closer to the edge of the building. And comparing the results in Table 7 with the literature, Karthikeya et al. (2016) found in their results wind power densities ranging between 45 and 15 W/m^2 for different locations in the coastal area of Singapore.

Taking into consideration that coastal areas usually present higher wind speeds, our measured wind power density of 29 W/m^2 doesn't look too bad for a built environment. Let's note that the windiest season of the year range between spring and summer, meaning that the wind power density could be increased with a year round analysis.

The distribution of wind power as a function of the wind velocity was plotted using data from the Wind Monitor #1, since it presents the highest wind speed readings. Because of the way that the wind power distribution as a function of the wind speed is determined, a scatter plot was computed and the Rayleigh curve from the wind monitor added for comparison, because the curve shows the frequency of the wind speed. The plot is shown in Figure 29.

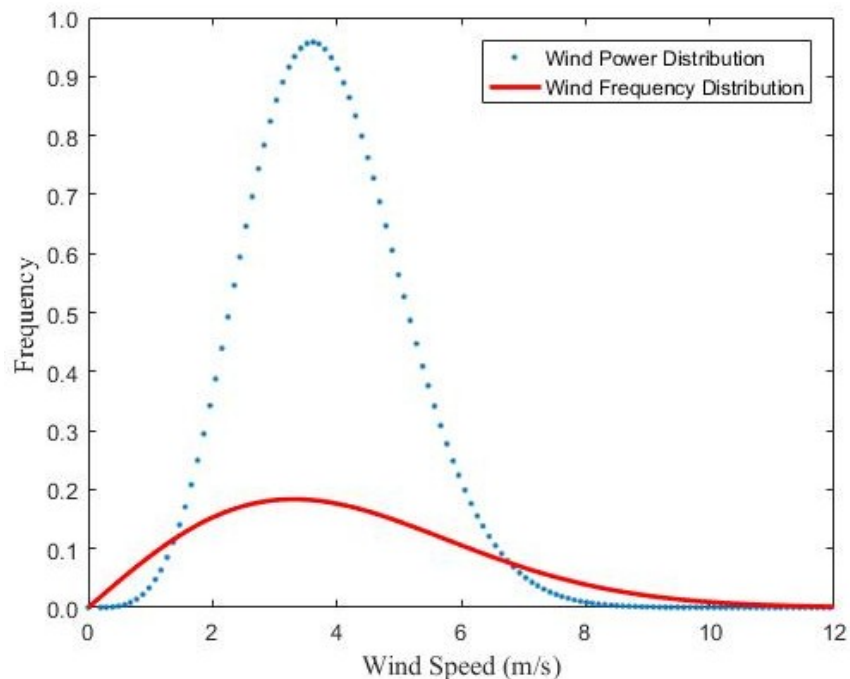


Figure 29 Wind Frequency and Power Distributions, Wind Monitor 1

Figure 29 shows that most of the wind power fraction is contained in the range of the wind speeds that are higher than 3 m/s according to the wind distribution. Between 3.5 and 5 m/s appears to be the zone with the highest wind power distribution. At wind speeds higher than 6m/s the wind power fraction is small.

4.6 Turbulence Study

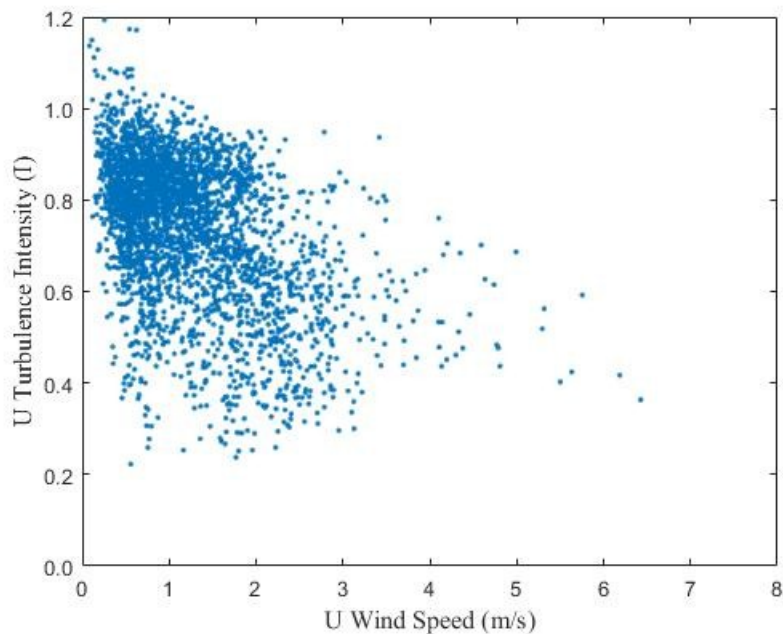
This section covers the study of the turbulence of the wind flow around the DICE building. To conduct the study, data from the ultrasonic anemometer were used, since it contains information regarding the fluctuating components of u , v and w .

First, we will cover the turbulence intensity. This parameter was defined in Chapter 2 by the equation 2.9.

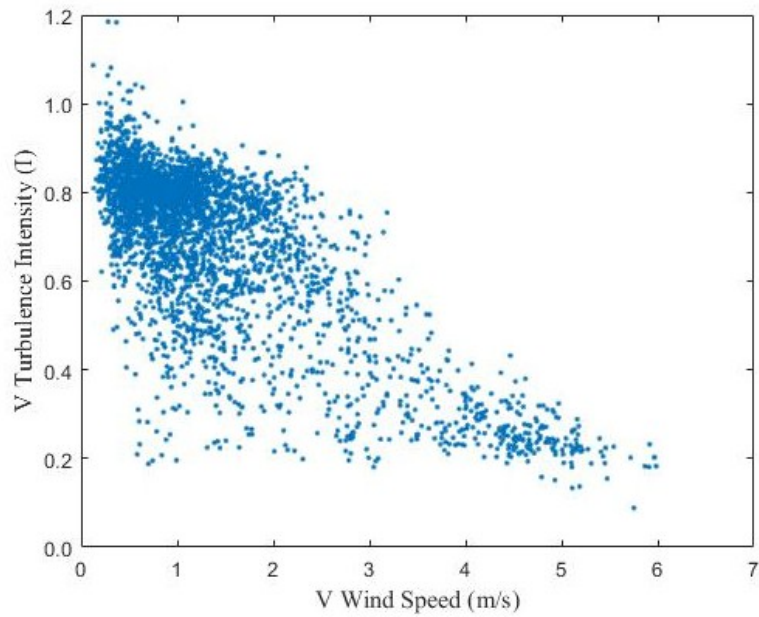
As noted before, turbulence intensity is used to quantify how turbulent the flow is in certain locations where energy harvesting is of interest.

Two approaches were taken to determine the turbulence intensity. With a sampling rate of 10Hz and an averaging time of 10 minutes, the turbulence intensity for the longitudinal, lateral and vertical components of wind velocity (u , v and w) were computed based on equation 2.9. The resulting plots are shown in Figure 30.

(a)



(b)



(c)

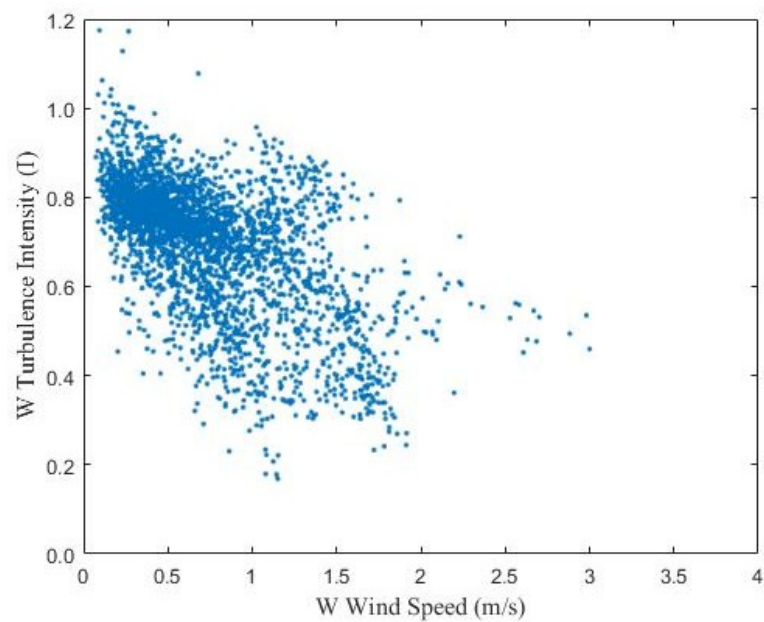
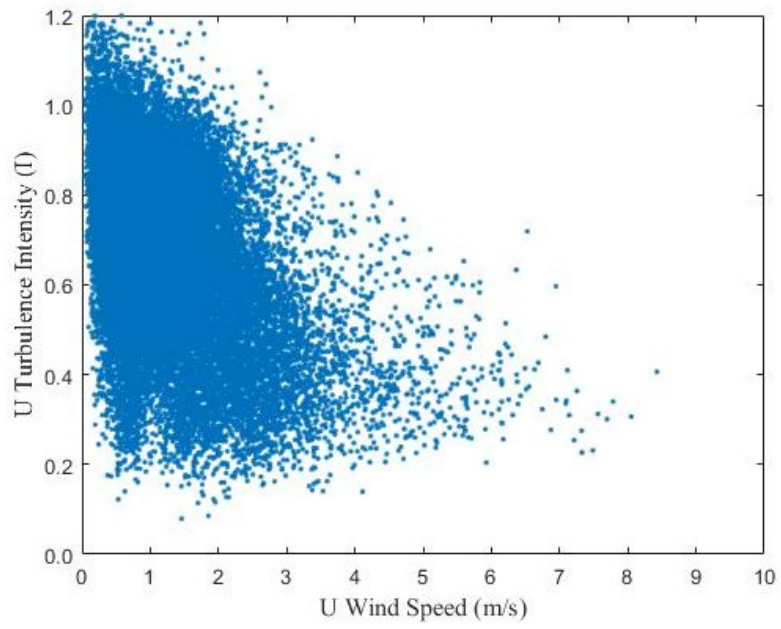


Figure 30 Turbulence Intensity 10 min. Average: (a) u component, (b) v component, (c) w component.

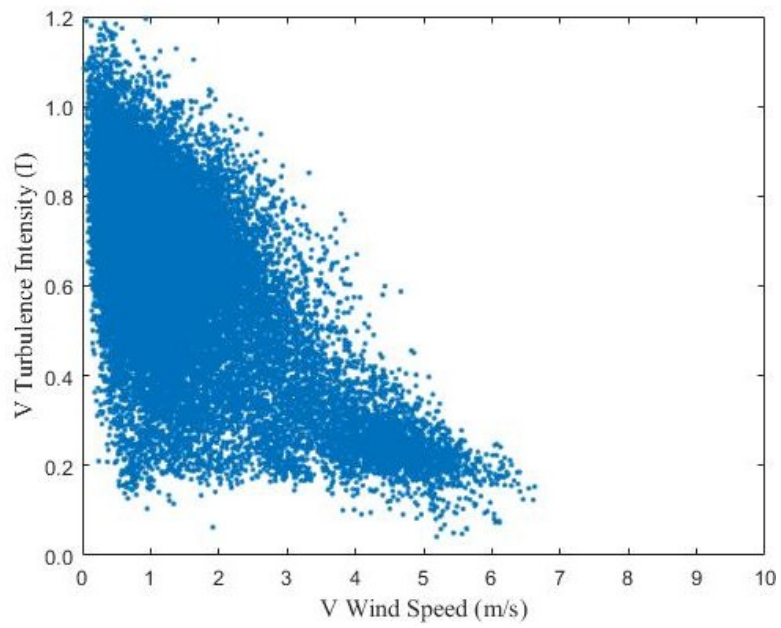
In Figure 30 it is observed how most of the scatters of the points are concentrated around the turbulence intensity value of 0.8.

The plots of the turbulence intensity for the same components of wind velocity (u , v and w), determined with a sampling rate of 10 Hz and 1 minute averaging time, are presented in Figure 31.

(a)



(b)



(c)

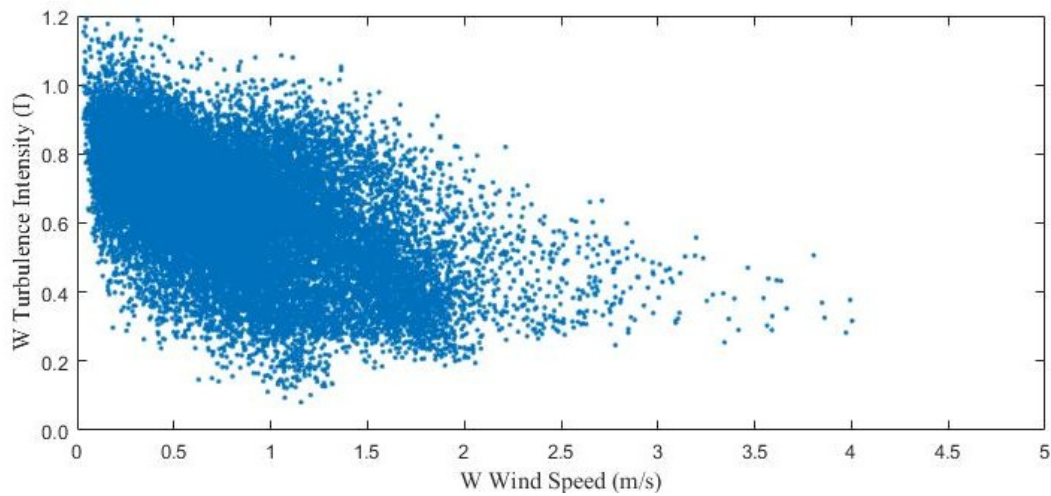


Figure 31 Turbulence Intensity 1min. Average: (a) u component, (b) v component, (c) w component.

As observed in Figure 30 and Figure 31, turbulence intensity shows a decreasing behavior as wind speed increases. This pattern agrees with the consulted literature; Karthikeya et al. (2016) found results with a similar behavior of decreasing turbulence intensity, presenting values between 0.25 and 0.15 for wind speeds approaching 15 m/s.

Turbulence described by Neuman et al. (2006) and Emeis (2013), explains that the normal wind turbulence model defines a monotone decline of turbulence intensity as the wind speed increases. For offshore regimes, the turbulence intensity decreases rapidly until 12 m/s because of the dominance of the thermal induced turbulence at low wind speed, this originates from unstable atmospheric conditions when the water surface temperature is much higher than air temperature. However, with increasing wind speeds and increasing roughness length z_0 , the mechanical part of the turbulence intensity becomes dominant over the thermal effects and turbulence intensity starts to increase (Barthelmie, 2000).

A similar increase in turbulence intensity was found by Karthikeya et al. (2016) when studying turbulence intensities at different heights. By using a LiDAR unit, they found that for heights of 50, 80 and 100 m the turbulence intensity increased for wind speed values higher than 8 m/s.

In this study there is not enough data after 8 m/s, so this phenomenon was not found. Only Figure 31-(a) shows a lightly increasing trend after 8 m/s.

Observing Figure 30 and Figure 31, we note empty spaces without data between the values of 0.1 and 0.2 of turbulence intensity along the wind speed axis. Since turbulence intensity is basically a statistical tool, only one month of data is not enough to get a plot similar to Figure 4. It misses atmospheric information that would add more data to the study. Another noticeable difference between the figures is the much higher turbulent regime found in the built environment compared to an offshore location. This is noticed by the high concentration of scattered points between 0.4 and 1.0 at low wind speeds.

The averaged turbulence intensity is presented in Table 8.

Table 8 Averaged Turbulence Intensity

Wind Velocity Component	Turbulence Intensity (I) 10 min.	Turbulence Intensity (I) 1 min.
<i>u</i>	0.76	0.69
<i>v</i>	0.70	0.64
<i>w</i>	0.72	0.67

As shown in Table 8, the turbulence intensity at the DICE building for the month of February 2017 was between 0.64 and 0.76 depending on the averaged time and the component of the wind velocity.

It is consistent with the dominance in turbulence intensity from the *u* component of the wind velocity. In both averaging cases it presents the higher turbulence intensity, followed by the vertical component *w*.

Table 8 reflects a highly turbulent regime, considering that according to NREL the turbulent intensity should be less than 18% for sites where urban wind turbines are considered (Fields et al., 2016). As discussed in Chapter 2, high turbulence intensity affects the overall performance of a wind turbine, compromising the power production and service life.

However, some wind turbine designs may overcome the turbulence issue and perform well in the urban environment. As an idea of which design would work better, Pagnini et al. (2015) concluded that vertical axis wind turbines perform better in turbulent flows compared to horizontal axis wind turbines. A key aspect is that the VAWT does not have a yawing mechanism and it can produce power with wind blowing from any direction, including wind gusts or eddies. According to Lubitz (2014), HAWT seems to be affected by changes in wind speed, presenting a time lag of 2 seconds between the change of wind speed and the change in power production. When operating in a turbulent regime with constant changes in wind speeds and direction, it is common to see a decrease in performance.

This has been documented by researchers, with turbulence studies showing that at low wind speeds, high turbulence intensity ($I > 0.14$) increased power production for 2%, however high turbulence intensity affected the overall performance of the turbine (Lubitz, 2014).

When analyzing the difference in time averaging at computing turbulence intensity, our results show a decrease of 9.2% for the longitudinal (u) component of the wind velocity when calculating the intensity with 1 minute averaging time compared to 10 minutes.

In terms of the lateral component (v), there is a reduction in the turbulence intensity value of 8.6% when computing 1 minute averaging time compared to 10 minutes. And in terms of the vertical component (w), the reduction was 6.9% using 1 minute averaging time instead of 10 minutes.

This can be explained as the existence of an overestimation in the turbulence intensity when using 10 minutes. The use of 10 minutes assumes that all of the fluctuations are part of the turbulence and adds that information to the final result. While having 1 minute average, the data are more specific, yielding a lower estimation of turbulence intensity.

Similar decrease in turbulence intensity was found by Tabrizi et al. (2015b), where the longitudinal and lateral (u, v) turbulence intensity presented a reduction of 25% when it was determined with 1 minute compared to 10 minutes averaging time. The vertical component of the wind velocity presented a lower change in the turbulent intensity, varying 11% between the two averaging times (Tabrizi et al., 2015b).

Our results show that the horizontal components (u, v) of the wind velocity are more sensitive to time averaging than the vertical component (w). Similar results were obtained by Tabrizi et al. (2015b), as discussed before the vertical component presented the lowest difference with the varying averaging time.

The wind flow at the roof top of the DICE building is highly turbulent; the decision of using 10 minute or 1 minute will depend on how accurate we want the results to be.

The researchers Tabrizi et al. (2015b), concluded that choosing 10 minutes would give an upper value for the turbulence intensity that can assure that the wind resource assessments captures the turbulent inflow that would allow one to calculate the loads on a wind turbine. This would be most conservative approach, which also consumes less computational power.

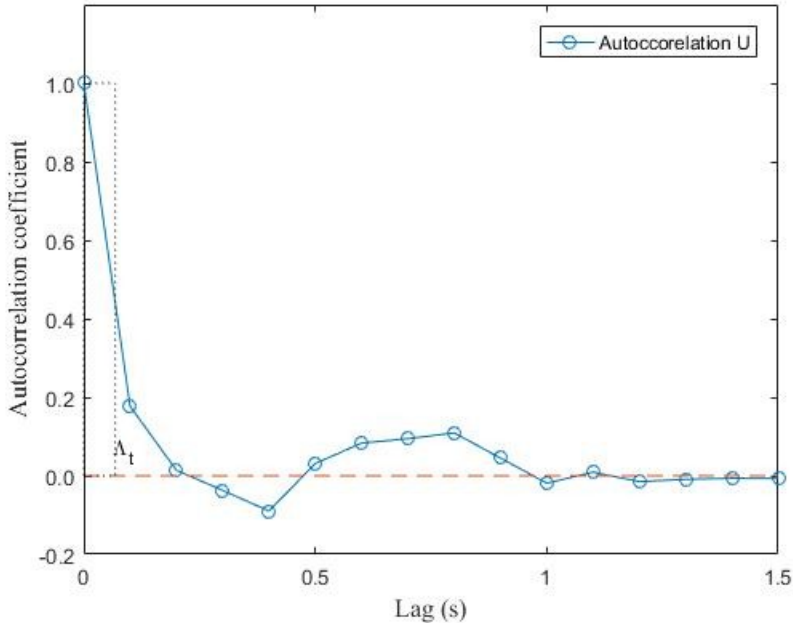
4.7 Autocorrelation of Wind Velocity

Autocorrelations of the velocity components (u, v and w) were computed for one minute of measurements in the windiest day of February 2017.

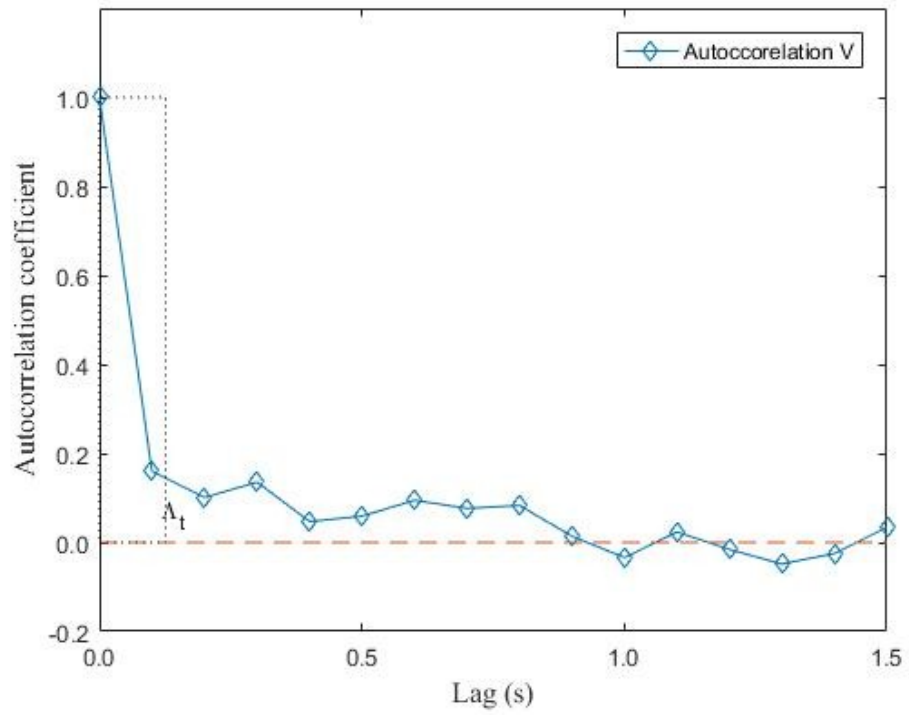
As it was discussed before, the windiest day was February 12th. From this day, two specific hours were chosen in order to conduct the study. First, the hour with the highest wind speed, this was 7 pm. Followed by the hour with the highest turbulence (4 pm).

The sampling of the data was 10Hz and the autocorrelation was computed for the first minute of each hour. The plots for the 7 pm autocorrelation are shown in Figure 32.

(a)



(b)



(c)

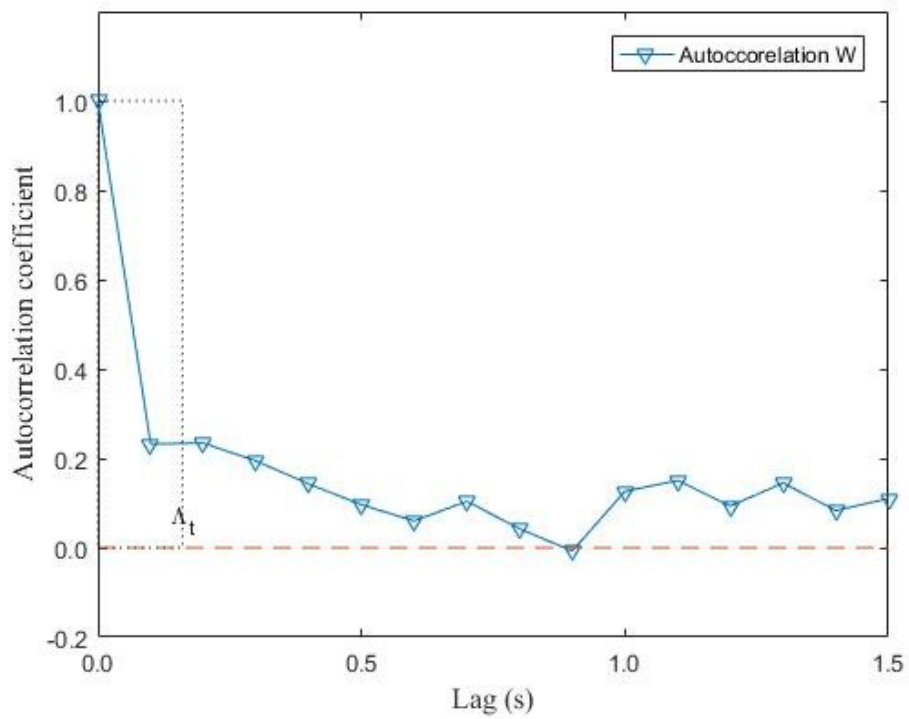


Figure 32 Autocorrelation at 7 pm: (a) u component, (b) v component, (c) w component.

In Figure 32-(a) it is observed that the autocorrelation of the u component of the velocity presents a steeper decrease to zero compared to (b) and (c). It crosses 0 at 0.227 seconds. Compared to Figure 32-(b) and (c), it also presents a shorter integral time scale Λ_t . This can be seen graphically since the area under the curve is smaller and it is represented by Λ_t on the plot.

The autocorrelation of v and w crosses zero at 0.93 and 0.88 seconds respectively. With a shorter integral time scale it is expected for this case that u presents a shorter integral length scale or spatial dimension. As discussed before, following Taylor's hypothesis, the length scale can be approximated to the time scale multiplied by the mean wind speed. Where the mean speed was defined: as the mean of the time series, in this case, 1 minute.

Taylor's hypothesis assumes that the turbulent eddies are carried by the mean wind speed and change slowly as they move. However, in order for this hypothesis to be valid, the turbulence needs to be stationary in time and homogeneous in the mean wind speed direction. These conditions are usually met in wind tunnels and approximately valid in the atmosphere when the measurement location and period are chosen carefully (Dutton & Panofsky, 1984).

In the lower 10% of the ABL at open field, the hypothesis could be valid. In this region the wind direction does not change significantly with height, the lateral wind component is zero and the vertical component is often negligible compared to its fluctuation. These conditions are not usually met in the urban environment, causing Taylor's hypothesis to hardly be valid. In this region, the wind flow tends to be multi-directional. As an example, when there are strong shears in the vertical direction, this will often distort the eddies as they move, breaking them apart (Dutton & Panofsky, 1984).

The results for the integral time scale, and the spatial dimension of the turbulence is presented in Table 9.

Table 9 Autocorrelation Parameters 7 pm

Velocity Component	Mean Wind Speed (m/s)	Integral Time Scale (s) Λ_t	Integral Length Scale (m) Λ_u
u	2.22	0.07	0.15
v	5.46	0.13	0.69
w	1.80	0.16	0.29

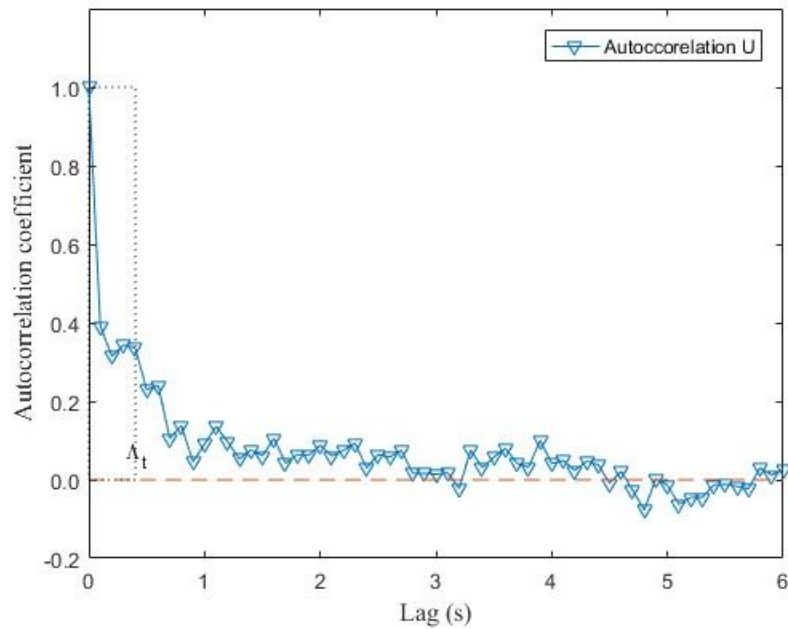
Table 9 shows how the integral time and length scale varies depending on the wind velocity component. It is observed how the u component is smaller than v and w .

It is noted a higher wind speed flowing in the lateral direction, creating a larger eddy compared to the other two components. This lateral component means that the wind was potentially blowing from the West. This wind direction is particularly open, since the DICE building doesn't have mayor obstacles on the West side of the building.

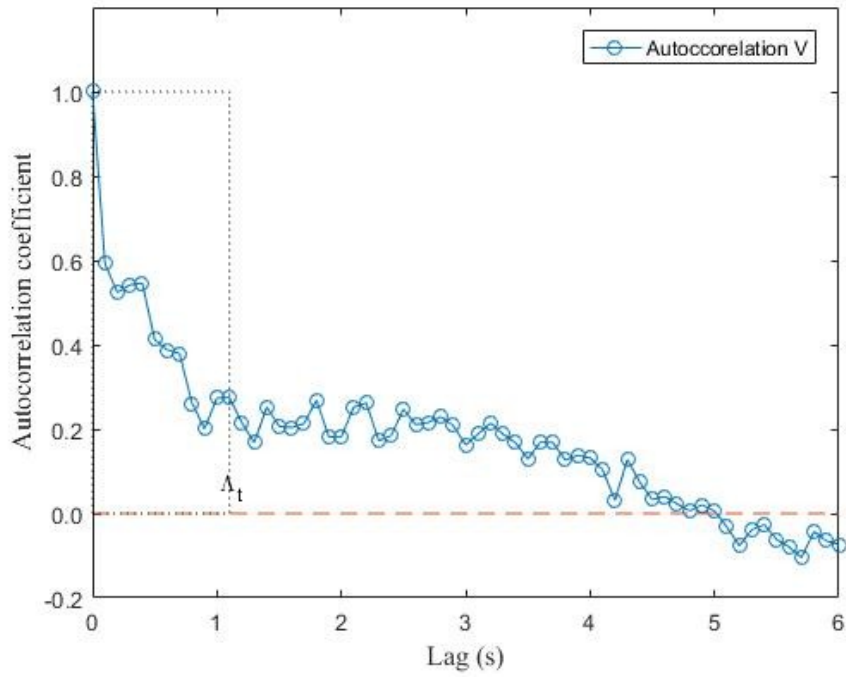
The vertical component also showed a higher integral length scale and time scale compared the longitudinal, showing some vertical flow dominance over the longitudinal component.

To have a better understanding of the results, the autocorrelations at the time when the hourly turbulence intensity was higher are presented in Figure 33. We would expect to see larger dimensions for the turbulent elements.

(a)



(b)



(c)

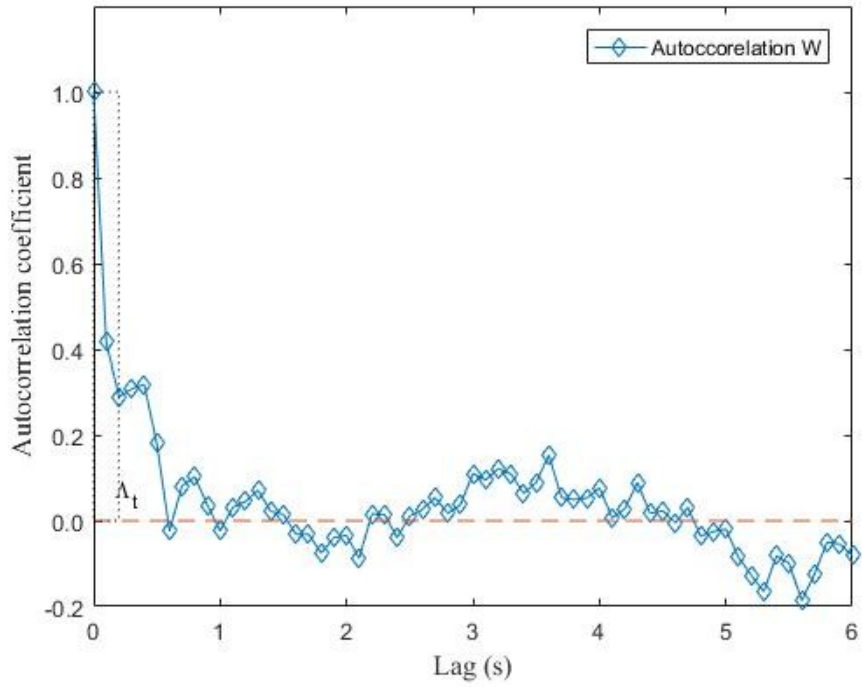


Figure 33 Autocorrelation at 4 pm: (a) u component, (b) v component, (c) w component.

Figure 33-(c), shows how the autocorrelation of the w component of the velocity decreases to zero faster than the other two components (u and v). This result differs from Figure 32, where we found this behavior in the u component. This will translate into larger elements in the horizontal component of the wind velocity.

Analyzing the plots, we notice that the autocorrelation of u crosses zero at 3.14 seconds, v at 5.02 seconds and w at 0.59 seconds. Once again the v component of the wind velocity will have the largest integral time scale between the other two, similar result compared to the windiest hour of the day.

The results for the integral time scale and the spatial dimension of the turbulence are presented in Table 10. It shows how the overall integral length scales of the components are smaller than the ones computed at 7 pm. This is due to the lower wind speeds that are present at 4 pm. Only the u component presents a bigger element compared to Table 9.

All the components presented larger integral time scales, being u and v , the ones with the highest increment. This reflects that the turbulent elements lasted for a longer time, in other words, their time memory was larger.

Table 10 Autocorrelation Parameters 4 pm

Velocity Component	Mean Wind Speed (m/s)	Integral Time Scale (s) Λ_t	Integral Length Scale (m) Λ_u
u	0.86	0.40	0.35
v	1.03	1.10	1.14
w	0.63	0.20	0.13

In terms of how does the element size of the turbulence affect the power production of a wind turbine, it will depend on the size of the turbine.

Urban wind turbines vary in size, ranging from micro turbines with 0.5 or 1.25 m rotor diameters; to household turbines ranging from 3 to 10m rotor diameter. Based on our results, a micro wind turbine could be affected by the element size we obtained, especially because the largest spatial dimensions of the turbulence were found in the longitudinal and lateral components of the wind.

Larger wind turbines, the ones with a swept are between 7 and 79 m, wouldn't be too affected by a vortex with 0.6m in diameter. The wind turbine wouldn't be much affected by a small turbulent element, compared to its size. What clearly affects the turbine is the presence of the three dimensional flow, and the constant appearance of these vortices in the turbulent regime. That is why intensity is quantified, to obtain a measure of the value and compare it to best practices.

A more detailed study of how the size of turbulent elements interact with turbine blades, and how this interaction affects the power performance should be carried in order to understand the relation between the integral time scale, length scale and power output. So far we have seen that with higher turbulence intensity, larger integral time scales are obtained. However, thanks to lower wind speeds the spatial dimension was smaller, in an overall sense.

The results regarding integral length scales are approximations based on Taylor's frozen turbulence hypothesis and one minute mean wind speed. If a smaller mean is taken the result may vary considerable, it will depend on how variable is the wind speed.

It is important to recall that in the environment there is no a constant mean flow like in wind tunnels or pipes. The wind is constantly changing in terms of time and it is disturbed by the landscape.

4.8 Tory Building 2016 Data Assessment

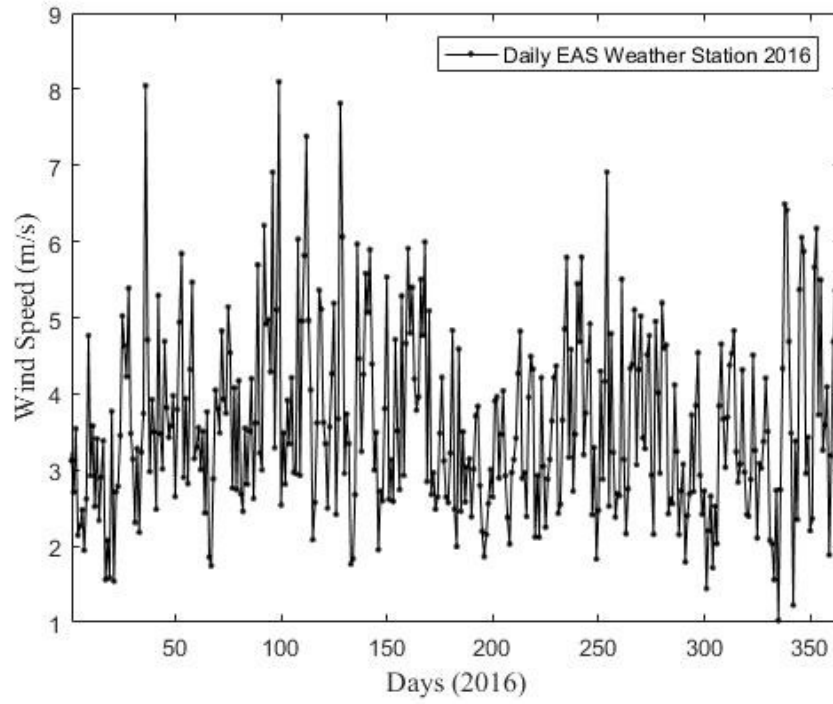
In order to have a resource assessment based on one year of wind data, we used TBWS and assessed hourly data from January 1st 2016 to December 31st 2016. These data are public and are available online in the EAS archive with a database going from the year 2000 to 2016.

Following the previous methodology to calculate the average air density, we obtained for the year 2016 an averaged air density of 1.17 kg/m³, with a standard deviation of 0.05 kg/m³. The average pressure was 94.07 kPa, with a standard deviation of 0.71 kPa; and the average temperature was 6.36°C, with a standard deviation of 10.80°C.

The air density was used later to determine the wind power density of the TBWS based on the Rayleigh parameters.

Daily and hourly wind speeds were plotted in order to analyze the wind behavior through the year. These plots are shown in Figure 34.

(a)



(b)

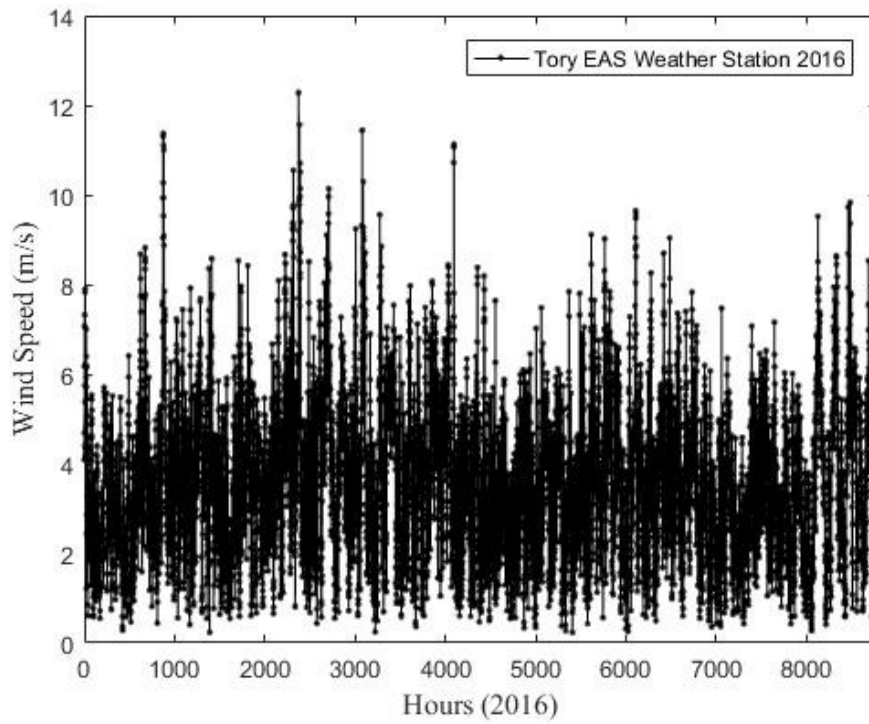


Figure 34 Daily and Hourly Wind Speed, EAS Weather Station 2016

Figure 34 shows how variable the wind speed is through the year. From (a) it seems that the highest wind speeds were present between March and April 2016.

In order to obtain a better understanding of the frequency of the wind velocity and principal wind direction, an hourly wind rose was plotted and presented in Figure 35.

Figure 35 reflects how the principal wind directions in 2016 were North-West and South-East. This agrees with our results for the month of February 2017 from the DICE and the TBWS. However, there is a peak in the South-West directions which has a frequency that surpasses 6%.

The same peak is present in Figure 27-(e), suggesting that for the month of February, wind coming from the South-West is frequent. It is so frequent that it actually dominates the overall frequency of the annual wind rose.

In terms of wind speeds, according to the wind rose, the most frequent ones were between 0 and 5 m/s. There is a higher frequency for higher wind speed for winds coming from the North-West, as shown in the wind rose.

A better representation of wind speed frequency and probability is shown in Figure 36, with the Rayleigh distribution.

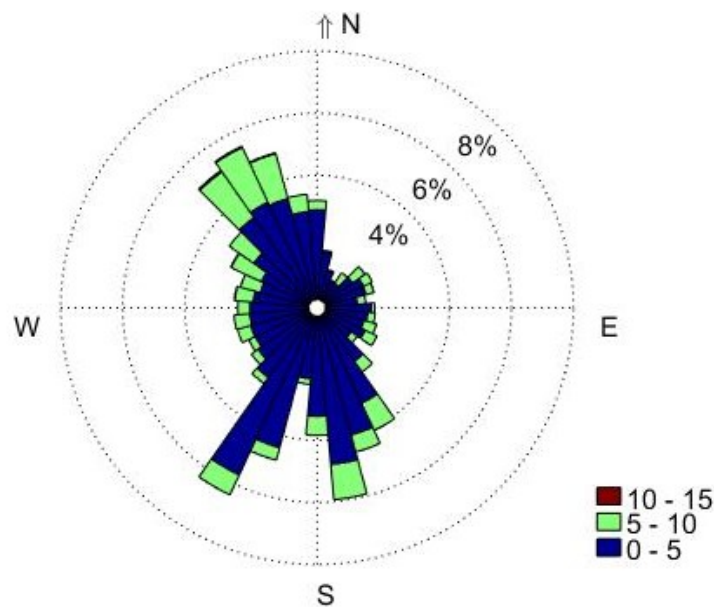


Figure 35 EAS Weather Station (TBWS) 2016 Wind Rose.

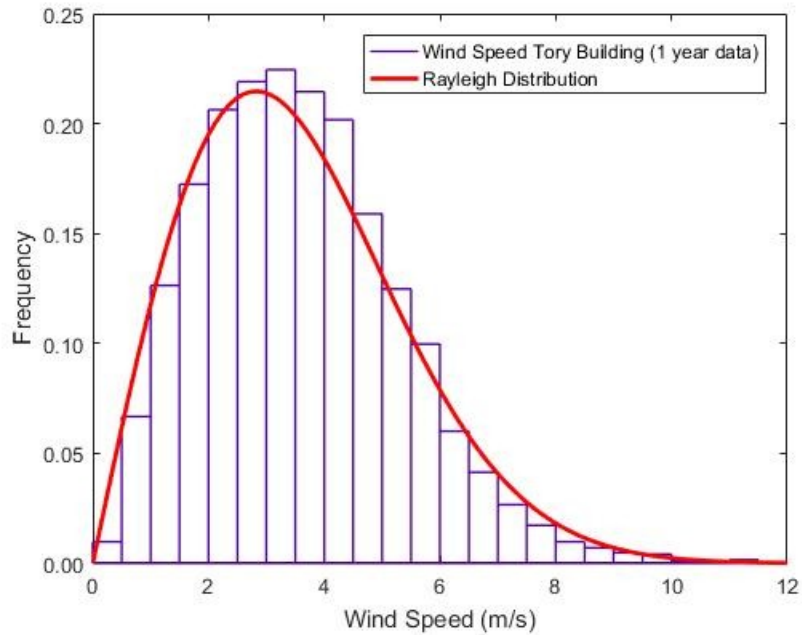


Figure 36 Rayleigh Distribution TBWS 2016.

The histogram shows how the most frequent wind speed fluctuated between 3.5 and 4 m/s. By analyzing graphically the plot, it can be noted how the distribution fit has a maximum showing the most frequent wind speed as 2.82 m/s. The mean wind speed according to the distribution is 3.54 m/s, and there is an approximated 50% probability of having wind speeds higher than 4 m/s through the year. This means that energy could potentially be harvested half a year, based on a cut in speed of 3.5 m/s.

The parameters of the Rayleigh distribution are presented in Table 11.

Table 11 Rayleigh Parameters EAS Weather Station 2016

Year 2016	Mean Wind Speed (m/s)	Rayleigh Scale Parameter (m/s)	Most Probable Wind Velocity (m/s)	Wind Power Density (W/m ²)
Tory EAS Weather Station	3.54	2.82	1.99	17.50

From the parameters in Table 11 we see that the mean wind speed and scale parameter are still lower than the ones obtained for Wind Monitor #1 and #2 shown in Table 6. However, these values are higher than the ones from TBWS on February 2017.

Table 11 also presents the most probable wind velocity and wind power density computed with that velocity. These two parameters were determined using equations 4.1 and 4.2.

For a year assessment the most probable wind speed seems to be considerable slow (1.99 m/s) compared to other assessments which found a 4.64 m/s scale factor that would be translated into 3.28 m/s as the most probable wind speed (Pagnini et al., 2015). However, in another assessment, Mazon et al. (2015) found the most frequent wind speeds to be lower than 3.5 m/s, meaning that their highest wind frequencies corresponded to low wind speeds. The researchers also showed a probability peak at 1.15 m/s, and in another period of the year a probability peak corresponding to 2.7 m/s. With the results, they obtained a 50% probability of having wind speeds lower than 3m/s for their location (Mazon et al., 2015).

From Table 11 we see that the wind power density for the whole 2016 is higher than the power density determined for the month of February 2017 shown in Table 6. However 17.50 W/m² still a small number that corresponds to a class 1 in wind power category.

Comparing this result to other urban assessments, as discussed previously Karthikeya et al. (2016), estimated a wind power density of 15 W/m² for one of their coastal location in Singapore. This would set Tory building as comparable to other urban settings.

The wind power distribution in terms of the wind velocity was also plotted for the year of data from the TBWS. Similar to Figure 29, a scatter plot was computed and because of the amount of data contained in one year of hourly data, the plot seems to be a continuous line instead of scattered data. The Rayleigh curve from the TBWS was added for comparison. This plot is shown in Figure 37.

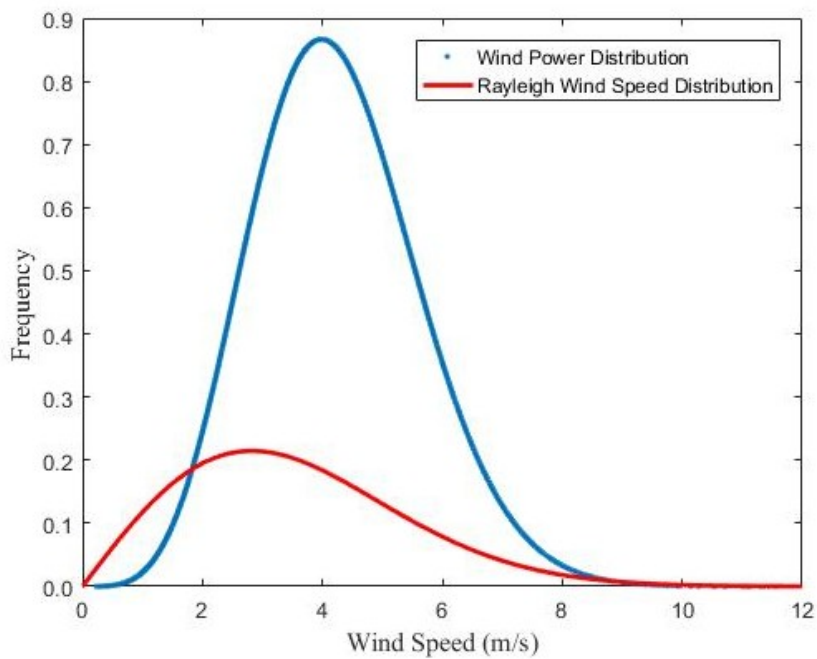


Figure 37 Wind Frequency and Power Distributions, TBWS 2016.

Figure 37 shows that most of the wind power fraction is contained in the range of the highest wind speeds according to the Rayleigh wind distribution, which is shown as the smaller curve.

A peak in the wind power distribution is shown at 4m/s. and most of the power distribution is ranging between 3.5 and 5 m/s. This is good since as discussed before, there is a 50% probability of having 4m/s or higher wind speeds through the year.

Similar to Figure 29, at wind speeds higher than 6 m/s the wind power fraction is small based on the wind frequency distribution. Also, at the point where the wind speed frequency is a maximum the fraction of available power is small.

As we have seen, most of the urban assessments show the same results in terms of wind speed. They are based on Weibull or Rayleigh distributions yielding wind speeds between 1.15 and 4 m/s and scale factors between 2 and 4 m/s, and probabilities between 40 and 50% for wind speed higher than 4 m/s.

Considering that most of the small wind turbines have a cut in speed of 3.5 m/s (Mazon et al., 2015; The City of Calgary, 2017), and that there is a 40% probability of having wind speeds higher than 4 m/s for both of the analyzed locations; it could be feasible to produce power at least half of the year, especially if turbines able to be more efficient in high turbulence zones are designed.

As a general view of the obtained results from both buildings, we have seen that the maximum available power was close to 30 W/m^2 and the literature have shown a maximum concentration of 45 to 50 W/m^2 . By comparing these results to wind energy applications, we have that a project in considered to be attractive if the assessed location has a wind potential of 250 W/m^2 at a 10 m height, and 400 W/m^2 at 40 m. These wind power density values are considerable bigger that the ones obtained in urban settlements, showing why wind energy in the urban environment still have a lot of obstacles to overcome in order to be fully applicable.

5. Conclusion

5.1 Summary

The goal of this thesis was to study the wind field around the edge of a high rise building, in this case the DICE building at the University of Alberta North Campus. The purpose was to determine if there is an existence of an accelerated region which could potentially increase the power produced by a small wind turbine. This work is the beginning of a growing interest in wind resource assessment research, including urban wind power and wind monitoring in the Mechanical Engineering department at the University of Alberta.

Chapter 2 presented the challenge of designing and constructing our own data acquisition system using low cost equipment. The system needed to be able to perform at a high sampling rate, record data simultaneously from the 4 anemometers and have enough storage capacity to save more than 6 months of continuous data. From this first objective the following conclusions were made:

- An Arduino Mega board, equipped with a data logging shield proved to be a low cost system able to perform as a basic data acquisition device and store data simultaneously.
- When using the four anemometers, the highest sampling rate possible was 10Hz. Trying to get a higher sampling rate led to unstable data recording.
- Based on the data file format (.txt), a 16 GB SD card has enough storage capacity to store at least 9 months of continuous data at a 10Hz rate.

Chapter 3 discussed the results of the wind assessment and the turbulence study at the DICE building for the month of February 2017. Comparisons between the recordings of the anemometers at different positions near the edge were made. It also compared results between the DICE and the TBWS, including a wind assessment for TBWS using one year of data. From this chapter the following conclusions were made:

- The wind resource at DICE building showed that: closer to the edge, the wind speed was higher. The DICE building showed a higher wind power density compared to the Tory building, which is located in the free stream, showing that higher wind speeds and power density were recorded at the location where sensors were set close to the edge. In other words, there is a higher wind power density closer to the edge.
- For the month of February 2017 the main wind directions for the North Campus were North-West and South-East, with frequent wind speeds varying between 0 and 5m/s.

- Based on Rayleigh distributions: the DICE building has higher probabilities of experiencing higher wind speeds, confirming that at larger heights, higher wind speeds.
- DICE building has a high turbulence intensity that may affect the power performance of a wind turbine. Probably a VAWT would be a better option for this highly turbulent environment.
- In terms of the integral length of the turbulence, it seems that the size of the elements should not affect much the operations of the turbines. The dimensions are smaller than the regular size of a small wind turbine; however, the overall effect of the turbulence would affect the performance because of the recirculation and the complex wind flow.
- These results are comparable to other research studies done in coastal areas in terms of wind speeds. And for Edmonton, a city far from the coast, having similar results in terms of power density and wind frequency is a positive thing.
- Urban settings don't present high wind speeds like prairies or offshore locations, which would be translated into higher wind power densities. However this does not discard the implementation of small wind turbines in the built environment. As we have seen, the anemometers located near the edge of the building recorded wind speeds over 4m/s through the month of February 2017, yielding wind power densities comparable to coastal locations.
- The TBWS, a measurement location that it is supposed to be set in the free stream, registered lower wind speeds compared to the DICE. Both locations would be able to produce power at least half of the year based in a cut in speed of 3.5m/s. The amount of energy able to be harvested will depend on the size of wind turbines; let's note that bigger turbines produce more power.
- Urban settlements present a lower wind power density compared to open field applications. Even though there is a increase in the amount of energy available at the edge of the building, the quantity still under the 250 W/m^2 that makes a location fall in the category of "good" for wind energy harvesting.

5.2 Future Work

The work performed in this study encountered some areas that can be improved for future work. These improvements and recommendations are listed next:

- Improvements regarding the data acquisition system should be done. In terms of sampling rate, a higher frequency would be beneficial in order to study in a more detailed way the turbulence flow that surrounds the building. In terms of the Arduino system, a more accurate GPS and more reliable data storage should be researched and applied.

- The anemometers location can be changed to a height out of the recirculation zone, and with the sonic anemometer, a study of the turbulence of the flow over the building.
- Run a full year wind resource assessment at the North Campus. Running a group of buildings would be beneficial to get an idea of which building has the highest wind energy concentration.
- Install a wind turbine to study the performance and power output under real urban conditions. Determine the real power curve of the turbine and compare it to the manufacturer curve. Run this study combined with the ultrasonic anemometer to study how the turbulence affects the performance of the turbine.
- After studying the power performance of a wind turbine under real conditions, a techno economic assessment would be beneficial to get an idea of how much money could be saved; and quantify the potential reduction of the carbon footprint in campus by using wind power.

References

- Abohela, I., Hamza, N., & Dudek, S. (2013). Effect of roof shape, wind direction, building height and urban configuration on the energy yield and positioning of roof mounted wind turbines. *Renewable Energy*, *50*, 1106–1118. <https://doi.org/10.1016/j.renene.2012.08.068>
- Albers, A., Jakobi, T., Rohden, R., & Stoltenjohannes, J. (2007). Influence of Meteorological Variables on Measured Wind Turbine Power Curves. *Proceedings of EWECE 2007*, (0), 7.
- Archer, C. L. (2005). Evaluation of global wind power. *Journal of Geophysical Research*, *110*(D12), D12110. <https://doi.org/10.1029/2004JD005462>
- Ayhan, D., & Sağlam, Ş. (2012). A technical review of building-mounted wind power systems and a sample simulation model. *Renewable and Sustainable Energy Reviews*, *16*(1), 1040–1049. <https://doi.org/10.1016/j.rser.2011.09.028>
- Bai, G., Fleck, B., & Zuo, M. J. (2016). A stochastic power curve for wind turbines with reduced variability using conditional copula. *Wind Energy*, *19*(October 2015), 1519–1534. <https://doi.org/10.1002/we>
- Barthelmie, R. J. (2000). Monitoring offshore wind and turbulence characteristics in Denmark. *Wind Energy 1999: Wind Power Comes of Age*, 311–321.
- Beller, C. (2011). *Urban Wind Energy Risø-PhD-Report* (Vol. 89).
- Cace, J., Horst, E., Syngellakis, K., Niel, M., Clement, P., Heppener, R., & Peirano, E. (2007). Urban wind turbines - guidelines for small wind turbines in the built environment, 1–41.
- Caretto, L. (2010). *Use of Probability Distribution Functions for Wind*.
- Centre for Atmospheric Science The University of Manchester. (2017). Sonic Anemometers. Retrieved from <http://www.cas.manchester.ac.uk/restools/instruments/meteorology/sonic/>
- CESAR. (2017). Canadian Energy Systems Analysis System (CESAR). Retrieved from <http://www.cesarnet.ca/user-s-guide-cesarcaness-energy-carbon-sankey-diagrams-canada>
- Dayan, E. (2006). Wind energy in buildings. Power generation from wind in the urban environment - where it is needed most. *Refocus*, *7*(2). [https://doi.org/10.1016/S1471-0846\(06\)70545-5](https://doi.org/10.1016/S1471-0846(06)70545-5)
- Dutton, J. A., & Panofsky, H. A. (1984). *Atmospheric Turbulence*.
- Elliot, D., & Infield, D. (2014). An assessment of the impact of reduced averaging time on small wind turbine power curves, energy capture predictions and turbulence intensity measurements. *Wind Energy*, *17*(December 2012), 337–342. <https://doi.org/10.1002/we>
- Emeis, S. (Karlsruher I. für T. (2013). *Wind Energy Meteorology*. Karlsruher Institut: Springer.
- Eriksson, S., Bernhoff, H., & Leijon, M. (2008). Evaluation of different turbine concepts for wind power. *Renewable and Sustainable Energy Reviews*, *12*(5), 1419–1434. <https://doi.org/10.1016/j.rser.2006.05.017>

- ExxonMobil. (2016). The Outlook for energy: a view to 2040, 1–16. <https://doi.org/10.1080/01998595.2012.10491656>
- Fields, J., Oteri, F., Preus, R., & Baring-gould, I. (2016). Deployment of Wind Turbines in the Built Environment : Risks , Lessons , and Recommended Practices Deployment of Wind Turbines in the Built Environment : Risks , Lessons , and Recommended Practices, (June).
- Fleck, B., & Huot, M. (2009). Comparative life-cycle assessment of a small wind turbine for residential off-grid use. *Renewable Energy*, *34*(12), 2688–2696. <https://doi.org/10.1016/j.renene.2009.06.016>
- Google. (2017). Google My Maps. Retrieved from <https://www.google.com/maps/d/>
- Grieser, B., Madlener, R., & Sunak, Y. (2013). Economics of Small Wind Power Plants in Urban Settings : An Empirical Investigation for Germany Benno Grieser , Reinhard Madlener and Yasin Sunak January 2013 Institute for Future Energy Consumer Needs and Behavior (FCN), (1).
- Gsänger, S., & Pitteloud, J.-D. (2015). 2015 Small Wind World Report Summary., 15.
- GWEC. (2017). Global Wind Statistics 2016, 4. <https://doi.org/10.2.2017>
- IEA-Wind. (2011). Recommended Practices for Wind Turbine Testing for Small Wind Turbines - 12. CONSUMER LABEL FOR SMALL WIND TURBINES.
- IEA-Wind. (2016). IEA Wind Task 27. Retrieved January 1, 2017, from https://www.ieawind.org/task_27_home_page.html
- IEC. (2005a). Iec 61400-12-1. *International Electrotechnical Commission, 2005*, 179.
- IEC. (2005b). IEC 61400-1 Wind turbine - part 1:design requirement. *International Electrotechnical Commission, Third edit.*
- IEC. (2013). Wind turbines – Part 2: Design requirements for small wind turbines, *3rd editio*, 282. Retrieved from https://webstore.iec.ch/p-preview/info_iec61400-2%7Bed2.0%7Den_d.pdf
- IRENA. (2012). RENEWABLE ENERGY TECHNOLOGIES: COST ANALYSIS SERIES Wind Power. *Power Generation Technologies*, *1*(5), 223–242. <https://doi.org/10.1016/B978-0-08-098330-1.00011-9>
- Islam, M. R., Mekhilef, S., & Saidur, R. (2013). Progress and recent trends of wind energy technology. *Renewable and Sustainable Energy Reviews*, *21*(August 2015), 456–468. <https://doi.org/10.1016/j.rser.2013.01.007>
- Jian-Zhong, L., Hui-Jun, L., & Kai, Z. (2007). New expressions for the surface roughness length and displacement height in the atmospheric boundary layer. *Chinese Physics*, *16*(7), 2033–2039. <https://doi.org/10.1088/1009-1963/16/7/038>
- Karthikeya, B. R., Negi, P. S., & Srikanth, N. (2016). Wind resource assessment for urban renewable energy application in Singapore. *Renewable Energy*, *87*, 403–414. <https://doi.org/10.1016/j.renene.2015.10.010>
- Krishnan, A., & Paraschivoiu, M. (2015). 3D analysis of building mounted VAWT with diffuser shaped shroud. *Sustainable Cities and Society*. <https://doi.org/10.1016/j.scs.2015.06.006>

- Kundu, P. K., Cohen, I. M., & Dowling, D. R. (2012). *Fluid Mechanics. Turbulence* (5th Edition). Waltham: Elsevier Inc. <https://doi.org/10.1016/B978-0-12-382100-3.10012-5>
- Larin, P., Paraschivoiu, M., & Aygun, C. (2016). CFD based synergistic analysis of wind turbines for roof mounted integration. *Journal of Wind Engineering and Industrial Aerodynamics*, 156, 1–13. <https://doi.org/10.1016/j.jweia.2016.06.007>
- Ledo, L., Kosasih, P. B., & Cooper, P. (2011). Roof mounting site analysis for micro-wind turbines. *Renewable Energy*, 36(5), 1379–1391. <https://doi.org/10.1016/j.renene.2010.10.030>
- Loomis, D. (2011). Are There Economies of Scale in Wind Energy? Retrieved from <http://linkinghub.elsevier.com/retrieve/pii/B9780080983301000119>
- Lu, L., & Ip, K. Y. (2009). Investigation on the feasibility and enhancement methods of wind power utilization in high-rise buildings of Hong Kong. *Renewable and Sustainable Energy Reviews*, 13(2), 450–461. <https://doi.org/10.1016/j.rser.2007.11.013>
- Lu, X., McElroy, M. B., & Kiviluoma, J. (2009). Global potential for wind-generated electricity. *Proceedings of the National Academy of Sciences*, 106(27), 10933–10938. <https://doi.org/10.1073/pnas.0904101106>
- Lubitz, W. D. (2014). Impact of ambient turbulence on performance of a small wind turbine. *Renewable Energy*, 61, 69–73. <https://doi.org/10.1016/j.renene.2012.08.015>
- Makkawi, a., Celik, a., & Muneer, T. (2009). Evaluation of micro-wind turbine aerodynamics, wind speed sampling interval and its spatial variation. *Building Services Engineering Research and Technology*, 30(1), 7–14. <https://doi.org/10.1177/0143624408096343>
- MATLAB. (2017). Curve Fitting and Distribution Fitting. Retrieved from <https://www.mathworks.com/help/stats/examples/curve-fitting-and-distribution-fitting.html>
- Mazon, J., Rojas, J. I., Jou, J., Valle, A., Olmeda, D., & Sanchez, C. (2015). An assessment of the sea breeze energy potential using small wind turbines in peri-urban coastal areas. *Journal of Wind Engineering and Industrial Aerodynamics*, 139, 1–7. <https://doi.org/10.1016/j.jweia.2015.01.002>
- Measnet. (2009). POWER PERFORMANCE MEASUREMENT Version 5 December - 2009. *Measurement*, (December), 1–12.
- Measnet. (2014). Calculation of Specific Site AEP, 1–4.
- Mertens, S. (2006). Wind Energy in the Built Environment Concentrator Effects of Buildings Wind Energy in the Built Environment Concentrator Effects of Buildings, 1–180.
- Natural Resources Canada. (2003). *Stand-Alone Wind Energy Systems: A Buyer's Guide*. Ottawa.
- Natural Resources Canada. (2017). Magnetic declination calculator. Retrieved from <http://www.geomag.nrcan.gc.ca/calc/mdcal-en.php>
- Neuman, T., Emeis, S., & Illig, C. (2006). Report on the Research Project OWID – Offshore Wind Design Parameter. In J. Peinke, P. Schaumann, & S. Barth (Eds.) (pp. 81–85). Springer. <https://doi.org/10.1007/3-540-30906-3>

- Oke, T. R. (1990). *Boundary layer climates*. *Earth-Science Reviews* (Vol. 27). [https://doi.org/10.1016/0012-8252\(90\)90005-G](https://doi.org/10.1016/0012-8252(90)90005-G)
- Oliver, B., Pacifico, S., May, D., Ungard, K., Eret, M., White-Argumedo, B., ... Gill, S. (2016). *Primer on Energy Systems in Canada* (Second Edi). Toronto: Pollution Probe. Retrieved from <http://www.pollutionprobe.org/>
- Pagnini, L. C., Burlando, M., & Repetto, M. P. (2015). Experimental power curve of small-size wind turbines in turbulent urban environment. *Applied Energy*, *154*, 112–121. <https://doi.org/10.1016/j.apenergy.2015.04.117>
- Paraschivoiu, I. (2002). *Wind turbine design: with emphasis on Darrieus concept*. Montreal, Quebec: Presses inter Polytechnique.
- Plate, E. J. (1995). *Urban Climates and Urban Climate Modelling: An Introduction*. Dordrecht: Springer.
- R.M. Young. (2017). Sonic Anemometer 81000 Manual. *Manual*, (231). Retrieved from <http://www.youngusa.com/products/11/3.html>
- R M Young Company. (2000). Wind monitor - SE model 09101 instructions, (231).
- Ramenah, H., & Tanougast, C. (2016). Reliably model of microwind power energy output under real conditions in France suburban area. *Renewable Energy*, *91*, 1–10. <https://doi.org/10.1016/j.renene.2015.11.019>
- Romanic, D., Rasouli, A., & Hangan, H. (2015). Wind resource assessment in complex urban environent. *Wind Engineering*, *39*(2), 193–212.
- Saidur, R., Islam, M. R., Rahim, N. A., & Solangi, K. H. (2010). A review on global wind energy policy. *Renewable and Sustainable Energy Reviews*, *14*(7), 1744–1762. <https://doi.org/10.1016/j.rser.2010.03.007>
- Sathyajith, M. (2006). *Wind Energy: Fundamentals, Resource Analysis and Economics*. Berlin: Springer.
- Simões, T., & Estanqueiro, A. (2016). A new methodology for urban wind resource assessment. *Renewable Energy*, *89*, 598–605. <https://doi.org/10.1016/j.renene.2015.12.008>
- Tabrizi, A. B., Whale, J., Lyons, T., & Urmee, T. (2015a). Extent to which international wind turbine design standard, IEC61400-2 is valid for a rooftop wind installation. *Journal of Wind Engineering and Industrial Aerodynamics*, *139*, 50–61. <https://doi.org/10.1016/j.jweia.2015.01.006>
- Tabrizi, A. B., Whale, J., Lyons, T., & Urmee, T. (2015b). Rooftop wind monitoring campaigns for small wind turbine applications: Effect of sampling rate and averaging period. *Renewable Energy*, *77*, 320–330. <https://doi.org/10.1016/j.renene.2014.12.037>
- Tennekes, H., & Lumley, J. L. (1999). *A first course in turbulence* (17th editi). Cambridge, Massachusetts: The MIT Press.
- The City of Calgary. (2017). How much wind is needed for a small wind turbine? Retrieved from <http://www.calgary.ca/CS/CPB/Pages/Operations-WorkPlace-Centre/Bearspaw-OWC/Wind-need-for-small-turbine.aspx>

- Toja-Silva, F., Lopez-Garcia, O., Peralta, C., Navarro, J., & Cruz, I. (2016). An empirical-heuristic optimization of the building-roof geometry for urban wind energy exploitation on high-rise buildings. *Applied Energy*, *164*, 769–794. <https://doi.org/10.1016/j.apenergy.2015.11.095>
- Tummala, A., Velamati, R. K., Sinha, D. K., Indrajaya, V., & Krishna, V. H. (2016). A review on small scale wind turbines. *Renewable and Sustainable Energy Reviews*, *56*, 1351–1371. <https://doi.org/10.1016/j.rser.2015.12.027>
- UNFCCC. Conference of the Parties (COP). (2015). Adoption of the Paris Agreement. Proposal by the President. *Paris Climate Change Conference - November 2015, COP 21, 21932*(December), 32. <https://doi.org/FCCC/CP/2015/L.9/Rev.1>
- Van der Hoven, I. (1957). Power Spectrum of Horizontal Wind Speed in the Frequency Range From 0.0007 To 900 Cycles Per Hour. *Journal of Meteorology*. [https://doi.org/10.1175/1520-0469\(1957\)014<0160:PSOHWS>2.0.CO;2](https://doi.org/10.1175/1520-0469(1957)014<0160:PSOHWS>2.0.CO;2)
- Wind Empowerment. (2017). Wind resource assessment - The basics. Retrieved from <http://windempowerment.org/wind-resource-assessment-the-basics/>
- Wood, D. (2011). *Green Energy and Technology: Small Wind Turbines*. <https://doi.org/10.2174/97816080528511060101>

Appendix A: Anemometers Technical Information

A.1 Ultrasonic Anemometer Model 81000 (R.M. Young, 2017).

Specification Summary

WIND SPEED

Range: 0 to 40 m/s (0 to 90 mph)
Resolution: 0.01 m/s
Threshold: 0.01 m/s
Accuracy: $\pm 1\%$ rms ± 0.05 m/s (0 to 30 m/s)
 $\pm 3\%$ rms (30 to 40 m/s)

WIND DIRECTION

Azimuth Range: 0.0 to 359.9 degrees
Elevation Range: ± 60.0 degrees
Resolution: 0.1 degree
Accuracy: $\pm 2^\circ$ (1 to 30 m/s)
 $\pm 5^\circ$ (30 to 40 m/s)

SPEED OF SOUND

Range: 300 to 360 m/s
Resolution: 0.01 m/s
Accuracy: $\pm 0.1\%$ rms ± 0.05 m/s (0 to 30 m/s wind)

SONIC TEMPERATURE

Range: -50 to +50 °C
Resolution: 0.01 °C
Accuracy: ± 2 °C (0 to 30 m/s wind)

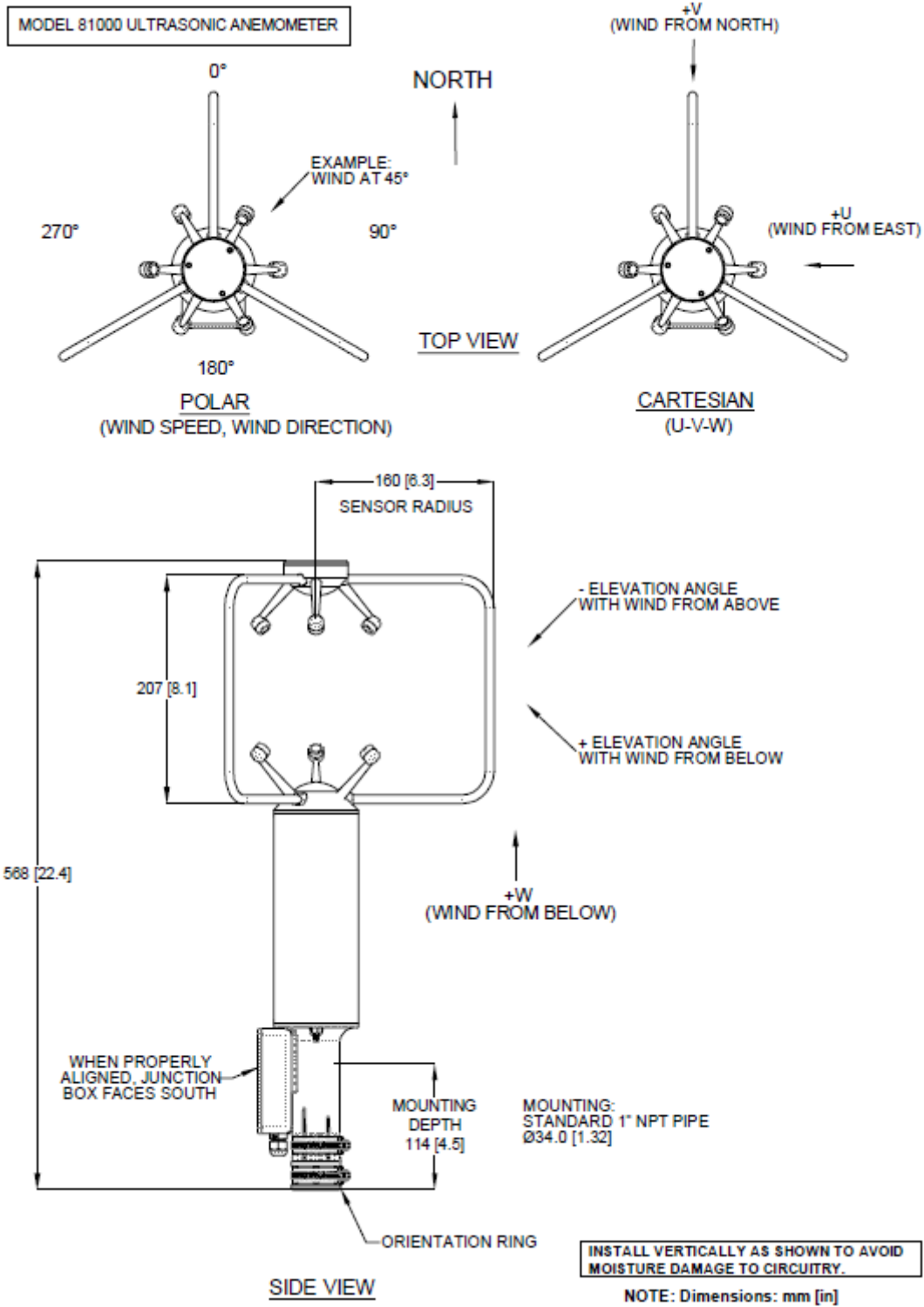
VOLTAGE OUTPUT (4 CHANNELS)

Range: 0 to 5000 mV
Resolution: 12 Bit
Accuracy: $\pm 0.1\%$ of full scale

GENERAL

Air sample column: 10 cm high X 10 cm diameter
Air sample path: 15 cm
Output rate: 4 to 32 Hz (selectable)
Output formats: Serial data (selectable)
RS-232 and RS-485
Baud Rates: 1200 to 38400
Power Supply: 12 to 24 VDC, 110 mA
Dimensions: Overall height 56 cm
Support arm radius 17 cm
Mounting 34 mm (1.34 in) diameter
(standard 1 inch pipe)
Weight: Sensor weight 1.7 kg (3.8 lb)

Sensor orientation and dimensions



A.2 Wind Monitor Model 09101 (R M Young Company, 2000).

Specification Summary

WIND SPEED SPECIFICATION SUMMARY

Range	0 to 100 m/s (224 mph)
Resolution:	0.1 unit
Accuracy:	±0.3 m/s (0.6 mph) or 1% of reading
Threshold:	1.0 m/s (2.2 mph)
Distance constant:	2.7 m (8.9 ft)
Transducer:	Rotating magnet and stationary coil.

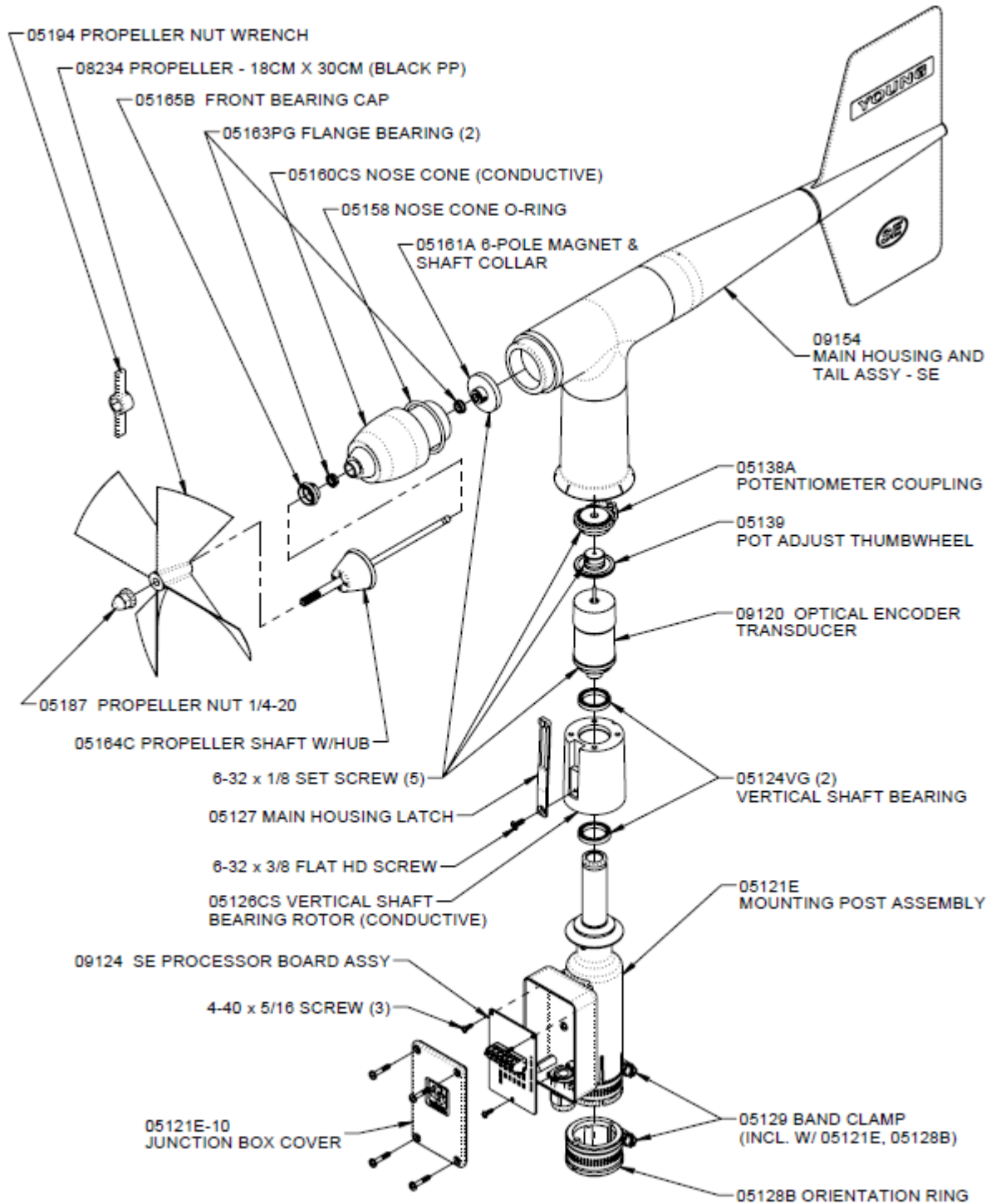
WIND DIRECTION (AZIMUTH) SPECIFICATION SUMMARY

Range:	0-360 degrees
Accuracy:	± 2 degrees
Resolution:	1 degree
Threshold:	1.1 m/s (2.5 mph) @ 10° displacement
Delay distance:	1.3 m (4.3 ft)
Damping ratio:	0.3
Transducer:	Absolute encoder

GENERAL

Power requirement:	11-24 VDC, 20 mA
Dimensions:	Overall height 37 cm Overall length 55 cm Propeller 18 cm diameter Mounting 34 mm (1.34 in) diameter (standard 1 inch pipe)
Weight:	Sensor weight 1.0 kg (2.2 lb) Shipping weight 2.3 kg (5.0 lb)
Voltage Output:	WS: 0-5 VDC for 0-100 m/s WD: 0-5 VDC for 0-540°
Serial RS-485:	2 wire-half duplex, 1200-9600 Baud RMY, NCAR, NMEA, or RMYT protocols Polled or continuous
Operating Temperature:	-50 to 50°C (-58 to 122°F)

General Assembly



Appendix B: The DICE building pictures



(a) The DICE building



(b) Anemometers at the DICE rooftop



(c) Ultrasonic anemometer and Wind Monitor #3



(d) Ultrasonic anemometer and Wind Monitor under icing conditions



(e) Anemometers under icing conditions